RCA REVIEW

a technical journal

RADIO AND ELECTRONICS
RESEARCH • ENGINEERING

Published quarterly by

RCA LABORATORIES

in cooperation with all subsidiaries and divisions of

RADIO CORPORATION OF AMERICA

VOLUME XXI | JUNE 1960 | NUMBER 2

CONTENTS

RCA REVIEW is regularly abstracted and indexed by *Industrial Arts Index Science Abstracts* (I.E.E.-Brit.), *Electronic Engineering Master Index, Chemical Abstracts, Proc. I.R.E.*, and *Electronic & Radio Engineer.*

RCA REVIEW

BOARD OF EDITORS

THE STRATOSCOPE I TELEVISION SYSTEM*†

By

L. E. Flory, G. W. Gray, J. M. Morgan and W. S. Pike

RCA Laboratories,
Princeton, N. J.

Summary—*Stratoscope I is a balloon-borne astronomical telescope designed for solar photography. When aloft, the telescope is remotely operated by radio command signals transmitted from a control station on the ground.*

A special television system has been developed to assist in aiming and focusing Stratoscope I. This equipment comprises a camera and transmitter on the telescope and a ground receiver driving several monitors. It permits the astronomers at the ground control station to visually aim and focus the telescope by inspection of the television monitors. The use of this technique has significantly increased the yield of useful photographs obtained with Stratoscope I.

Introduction

THE Stratoscope I Television System is a special-purpose slow-scan television chain comprising a balloon-borne camera and transmitter, and a ground receiving station. The Stratoscope itself is a balloon-borne telescope used for high-altitude solar photography. At its operating altitude of 80,000 feet, the disturbing effects of the turbulent atmosphere of the earth are greatly reduced. When aloft, the telescope is operated by radio command signals transmitted from the ground control point.

A typical flight starts before dawn with the launching of the balloon and telescope. About two hours are required to reach operating altitude. At altitude, the equipment is turned on by a timer, and automatic servos on the telescope orient it in azimuth and elevation so that it "sees" the sun. After a waiting period to permit the various portions of the telescope to come to thermal equilibrium, an automatic film camera on the telescope starts and exposes one frame of film each second. The television camera is also turned on, and the astronomer in charge can aim and focus the telescope by viewing the television screen at the ground control point. At the end of about three hours, the film is exhausted and automatic mechanisms stow the telescope

* Manuscript received February 15, 1960.

within its gimbal structure. The balloon is then cut loose, and the telescope with its film and TV cameras descends to earth on a parachute. The exposed film, which constitutes the useful result of the flight, is removed and developed. Figure 1 shows an over-all view of the balloon and telescope just after launching. The vertical distance from the top of the balloon to the bottom of the telescope gimbal structure is about 300 feet.

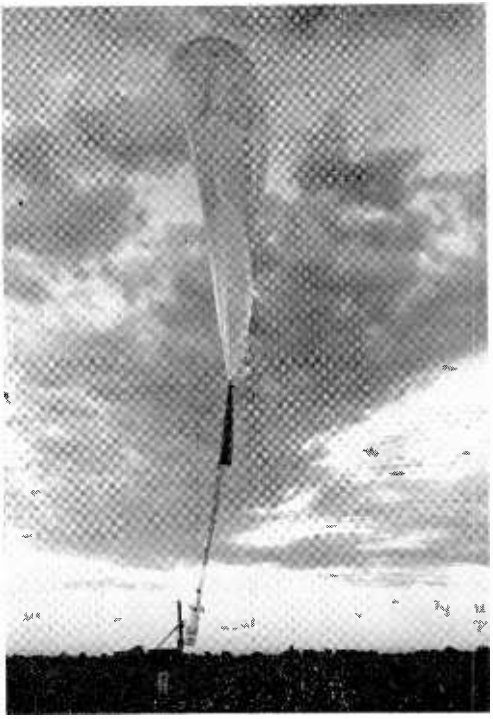

Fig. 1—Launching of Stratoscope I.

Integration of Television and Film Camera Systems

As the electrical and mechanical design of the television system had to be integrated rather carefully with the telescope itself, a number of problems arose requiring solutions and techniques quite different from those normally encountered in commercial broadcast practice. It was specified that the resolution of the television system was to be comparable to commercial television broadcast practice, and that a

range of 150 miles must be attainable. At the operating altitude of 80,000 feet, the temperature is about —55° C and the pressure about 1/40 atmosphere.

Rotating mechanical shutters in the telescope and film camera were arranged to expose the film at a rate of once per second with an exposure time of about 1.5 milliseconds. Therefore, a vertical-scanning frequency of one cycle per second was adopted for the television system. A 500-cycle-per-second horizontal-scanning frequency was used, thereby giving 500-line resolution. In order to avoid a complicated and possibly unstable sync generator aloft, interlace was not used.

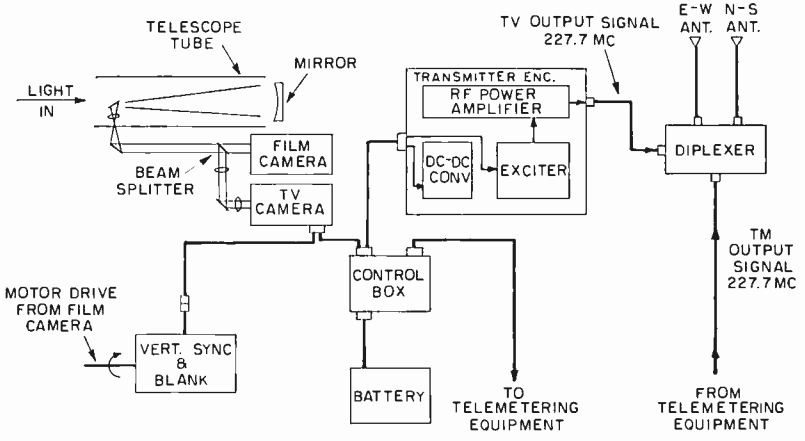

Fig. 2—Balloon-borne portion of Stratoscope I television system.

An advantage of the low frame rate is that lower bandwidth and transmitter power are required. A bandwidth of 200 kilocycles is adequate for 500-line resolution at these scanning frequencies. Calculation showed that an FM transmitter with 200-kilocycle deviation (modulation index = 1) and a power output of 0.8 watt would be ample under ideal conditions with the contemplated receiver and antennas. An actual power output of 10 watts was used.

A block diagram of the balloon-borne portion of the system is shown in Figure 2. Light entering the telescope is imaged at the film gate of the film camera and at the faceplate of the television pickup tube (Vidicon) by an optical system comprising a primary 12-inch parabolic mirror and a number of subsidiary mirrors and lenses. The exposure time and rate are controlled by the rotary shutter. A beam

splitter, which follows the shutter, apportions the light between the television and film cameras.

After some preliminary experimentation, an additional rotary shutter was installed in the path to the television camera only. This permits only every third exposure to reach the Vidicon, the two intervening ones being blanked out. This expedient was found necessary to reduce image blurring caused by the storage properties of the Vidicon when operated at the low scanning rate.

Vertical sawtooth and blanking signals for the camera were first generated electro-mechanically by means of a potentiometer and a

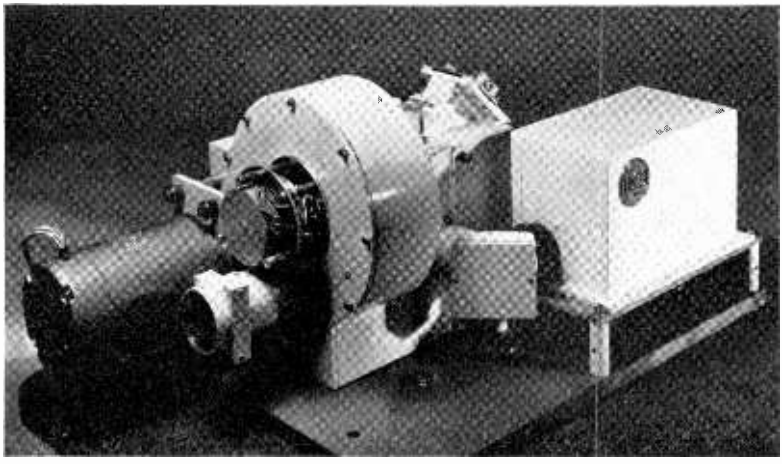

Fig. 3—Film and television cameras for Stratoscope I. The cylindrical drum contains the shutter mechanism.

cam-operated microswitch on the one-revolution-per-second shaft of the film camera. Initial experiments with this system established that the vertical sawtooth so produced was not sufficiently free of noise, having both cyclic and random disturbances of small amplitude superimposed upon it. These produced undesired shading in the picture. An electronic vertical sweep circuit driven from the blanking microswitch was finally substituted for the potentiometer, with entirely satisfactory results. The microswitch is phased with the shutter system so that the latter illuminates the Vidicon during the vertical retrace. Horizontal scanning and blanking signals are generated by circuits within the camera. Due to flashover problems associated with the high operating altitude of the equipment, any units involving potentials over about 200 volts must be pressurized. Thus, the camera

and transmitter are enclosed in pressure-tight housings. Figure 3 shows the film camera with its driving motor and the television camera.

Power for the balloon-borne television equipment is supplied by lead–acid storage cells. Although there are other batteries which offer advantages in weight and efficiency, lead cells are easy to maintain, will withstand many charge-discharge cycles, and are inexpensive. As weight was not a severe problem, they seemed the best compromise. A disadvantage of lead–acid cells is the relatively large drop in voltage which occurs during discharge. At the battery temperatures and discharge rates involved in this system, the drop is about 20 per cent. This problem was overcome by regulating all critical voltages in the television system with transistor regulators. Transistor dc-dc chopper-type converters were used to obtain the high voltages required by the Vidicon and the transmitter.

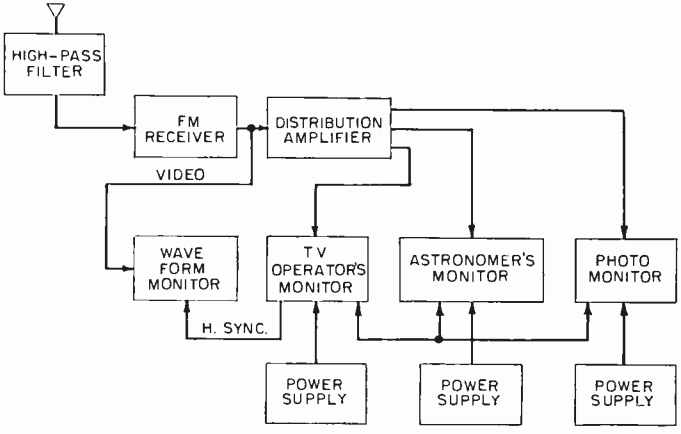

Fig. 4—Ground-station portion of Stratoscope I television system.

Receiving Equipment

A block diagram of the ground station television equipment is shown in Figure 4. Signals from the balloon are picked up on a pair of stacked Yagi antennas mounted on commercial antenna rotators. The antenna gain is about 15 decibels over an isotropic source. Motion in both azimuth and elevation may be controlled by the operator. A 200-megacycle high-pass filter is provided at the receiver input to ensure that no spurious signals are picked up from the command and communication transmitters, also located in the ground station. The command transmitter operates on 138 megacycles and is used to operate the air-borne focusing and pointing equipment on the telescope. The

communications transmitter is normally operated at about 7 megacycles and is used to maintain communication with the crew tracking the balloon for recovery purposes.

The incoming signal from the balloon television system, on 225.7 megacycles, is applied to a commercial FM telemetry receiver. Its bandwidth is about 0.5 megacycle and its noise figure is about 6 decibels. The receiver output, at a level of about 8 volts peak-to-peak, is applied to a distribution amplifier. The amplifier provides three isolated outputs for the three monitors, so that a defect in one will not disable the others. It also incorporates a small amount of high-frequency boost to improve the system response at the upper video frequencies. Conventional vacuum-tube circuitry is used in the receiver and distribution amplifier.

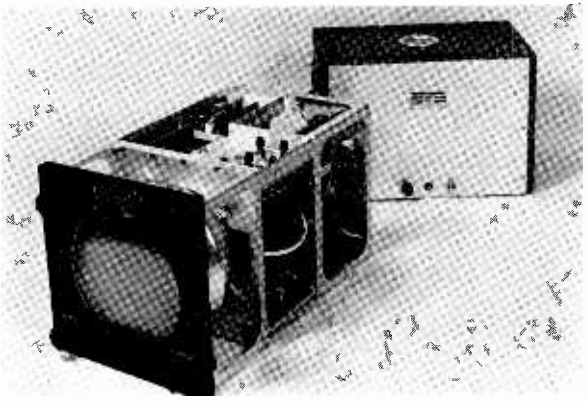

Fig. 5—Video monitor and power supply.

The three output signals from the distribution amplifier are applied to three television monitors. One of the monitors is used by the television operator, a second is at the operating position of the astronomer in charge, and the third provides signal to a continuously running photographic camera which records the pictures received. These photographs are used for check purposes only. Figure 5 is a photograph of one of the monitors with its power supply.

Television-Camera Design

As the balloon-borne portion of the system is inaccessible during flight, considerable attention had to be paid to thorough stabilization of all circuits. As mentioned earlier, a sync generator was eliminated on these grounds. The operating controls for the Vidicon target voltage and video black level are extended to the ground, via the telemetry

and command-radio circuits, for use during flight. All other controls are pre-set at launch and require no further adjustment.

A simplified circuit diagram of the camera is shown in Figure 6. The video amplifier is shown across the top of the diagram, vertical deflection and blanking in the middle, and the horizontal deflection circuit at the bottom.

The signal from the Vidicon target is applied first to a CK-5703 subminiature triode which is connected as a cathode follower. The voltage gain of this stage is about 0.9, but it serves as a comparatively noise-free impedance converter between the high output impedance of the Vidicon and the low input impedance of the following transistor amplifier.

To obtain maximum stability, an unconventional method of controlling the Vidicon beam current has been adopted. A 510,000-ohm resistor is placed in the cathode circuit and grid No. 1 is returned to the regulated —24 volt supply. Beam control is achieved by variation of the grid No. 2 voltage. By this means, the d-c beam current is degeneratively stabilized to the point where it requires no adjustment during flight.

Transistors Q1, Q2, and Q3 comprise a direct-coupled negative-feedback amplifier with a flat over-all voltage gain of about 300. A network interconnecting the emitters of Q1 and Q3 controls the ratio of a-c to d-c feedback and, thus, the stability and frequency response of the amplifier. Conventional high peaking is used to offset the drop in high-frequency response caused by the high-load impedance seen by the Vidicon. The high peaker consists of the compensated voltage divider following Q3. The lower resistive element of the high peaker is also used as a pre-set video gain control.

The gain control is followed by a two-transistor direct-coupled feedback amplifier stage comprising Q4 and Q5. Its gain is about 10. Note that in this amplifier, as in the previous one, the base potential of the input transistor is stabilized by a Zener diode. The output of Q5 is coupled to the following stage by a 2-microfarad coupling capacitor. Transistor Q6 is a keyed clamp which clamps the base of Q8 to a potential set by the remotely controlled black-level potentiometer at the start of each horizontal line. Clamp pulses are derived from the horizontal-rate generator. The video signal is amplified by Q8. In the collector circuit of Q8, a large pedestal at both horizontal and vertical frequencies is added to the video signal by Q7, which is driven with a mixed blanking signal derived from the vertical and horizontal rate generators. The diode which couples Q8 to Q9 opens during each blanking pulse, thus clipping out most of the added

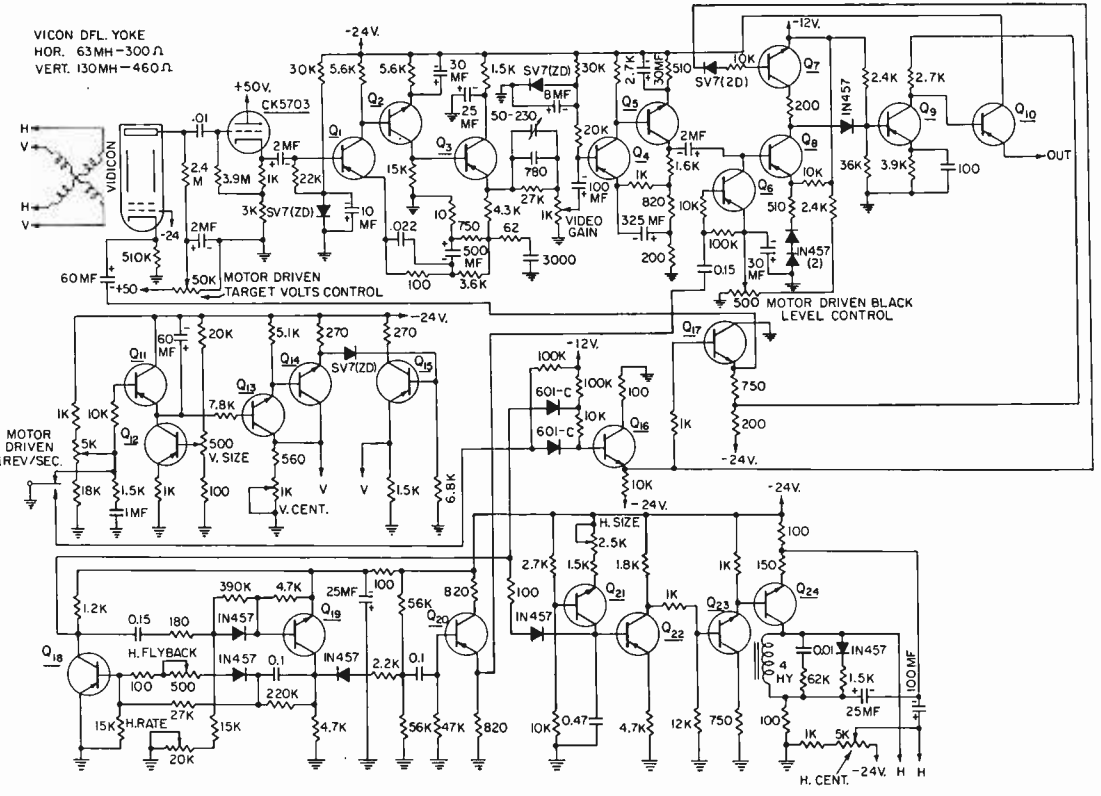

Fig. 6—Simplified schematic diagram of television camera circuit.

pedestal and providing Q9 with a composite signal which has a clean baseline during blanking time. As the black-level potentiometer indirectly controls the potential at the collector of Q8, the amount of pedestal not clipped by the diode (i.e., the black level) can be adjusted remotely. A fixed amount of mixed blanking is then added to the signal in the collector circuit of Q9, to serve as sync in the ground equipment. Q9 is directly coupled to Q10, an emitter follower, which drives the video transmitter. The emitter load for Q10 is a 3000-ohm resistor located at the transmitter.

Vertical deflection for the Vidicon is provided by transistors, Q11 through Q15. A switch on the one-revolution-per-second shaft in the film-camera drive train initiates the vertical deflection cycle. At the instant the vertical flyback is to be initiated, the upper contact of the switch opens and the lower contact closes. The switch stays in this position for about 50 milliseconds and then reverts to its original position.

When the switch operates, transistor Q11 conducts, discharging the 60-microfarad capacitor. This corresponds to the vertical flyback. At the conclusion of the flyback, when the switch reverts to its original position, transistor Q11 turns off and the capacitor recharges through constant-current transistor, Q12. The linear sawtooth generated across the capacitor is amplified in transistors Q13 through Q15 and applied to the vertical-deflection coils.

The horizontal rate generator, at the bottom left of the diagram, comprises transistors Q18 and Q19, which are connected in a stabilized multivibrator circuit. The two coupling time constants of the multivibrator are individually adjustable and one is about five times as long as the other. The longer one is used to adjust the horizontal frequency, while the shorter adjusts the length of the horizontal flyback and blanking. The output from the multivibrator is applied to a sawtooth generator which is similar to that used in the vertical-deflection circuit, except that the discharge device is a diode. Transistor Q21 is the constant-current charging transistor. The sawtooth produced is amplified by Q23 through Q24 and applied to the horizontal-deflection coils.

Mixed blanking is produced in transistors Q16 and Q17. Horizontal and vertical pulses are applied to the base of Q16 through a diode clipper network which ensures that both horizontal and vertical pulses are of the same amplitude. Transistors Q16 and Q17 are connected as emitter followers and distribute mixed blanking, at low impedance and the correct amplitude, to the circuits requiring it, including the Vidicon cathode.

The video output from the camera is applied to a commercial FM telemetry transmitter operating at 225.7 megacycles. It has a power output of 2 watts. This unit is used as an exciter to drive a 10-watt push-pull final amplifier. The latter uses a single 5894 double-tetrode tube in conventional circuitry. Because the 5894 is operated at only a fraction of its ratings at this power level, no blower is required to keep the seals below the critical temperature and, therefore, problems

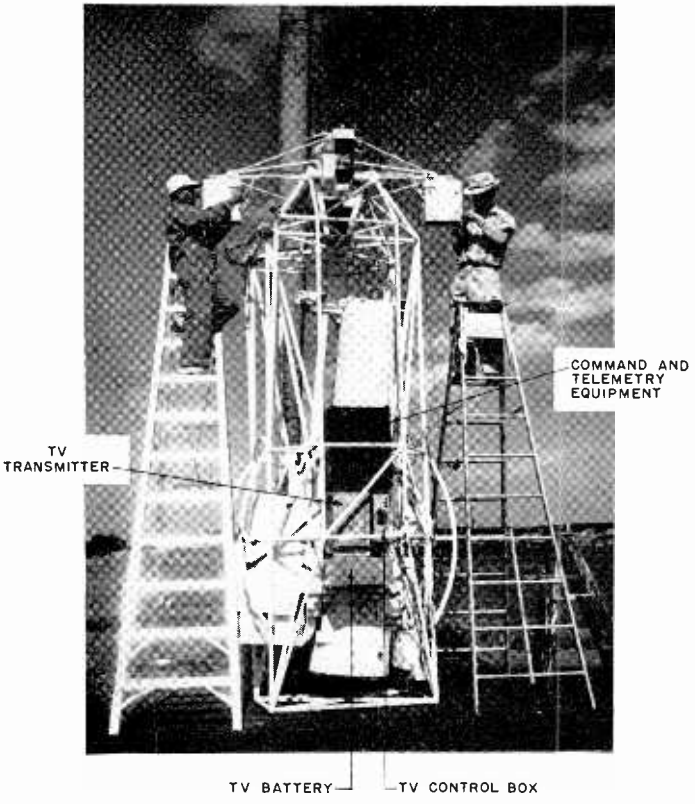

Fig. 7—Stratoscope I during ground testing.

of vibration are avoided. The amplifier, exciter, and a commercial transistor chopper-type dc-to-dc converter are housed in a large cast-aluminum pressure-tight housing.

Figure 7 shows the equipment mounted on the telescope. The battery case is at the bottom. Immediately above on the left is the transmitter housing. The unit to the right is a junction and control box containing the power relays, motor-driven target and black-level

potentiometers, and battery-voltage regulators for the entire television system.

Printed wiring boards are used for the camera circuits. Some of these are shown in Figure 8. The various boards plug into appropriate sockets in the camera case. This method of construction permits quite compact packaging while the plug-in feature allows ready replacement and servicing when required.

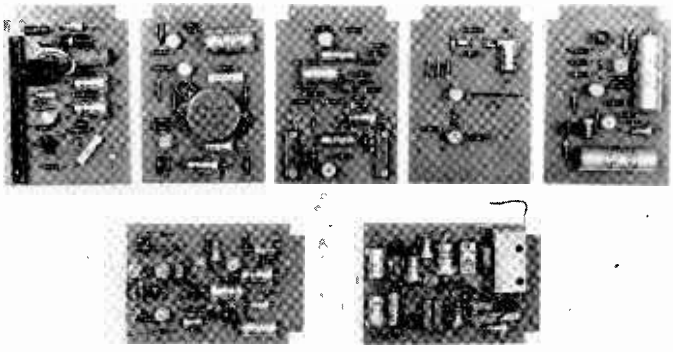

Fig. 8—Printed wiring boards for Stratoscope I television camera.

Transmitting Antenna

There were a number of considerations in the design of the transmitting antenna that warranted careful attention. First, Stratoscope I carries a telemetering system with its associated transmitter operating on a frequency only two megacycles removed from the television system. Second, as the orientation of the entire balloon with respect to the receiving station changes during flight, the air-borne antenna had to be omnidirectional in azimuth. Third, because the telescope tube traverses in elevation during flight and is several wavelengths long at the telemetry and television frequencies, the antenna must be located to minimize any anomalies in its directional pattern created by this motion.

An antenna and combining network were developed which would efficiently radiate both signals, while at the same time isolating the telemetry and television transmitters from each other. A vertically polarized antenna mounted below a ground plane located on the bottom of the telescope gimbal structure looked promising. Scale models of

several types of antenna were constructed for operation at about three times the desired frequency, and their patterns were measured.

A single vertical quarter-wave unipole below the ground plane was tried first. It proved to have two disadvantages. First, too much of the energy radiated from it was lost above the horizon. Second, because of the close frequency spacing of the transmitters, frequency diplexing was deemed to be impractical because too much selectivity would be required in the filters. The pattern of this simple antenna in the vertical plane is shown by the dashed line in Figure 9. Note the large amplitude lobes above the horizon.

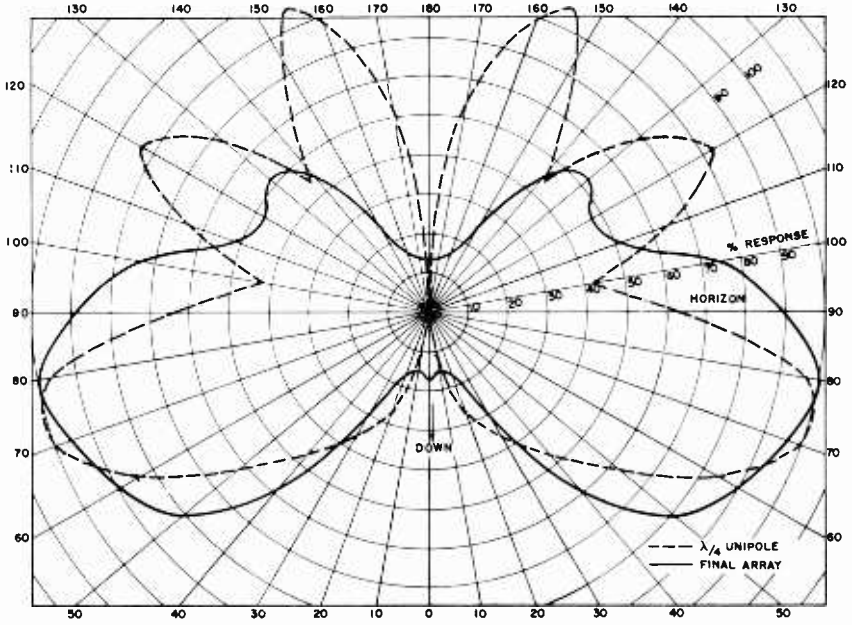

Fig. 9—Antenna patterns.

A four-element antenna was tried next. This consisted of four unipoles mounted symmetrically below a circular ground plane. It is shown mounted on the telescope in Figure 10. The feed system is shown schematically in Figure 11. The East–West pair of unipoles are interconnected by cables such that the currents in the East antenna lag behind those in the West by 180°. The North–South pair are similarly connected. If, now, an extra 90° phase shift is introduced into the cable driving the East–West pair, the antenna pattern will be omnidirectional in azimuth as desired. The antenna is similar to the

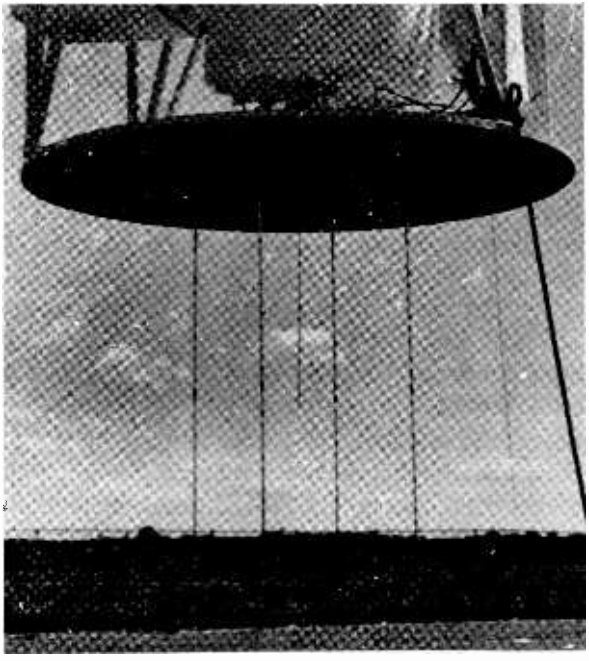

Fig. 10—Antenna.

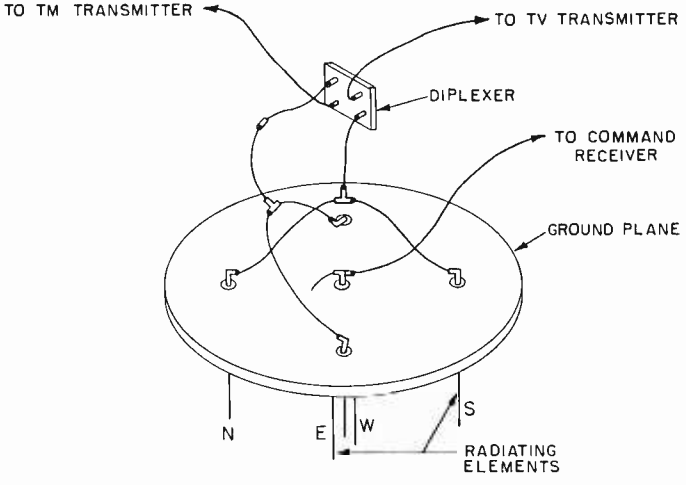

Fig. 11—Antenna arrangement.

"turnstile" array often used in television broadcasting, insofar as its feed arrangements are concerned. That is to say, it must be fed from two correctly phased sources. This requirement is easily met with the familiar bridge or "rat-race" type diplexer. Thus, all power produced by both transmitters is radiated, and a failure of either transmitter does not affect the other.

It was determined that this antenna pattern could be modified to direct more energy toward the horizon and suppress the upward lobes by the simple expedient of lengthening the unipoles to about 0.65 wavelength. The pattern of the final antenna in the vertical plane is shown by the solid line in Figure 9. Matching between the antenna and the diplexer was achieved by selecting appropriate lengths and impedances for the interconnecting cables.

A center quarter-wave unipole was installed in the antenna and used to energize the command receiver in the balloon. This operates on 138.38 megacycles. It may be shown that, due to the manner in which the transmitting unipoles are phased, the field from the balloon transmitters at the location of this receiving antenna is zero. The 138.38 megacycle receiver is thus immune to interference from the transmitters on the balloon.

Ground Station

A photograph of the ground station is shown in Figure 12. The double Yagi antenna receives the television signals from the balloon. As the receiver used was a commercial telemetry receiver, the principal item of interest in the ground station television equipment is the monitor. The monitor circuit is shown in Figure 13.

The video signal from the distribution amplifier enters the monitor at the jack shown in the upper left corner. It is applied to the sync separator comprising transistors Q1, Q2, and Q3 and to the video amplifier at the right center of the diagram. A gain-control contrast potentiometer adjusts the input level to the video amplifier.

In the video amplifier, transistors Q29 and Q30 are connected as a direct-coupled feedback amplifier having a gain of about 10. The output of Q30 is a-c coupled to Q31 with a large capacitor. D-C restoration is provided to keep the base of Q31 from swinging positive. Note the high collector supply voltage used on Q31. This transistor is direct-coupled to Q32, an emitter follower, which drives the kinescope grid. D-C restoration is also used in the emitter-follower circuit. This amplifier will deliver about 40 volts peak-to-peak signal to the kinescope grid.

Type 7ABP14 kinescopes are used in all three monitors. An orange filter is used over the kinescope at the two main viewing positions, the astronomer's monitor and the television operator's position. This filters out the short-persistence blue component of the phosphor luminescence. At the recording camera monitor, a blue filter is used to remove the long-persistence component.

Sync separation takes place principally in Q1. The video signal applied to the base of Q1 has positive-going sync. The base of Q1 goes into conduction on each sync tip, and, thus, builds up a bias on the base such that only the sync tips are amplified by Q1, the video signal being below cutoff. Q1 is direct coupled to Q2 which has fixed bias. Q2 further clips the video signal, again in the direction to

Fig. 12—Stratoscope I ground receiving station.

amplify only the tips of the sync pulses. In this manner, the collector of Q2 provides clean sync to the following circuits.

This signal is applied to Q3 where it is inverted and amplified. At the collector of Q3, the signal splits, vertical pulses being selected by integration in the base and collector circuits of Q4, and horizontal pulses being selected by differentiation in the base circuit of Q13.

Vertical sync pulses from Q4 are applied to transistors Q5 and Q6, which comprise the vertical oscillator. It is a stabilized multivibrator similar to the horizontal oscillator in the camera. Vertical sawtooth is generated in Q7 and Q8, Q7 being a constant-current charging transistor and Q8 an emitter follower. The 100-microfarad time-base capacitor is discharged by a diode directly coupled to the multivibrator.

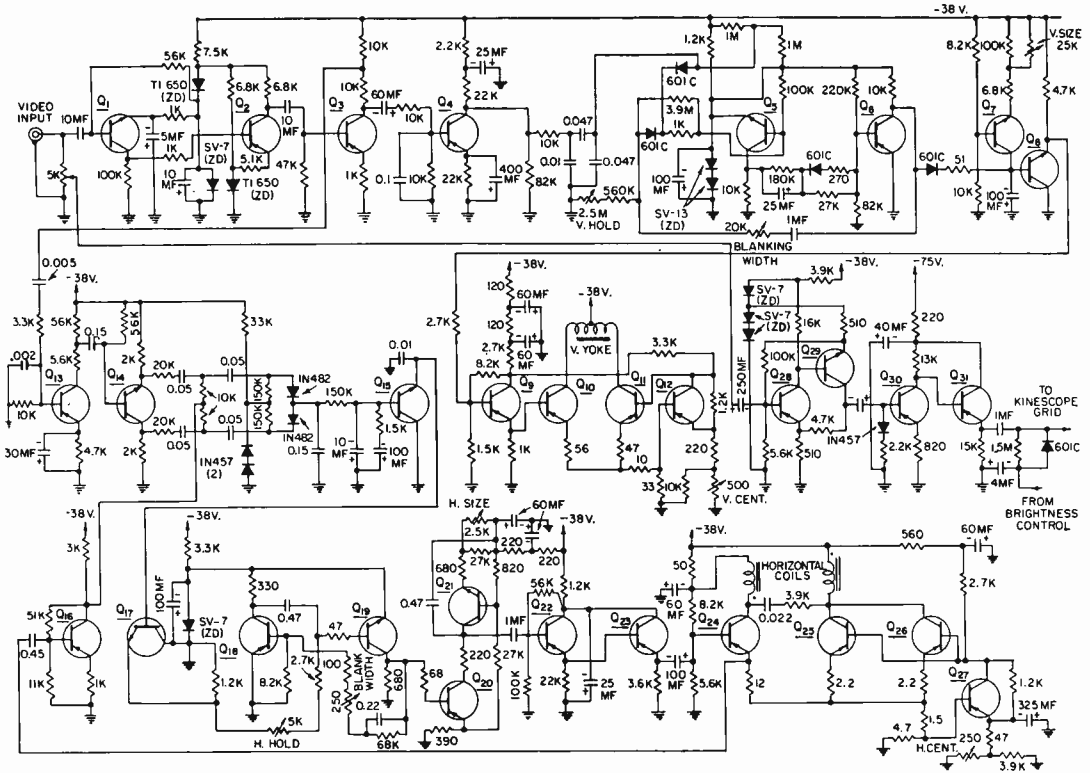

NOTES:

TRANSISTORS

2N585 - $Q_1, Q_7, Q_8, Q_{17}, Q_{19}, Q_{21}, Q_{29}$

2N404 - $Q_2, Q_3, Q_4, Q_6, Q_9, Q_{12}, Q_{13}, Q_{18}, Q_{20}, Q_{22}, Q_{23}, Q_{27}, Q_{28}$

2N335 - Q_5, Q_{15}

2N158 - $Q_{10}, Q_{11}, Q_{24}, Q_{25}, Q_{26}$

2N388 - Q_{14}

2N586 - Q_{16}

2N247 - Q_{30}, Q_{31}, Selected for $E_c = 75V$

Fig. 13—Simplified schematic diagram of slow-scan video monitor circuit.

The low frame rate introduces two problems. First, accurate reproduction of the vertical sawtooth virtually requires d-c amplification. Second, it is difficult, if not impossible, to filter out the 1-cycle component of the power supply by conventional means. Hence, wherever a 1-cycle component exists at high amplitudes, certain circuit precautions must be observed. The vertical-deflection amplifier is a case in point. It is a direct-coupled push-pull amplifier. The push-pull configuration greatly reduces the 1-cycle component of current drawn from the power supply.

The sawtooth from Q8 is applied to Q9, another emitter follower. From Q9 it is applied to Q10. The collector load of Q10 is half of the center-tapped vertical-deflection yoke winding. The emitter currents of both Q10 and Q11 are sampled by a common 33-ohm resistor. Q11 drives the opposite side of the center-tapped yoke winding. Any unbalance in the currents flowing in Q10 and Q11 will cause a signal to appear across the 33-ohm resistor connected to both emitters. This is amplified by Q12 and fed back to Q11 in the correct polarity to reduce the unbalance. The deflection yoke used in the monitor is unconventional. It is wound like a motor stator on a laminated core and the vertical winding actually consists of four identical windings connected in series. Q10 drives two of these windings, one on each side of the yoke, while Q11 does likewise. This arrangement ensures good coupling between the two sides of the push-pull system. The horizontal windings are similarly arranged.

The horizontal circuit is more complex. Horizontal sync from Q13 is applied to Q14, a phase splitter, which drives a balanced phase detector. A reference sawtooth is also supplied to the phase detector from the horizontal-deflection system via Q16. The d-c output of the phase detector is applied, via transistors Q15 and Q17, to the horizontal oscillator to control its frequency. Q15 and Q17 are connected as cascaded emitter followers in order to raise the impedance seen by the phase-detector output to the highest practically realizable value.

The horizontal oscillator is composed of transistors Q18 and Q19 which are connected to a multivibrator circuit similar to other oscillators previously described. The phase-detector output varies the voltage applied to one end of the horizontal-hold control to keep the oscillator locked to the incoming signal.

Pulses from the horizontal oscillator are applied to a sawtooth generator comprising transistors Q20 and Q21. Q20 discharges a 0.47-microfarad capacitor during the flyback. The capacitor then recharges through constant-current transistor Q21. The sawtooth is fed via a pair of cascaded emitter followers, Q22 and Q23, to the horizontal-output stage which comprises transistors Q24 through Q28.

The horizontal-output stage is basically similar to the vertical-output stage. Again, a push-pull type of circuit is used. There is an important difference, however, in the nature of the load impedance for the higher horizontal frequency. As might be expected, the yoke looks inductive, with the result that a large pulse is generated across it during the flyback. Although the working of the circuit is very similar to that of the vertical output circuit, the dissipation of the transistors driving one-half of the yoke is much higher than that of the transistor driving the other half, due to the assymetry of the signal caused by yoke inductance. For this reason two transistors, Q25 and Q26, are used in parallel to drive one side. Q28 is the error-detecting amplifier. Again, good coupling between the horizontal-yoke windings is required, so that the actual winding is composed of four sections of which two are wound on each side of the yoke.

Power for the monitor is supplied by an a-c operated unit which provides regulated voltages to all critical points. Voltage regulation has proven important because of the low frame rate and because of the unstable power supply from the gasoline-driven generator used in the field. A combination of transistor and tube circuitry is used in the power supply.

Operation

Stratoscope I made a total of four flights during the summer of 1959. In all of them, the television equipment functioned satisfactorily, enabling the telescope to be focused well within the theoretical focus tolerance. It also greatly assisted the astronomer in charge in finding sunspots and other areas of interest on the surface of the sun.

On the second flight, for example, over four hundred photographs were taken by the balloon camera which are superior in quality to any similar photographs ever taken before by any telescope. The use of the television system vastly increased the yield of useful pictures, one of which is shown in Figure 14. The large circular sunspot visible in the photograph is about 5000 miles in diameter.

A number of minor modifications were made to the system during this period. After the first flight, for example, the optical magnification in the path between the telescope and the television camera was reduced somewhat so that the television system "saw" a larger field. This increased the ease with which sunspots could be located and provided more light for the Vidicon. For the last two flights, an improved vertical-sawtooth generator was used in the camera in order to reduce a thermally produced change in the vertical deflection observed on Flights 1 and 2. This change would not have been necessary

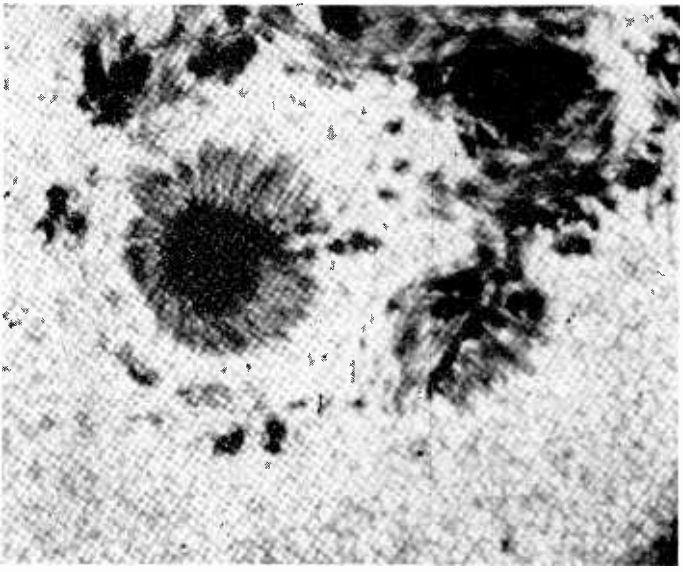

Fig. 14—Sunspots photographed by Stratoscope I at 11:01 AM, C.D.T., August 11, 1959.

if the vertical-deflection circuit had originally been installed in the camera, but when the electronic vertical sweep was substituted for the potentiometer it had to be located externally for space reasons. It thus was subjected to a lower temperature than the interior of the camera.

ACKNOWLEDGMENT

Project Stratoscope was sponsored by the Office of Naval Research and the National Science Foundation. It was under the direction of Dr. Martin Schwarzchild of Princeton University. It is a pleasure to acknowledge the interest and direction of Dr. V. K. Zworykin and the assistance of many members of the RCA Laboratories Staff. Some of the basic slow-scan circuitry was derived from designs of E. A. Boyd and R. Davidson. O. M. Woodward, J. Epstein, and W. Maxwell also rendered invaluable assistance in the design and testing of the antenna and diplexer.

HIGH-VOLTAGE ELECTRON EXTRACTION FROM AN ARC-DISCHARGE PLASMA*†

By

KARL G. HERNQVIST

RCA Laboratories,
Princeton, N. J.

Summary—A method of using an arc-discharge plasma as an electron source for producing very high current density electron beams in vacuum is described. Electrons are extracted from a magnetically confined mercury-pool arc. A theoretical upper limit for the vapor pressure in the extraction region is derived, and results of tests on an electrode configuration satisfying this pressure requirement are given. For a certain beam voltage, instabilities occur in the extracted current above a value of current density which can be directly related to the 3/2-power law for the electron sheath in the extraction region. Stable beams having current densities of 30 amperes/cm² have been obtained for beam voltages of 1000 volts.

INTRODUCTION

IN ATTEMPTS to extend the useful range of microwave generators into the millimeter wavelength region, the demand for super high current density electron beams *in vacuo* has been ever increasing.[1] This demand arises because, for millimeter waves, the interaction area between beam and microwave field becomes small and because the high circuit losses necessitate high starting currents to produce oscillations. At present, thermionic emitters[2] are limited to emission current densities of the order of 10 amperes/cm². It is well known, however, that the plasmas of some arc discharges have current-carrying capabilities as high as thousands of amperes per square centimeter. Used as an electron source, such a plasma should be capable of delivering extremely high current density electron beams.

There are two basic problems associated with the use of this type of electron source. One is that of maintaining the proper pressure conditions. Although the pressure in the discharge region is high, a reasonably good vacuum must be maintained in the region through which the extracted electron beam passes. Thus, some scheme for

† This work was supported by a Signal Corps contract.
* Manuscript received March 31, 1960.

[1] Arthur Karp, "Backward-Wave Oscillator Experiments at 100 to 200 Kilomegacycles," *Proc. I.R.E.*, Vol. 45, p. 496, April, 1957.

[2] R. Levi, "The Impregnated Cathode," *Philips Technical Review*, Vol. 19, p. 186, December, 1957.

maintaining a differential pressure is required. The other problem is that of preventing instabilities in the process of electron extraction from the plasma. This paper describes an arrangement in which satisfactory solutions to these problems have been found. Here, the edge of the plasma of a magnetically confined mercury-pool arc discharge is situated at the cathode plane of a conventional electron gun. Stable electron beams at current densities up to 30 amperes/cm^2 have been obtained. It is believed that considerably higher current densities can be obtained at higher arc currents.

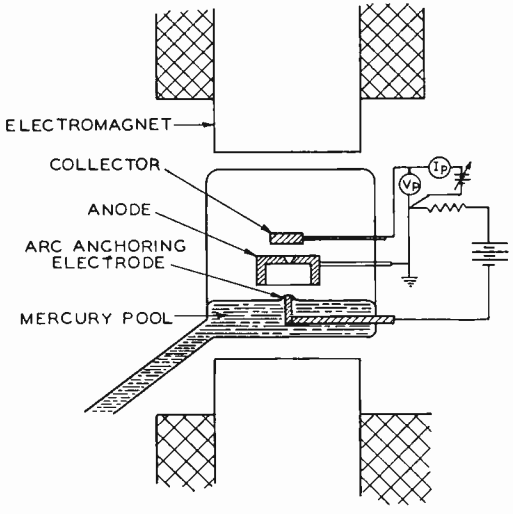

Fig. 1—Tube for studies of a magnetically confined arc.

Studies of a Magnetically Confined Arc Discharge

The type of arc discharge used for electron extraction studies is a mercury-pool arc having an anchored cathode spot.[3] Figure 1 shows the basic electrode geometry. An arc-anchoring electrode consisting of a 0.050-inch-diameter nickel rod, wetted with mercury, protrudes through the surface of a pool of mercury. A 0.013-inch-diameter hole is drilled in the stainless-steel anode directly above the anchoring electrode, and a collector is placed behind the anode. An electromagnet

[3] M. J. Druyvesteyn and F. M. Penning, "The Mechanism of Electrical Discharges in Gases of Low Pressure," *Review of Modern Physics*, Vol. 12, p. 87, April, 1940.

provides a variable magnetic field (up to 4000 gausses) oriented parallel to the tube axis.

Figure 1 also shows the test circuit for measuring the current density and electron temperature of the arc. When a d-c arc is fired in the tube, the arc cathode spot anchors at the anchoring electrode. In the tests, the d-c arc current was about 6 amperes and the arc drop about 10 volts. When the axial magnetic field is applied (~3000 gausses), the arc plasma takes the appearance of a bright narrow

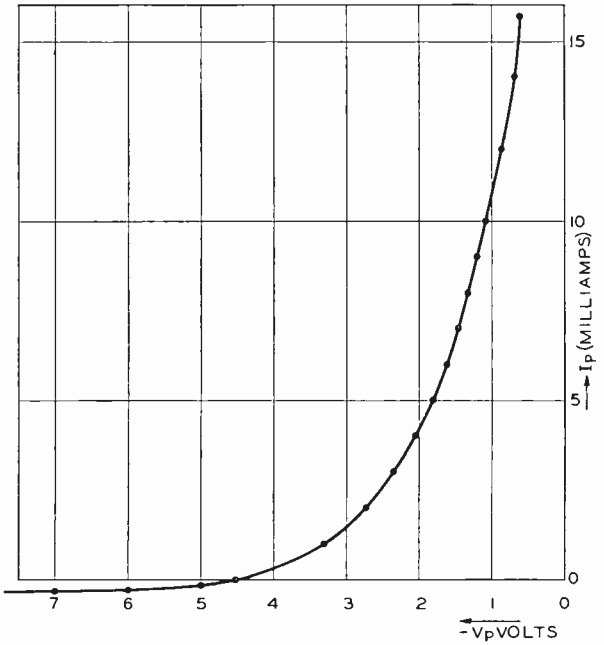

Fig. 2—Collector current I_p versus collector voltage V_p.

column extending from the cathode to the anode. The diameter of the arc column is approximately equal to that of the anchoring electrode, and part of the plasma extends through the hole in the anode to the collector. The potential of the collector with respect to the anode was varied from negative to positive values and the current to the collector recorded. Both d-c and a-c tests were made. The curve of current versus voltage is of course the probe characteristic of the plasma penetrating through the hole in the anode. Figure 2 shows the curve for voltage V_p between collector and anode versus collector current I_p obtained by point-by-point measurements. The curve yields

an electron plasma temperature of approximately 10,000°K. An oscilloscope picture of I_p versus V_p is shown in Figure 3. Here V_p was varied at 60 cps. The maximum electron-current density obtained was about 100 amperes/cm^2. It is seen that the current is quite unstable when V_p becomes positive. When V_p exceeds the ionization potential of the mercury vapor (~10 volts), excessive ionization sets in in the region between the anode and collector.

This experiment indicates that current densities larger than 100 amperes/cm^2 may easily be obtained in this discharge. For electron extraction, it is necessary to maintain a good vacuum in the region above the anode.

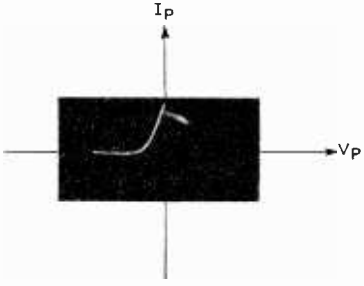

Fig. 3—Oscillogram showing I_p versus V_p.

Principle of Operation of the Electron Extractor

The electrode structure considered for extracting electrons from a magnetically confined mercury-pool arc discharge is shown schematically in Figure 4. Electrons are extracted from the arc plasma by applying a positive potential between the plasma and the electron extractor, thus separating electrons from the plasma ions. An arc discharge is operated in a discharge chamber between the cathode C and anode A_1. The arc discharge is confined in a narrow column by applying a magnetic field, parallel to the cathode, at the anode axis. Part of the plasma diffuses through the aperture in A_1, into a high-vacuum chamber. Figure 4 also shows the potential distribution along the tube axis with the potential at A_1, as a reference level. The electrodes G_1 to G_4 all have apertures lined up with the anode aperture. The plasma potential is very nearly equal to the anode potential. G_1 is operated at plasma potential, and G_2, the accelerator, is operated at a high potential. G_3 and G_4 are operated at a potential slightly nega-

tive with respect to G_2 and the collector A_2 in order to ensure ion trapping[4] in the drift space between G_3 and G_4.

The plasma extends to the plane P. For space-charge-limited current, the distance x in centimeters between G_2 and P is determined by the 3/2 power law

$$x^2 = 2.33 \times 10^{-6} \frac{V_a^{3/2}}{j_e} \tag{1}$$

where V_a is the acceleration voltage and j_e is the electron current density in amperes/cm^2.

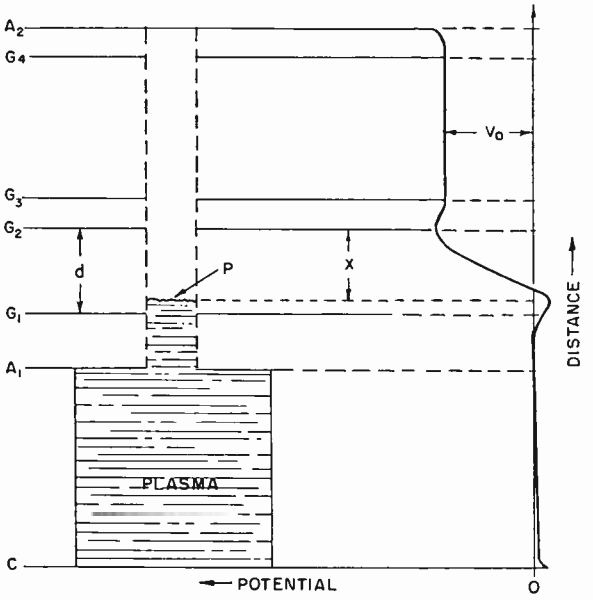

Fig. 4—Electrode structure and potential distribution for high-voltage electron-extraction studies.

Pressure Requirements for High-Voltage Electron Extraction

The basic technological problem of electron extraction from a plasma is that of maintaining the pressure differential necessary for acceleration of extracted electrons. While the pressure in the dis-

[4] L. M. Field, K. Spangenberg, and R. Helm, "Control of Electron-Beam Dispersion at High Vacuum by Ions," *Electrical Communication*, Vol. 24, p. 108, March, 1947.

charge region may be of the order of 10^{-1} mm of Hg, the pressure in the electron-beam region must be several orders of magnitude lower to avoid excessive ionization and scattering of the electron beam.

Of particular importance is the effect of the positive ions in the acceleration region (between G_1 and G_2). Ions formed in this region will neutralize the negative space charge of the electrons and increase the current demand from the plasma. This increase in electron current will result in formation of additional ions and so on. As a result, the electron-extraction process will become unstable unless the pressure in the acceleration region is kept below a certain value. The ions generated in the drift space (between G_3 and G_4) will be trapped and need not be considered.

To find an approximate value for the upper pressure limit for stable electron extraction, it will be assumed that the ions formed throughout the space between the plane P and the accelerator G_2 can, for purposes of analysis, be replaced by a small ion current injected opposite to the electron flow at the plane G_2. This artifice is valid when the ion-generation rate is low, so that ions do not accumulate in the acceleration region but are swiftly swept out at the plane P. The equivalent ion current is

$$j_p = j_e s_o p x, \tag{2}$$

where s_o is the number of ions formed per electron per centimeter path at a pressure of 1 mm of Hg, and p is the pressure, in mm of Hg. It must be remembered that s_o depends on the electron velocity and, thus, varies through the acceleration region. To find the approximate upper pressure limit, however, the maximum value of s_o may be used ($s_{o\max} = 20$ for mercury vapor[5] and an electron energy of about 80 volts).

This small injected ion current will cause a slight increase Δj_e in the electron current, which is given by[6]

$$\Delta j_e = 0.378 \sqrt{\frac{m_p}{m_e}}\, j_p \tag{3}$$

where m_p is the ion mass and m_e the electron mass. This increase in electron current will increase the ion current, and so on. Considering

[5] M. Knoll, F. Ollendorff, and R. Rompe, *Gasentladungstabellen*, J. Springer, Berlin, 1935, p. 66.

[6] I. Langmuir, "The Interaction of Electron and Positive Ion Space Charges in Cathode Sheaths," *The Physical Review*, Vol. 33, p. 954, June, 1929.

the cumulative effects of small increments of Δj_e, the total electron current j_{et} may be written as

$$j_{et} = j_e \left[1 + 0.378 s_o p x \sqrt{\frac{m_p}{m_e}} + \left(0.378 s_o p x \sqrt{\frac{m_p}{m_e}} \right)^2 + \cdots \right],$$

or

$$j_{et} = \frac{j_e}{1 - 0.378 s_o p x \sqrt{\frac{m_p}{m_e}}}. \tag{4}$$

For stability of electron extraction, $0.378 s_o p x \sqrt{\frac{m_p}{m_e}} \ll 1$,

and therefore

$$p \ll \frac{1}{0.378 s_o x} \sqrt{\frac{m_e}{m_p}}. \tag{5}$$

For mercury, and assuming $x = 1$ mm, Equation (5) yields $p \ll 2.2 \times 10^{-3}$ mm of Hg. This requirement can be fulfilled by keeping the walls surrounding the acceleration region at a temperature of about 0°C, which corresponds to a vapor pressure for mercury of about 2.5×10^{-4} mm.

In addition to the background pressure, consideration must be given to the density of the atomic beam emerging from the aperture in anode A_1. This atomic beam is, of course, present even when the background pressure in the electron-extraction region is zero. The pressure in the electron-extraction region is given by[7]

$$p_B = p_D \times \frac{1.13}{1.33} \frac{1}{4\pi} \frac{A_B}{l_0^2} \tag{6}$$

where A_B is the area of the beam cross section, l_0 is the distance between A_1 and the plane P (Figure 4), and p_D is the vapor pressure in the arc-discharge region. As an example, assume $p_D = 0.1$ mm of Hg, $p_B = 2 \times 10^{-4}$ mm of Hg, and a beam diameter of 0.013 inch. Then, Equation (6) yields $l_0 = 1.7$ mm. Thus, by keeping the acceleration region sufficiently far away from A_1, the pressure requirements can be met.

[7] N. F. Ramsey, *Molecular Beams*, Oxford Clarendon Press, 1956.

Experimental Tube

Analysis of the pressure requirements for high-voltage electron extraction indicates that the mercury-vapor pressure in the region where the electrons are accelerated must not exceed 10^{-3} mm. Since the pressure in the arc-discharge region (between the anode and cathode of the arc) is of necessity larger than this value, the following must be provided: (1) some system of differential pumping to provide a low pressure in the acceleration region, (2) the main arc-discharge region must be separated from the acceleration region by a minimum distance to allow the density of the neutral atomic beam projected into the high-vacuum region to decrease sufficiently, and (3) part of the arc-discharge plasma must be allowed to diffuse into the high-vacuum region to the cathode plane of the electron gun.

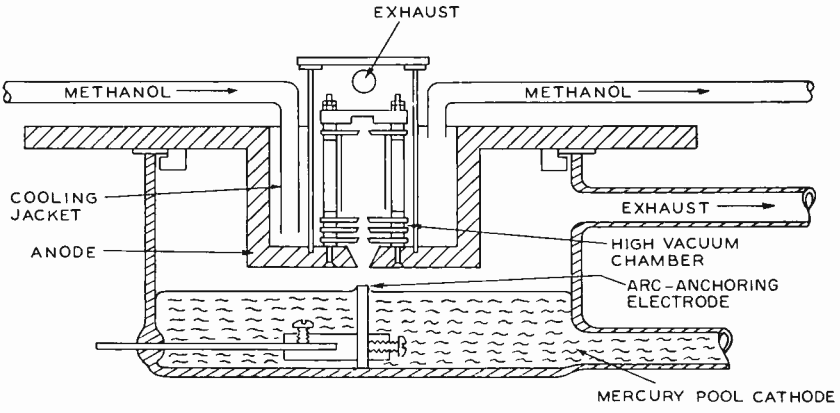

Fig. 5—Tube for studies of high-voltage electron extraction.

A tube geometry satisfying these conditions is shown schematically in Figure 5. It consists of two continuously pumped chambers separated by a stainless steel wall. The high-vacuum chamber protrudes into the discharge chamber. The two chambers are connected through the 0.013-inch-diameter hole in the wall of the high-vacuum chamber which also serves as the anode for the arc. The main arc is operated in the lower chamber. The arc-anchoring-electrode, located in the mercury pool cathode immediately underneath the 0.013-inch-diameter hole in the anode, is a 0.040-inch-diameter nickel rod well wetted with mercury. The cathode-to-anode distance is about 0.100 inch. This relatively short cathode-to-anode distance is necessary in order to avoid the formation of a positive anode drop which would prevent ion diffusion into the vacuum chamber.

The cooling liquid, which circulates through the jacket surrounding the high-vacuum chamber, is methanol, and its temperature is reduced by passing it through a copper coil submerged in a dry-ice–acetone solution. The stabilizer electrode G_1 is placed immediately above the anode and is run at a potential equal to or slightly negative with respect to A_1 in order to ensure stability. G_2 is the accelerator. G_3 and G_4 shield the drift space and are run slightly negative with respect to G_2 to ensure ion trapping for space-charge neutralization of the electron beam. Finally, A_2 is the collector. The electrodes G_1,

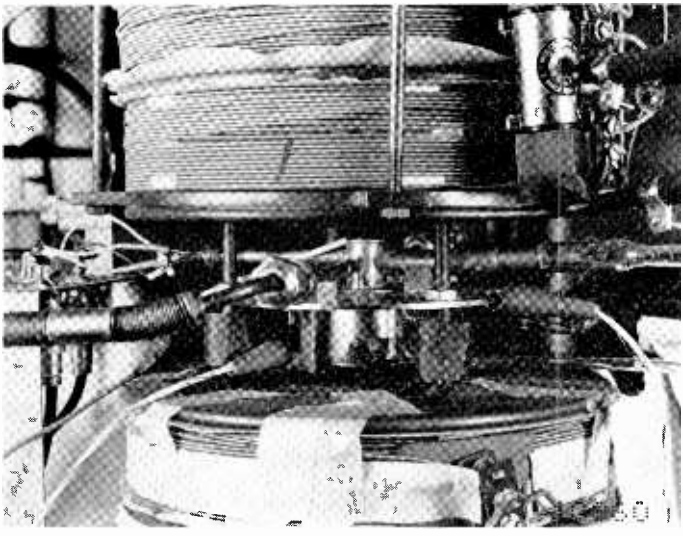

Fig. 6—Photograph of tube shown in Figure 5.

G_2, and G_3 have 0.013-inch-diameter apertures. G_4 has a 0.010-inch-diameter aperture. An electromagnet provides a variable magnetic field (up to 3500 gausses) oriented parallel to the tube axis. Figure 6 is a photograph of the tube.

Test Circuit

The studies of electron extraction were performed using a pulse technique. This was done for several reasons. First, the tube is demountable and does not allow baking. The use of low-duty-cycle pulse operation cuts down the heat dissipation at the electrodes and prevents excessive release of gas. Second, at a current density of 30 amperes/cm^2 and a beam voltage of 1000 volts, the energy input to

the collector for a d-c beam is 30 kilowatts/cm². This high density of energy input cannot be accepted by any electrode material without local fusing except at low duty cycles. Thus, a scheme for beam diffusing at the collector side would be called for. It should be emphasized that the use of pulse techniques is a convenience and does not mean that the electron source is incapable of supplying a d-c beam. In the tests, the pulse length used was usually about 50 microseconds at a repetition rate of 40 cps. There was no slackening of emission during the pulse.

The circuit used for studies of high-voltage electron extraction is shown schematically in Figure 7. In order to display the currents

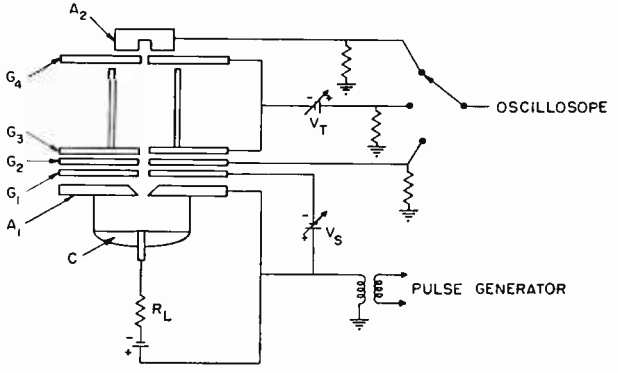

Fig. 7—Circuit for measurements on high-voltage electron extraction.

flowing to the various gun electrodes on an oscilloscope, it was necessary to pulse the arc discharge supply negative. All voltages are referred to the arc anode A_1. The stabilizer G_1 is operated at a negative potential V_s. The ion-trapping electrodes, G_3 and G_4, are operated negative with respect to G_2 and A_2. The gun electrodes are connected to ground through small resistors allowing current display on an oscilloscope.

In the tests, the arc current was about 5 amperes delivered through the current-limiting register R_L from a 50-volt d-c supply. The acceleration voltage was in the range 250 to 1000 volts. The effect of the ion-trapping voltage V_T was demonstrated. For best results, V_T was in the range —20 to —40 volts. To prove that a true high-velocity electron beam was achieved, measurements of collector current I_{A_2} versus collector voltage V_{A_2} were made. If, instead of a beam, a second plasma had developed, I_{A_2} would have gone to zero if A_2 were only a few volts negative with respect to G_4. Figure 8 shows the re-

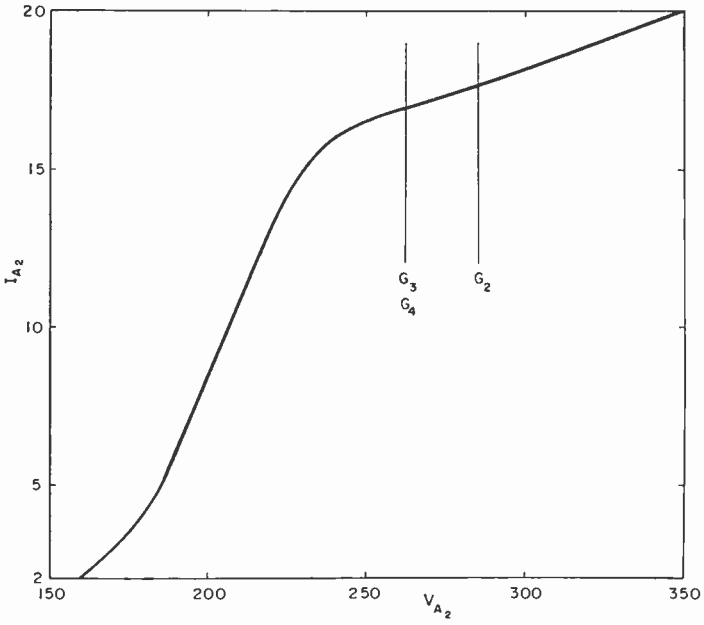

Fig. 8—Collector current I_{A_2} versus collector voltage V_{A_2}.

tarding voltage characteristic when V_{G_2} is 285 volts and V_{G_3} and V_{G_4} are 262.5 volts. It is seen that the collector current first decreases appreciably when A_2 is made more than 30 volts negative with respect to G_4. The current is transferred to G_4 due to secondary emission

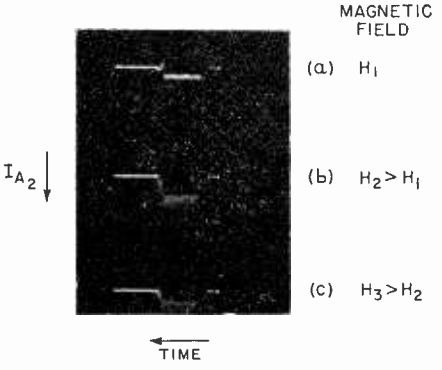

Fig. 9—Oscillograms of current flowing to collector A_2 at various magnetic field strengths.

from A_2 and/or to cancelled ion-trapping effect. The measurements shown in Figure 8, therefore, verify that a true high-velocity electron beam was obtained.

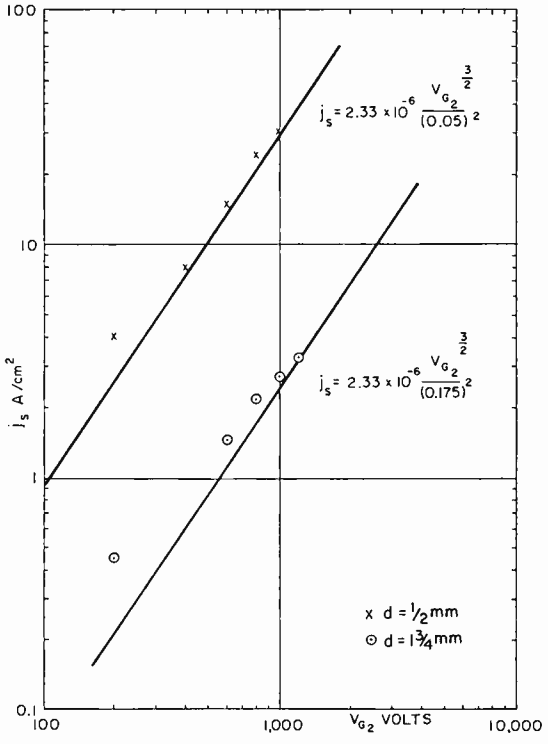

Fig. 10—Diagram showing maximum stable current density for electron extraction as a function of beam voltage.

Stability of Electron Extraction

The extracted current was found to be stable only below a certain critical value of current density. Above this current density, violent fluctuations occur in the current. This effect is demonstrated in Figure 9, which is an oscillogram of the current flowing to A_2. The current is varied by changing the strength of the magnetic field confining the arc discharge. Figure 9a shows the current at the threshold of instabilities. In Figure 9b, taken at a slightly higher current, the instabilities cause about 25 per cent modulation of the extracted current. In Figure 9c, at a still higher current level, almost 100 per cent modulation occurs.

Measurements of the current at the threshold for instabilities as a function of beam voltage indicated a relation

$$j_s = 2.33 \times 10^{-6} \frac{V_{G_2}^{3/2}}{d^2}, \tag{7}$$

where j_s is the maximum stable current density, and d is the distance between the stabilizer G_1 and the accelerator G_2. Measurements of

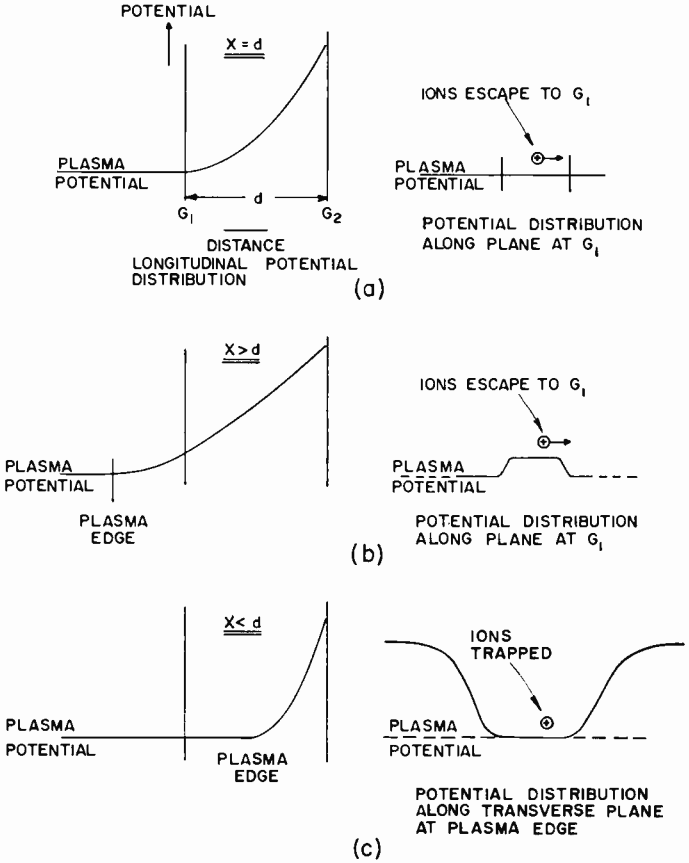

Fig. 11—Longitudinal and transverse potential distributions for different sheath thicknesses.

the current at the threshold for instabilities as a function of accelerator voltage were made for two structures, one in which $d = \frac{1}{2}$ millimeter and one in which $d = 1\frac{3}{4}$ millimeter. The results are shown in Figure

10; a beam diameter of ¼ millimeter was used in computing the current density. Figure 10 also shows j_s as calculated from Equation (7). It is seen that the measurements agree with Equation (7) quite well. These studies indicate that the thickness x of the space-charge sheath separating the plasma and the accelerator must not be less than the spacing between the stabilizer and the accelerator. The space-charge-sheath thickness x is given by the 3/2 power law, Equation (1).

The reason for this behavior may be understood by referring to Figure 11. Figure 11a shows the longitudinal and transverse potential distributions for the case $x = d$. Here, ions at the plasma edge can escape to G_1. In Figure 11b, the case for $x > d$, ions are stopped at the plasma edge but may escape sideways to G_1. In Figure 11c, the plasma edge is located between G_1 and G_2. Here, ions are trapped and can only be collected at G_1 by being reflected at the plasma edge. This is the condition that results in instabilities. Presumably, as ions accumulate in the trap, the current rises until the current-carrying capability of the plasma is exceeded. A complicated set of potential readjustments may then take place which brings the current back to a low value. Such relaxation phenomena are quite common in gas discharge devices.

Conclusion

The condition for stability (Equation (7)) has been verified, and stable beams with current densities up to 30 amperes/cm^2 have been obtained at 1-kilowatt beam voltage. This current density points up the potentialities of the method, but does not indicate the limit of its ultimate capabilities.

ABSOLUTE SPECTRAL RESPONSE CHARACTERISTICS OF PHOTOSENSITIVE DEVICES*

By

R. W. Engstrom

RCA Electron Tube Division,
Lancaster, Pa.

Summary—*Data are presented comparing absolute response characteristics associated with the various commercial-type photocathodes. A tabulation is provided of luminous sensitivity, dark emission, and quantum efficiency typical of these photocathodes. Some similar data are presented for photoconductive devices.*

Introduction

SPECIFICATIONS of photoelectric devices are frequently quoted in terms of lumens. The industrial standard test source in the United States is a tungsten-filament lamp operated at a color temperature of 2870 degrees Kelvin. In many applications, however, it is necessary to know the output of photosensitive devices not in terms of lumens, but in terms of watts of radiant energy. Radiant-sensitivity values can be computed from luminous-sensitivity values provided the relative spectral-response characteristic of the photosensitive device and the spectral-emission characteristic of the standard lamp source are known.[1]

Thus, if $R(\lambda)$ is the normalized spectral-response characteristic of the photosensitive device as a function of wavelength, the radiant sensitivity σ of the device in amperes per watt at the wavelength of maximum sensitivity can be expressed as follows:

$$\sigma = \left[\frac{680 \int_0^\infty \bar{y}(\lambda) \cdot W(\lambda)\, d\lambda}{\int_0^\infty R(\lambda) \cdot W(\lambda)\, d\lambda} \right] s \qquad (1)$$

* Manuscript received February 5, 1960.

[1] R. W. Engstrom, "Calculation of Radiant Photoelectric Sensitivity from Luminous Sensitivity," *RCA Review*, Vol. 16, p. 116, March, 1955.

where s is the luminous sensitivity of the device in amperes per lumen, $W(\lambda)$ is the relative distribution of radiant energy from the standard lamp, and $\bar{y}(\lambda)$ is the relative sensitivity of the average human eye. The figure 680 denotes sensitivity of the eye at the wavelength of maximum sensitivity measured in lumens per watt. The quantity within the brackets of Equation (1) represents a conversion factor k, in lumens per watt, which relates s and σ for a particular photodetector. Thus, Equation (1) may be rewritten

$$\sigma = ks. \tag{2}$$

In a previous paper,[1] $W(\lambda)$ was approximated by the distribution of energy of a black-body at 2870° Kelvin. Planck's black-body function provides a good approximation of the true radiation of a tungsten-filament lamp in the range of visible sensitivity, but outside the visible range the approximation is less accurate because of variations in the emissivity of tungsten and in the transmission of the lamp envelope. In the present paper, the function $W(\lambda)$ is evaluated by use of tungsten emissivity data[2] and transmission data* for 0081 lime glass, which is typical of the bulbs used in test lamps. Figure 1 shows these functions together with the calculated spectral-emission function for the test lamp.

By use of $W(\lambda)$, as shown in Figure 1, together with the latest relative spectral-response data, conversion factors (k) have been calculated for a number of spectral-response characteristics. These conversion factors as well as other related data are given in Table I. Also given in Table I are typical data on dark emission for various photocathodes. Dark emission from the photocathodes varies widely even for a given tube type because of small differences in processing. Values quoted are typical in most cases of measurements made on multiplier phototubes.

From the data in Table I, a composite graph, shown in Figure 2, has been constructed showing spectral-response characteristics of photoemissive devices on an absolute scale. Radiant sensitivities (identified by S-designation) refer to the photocathode (including transmission losses of the envelope). The graph permits direct comparison of absolute sensitivities at all wavelengths, and in relation to

---

[2] J. C. DeVos, "A New Determination of the Emissivity of Tungsten Ribbon," *Physica*, Vol. 20, p. 690, October, 1954.

* Transmission data supplied through the courtesy of C. J. Parker of the Corning Glass Company, Corning, New York.

lines of constant quantum efficiency (100 per cent quantum efficiency $= \lambda/12{,}395$ amperes per watt).

Although the calculations of Table I and Figure 2 concern only spectral characteristics of photoemissive devices, the same principle can be used to relate luminous and radiant sensitivities of photocon-

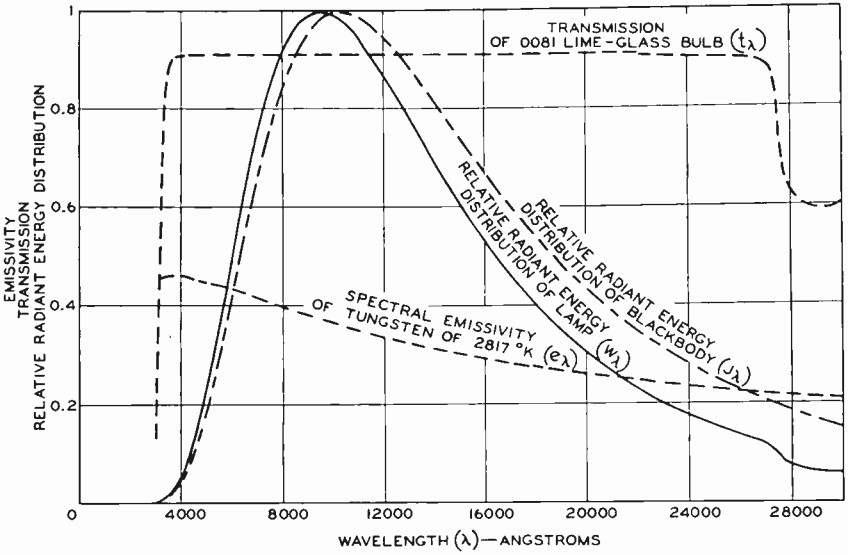

Fig. 1—Relative energy distribution of test lamp W_λ, and those factors involved in the calculation of W_λ. J_λ is the relative energy distribution of a blackbody at 2817 degrees Kelvin, the true temperature[3] of a tungsten lamp operating at a color temperature of 2870 degrees Kelvin. e_λ is the spectral emissivity of tungsten at 2817 degrees Kelvin, and t_λ is the relative transmission of 0081 lime-glass envelope of the test lamp. W_λ is proportional to $J_\lambda \cdot e_\lambda \cdot t_\lambda$.

ductive or photovoltaic devices. Table II is an abbreviated tabulation of properties of spectral-response characteristics relating to solid-state photodevices. Figure 3 shows relative spectral-response characteristics corresponding to the data of Table II.

Conclusion and Recommendations

Data have been presented in graphical and tabular form relating a number of photoelectric spectral-response characteristics on an

[3] G. A. Rutgers and J. C. DeVos, "Relation between Brightness, Temperature, True Temperature and Color Temperature of Tungsten," *Physica*, Vol. 20, p. 715, October, 1954.

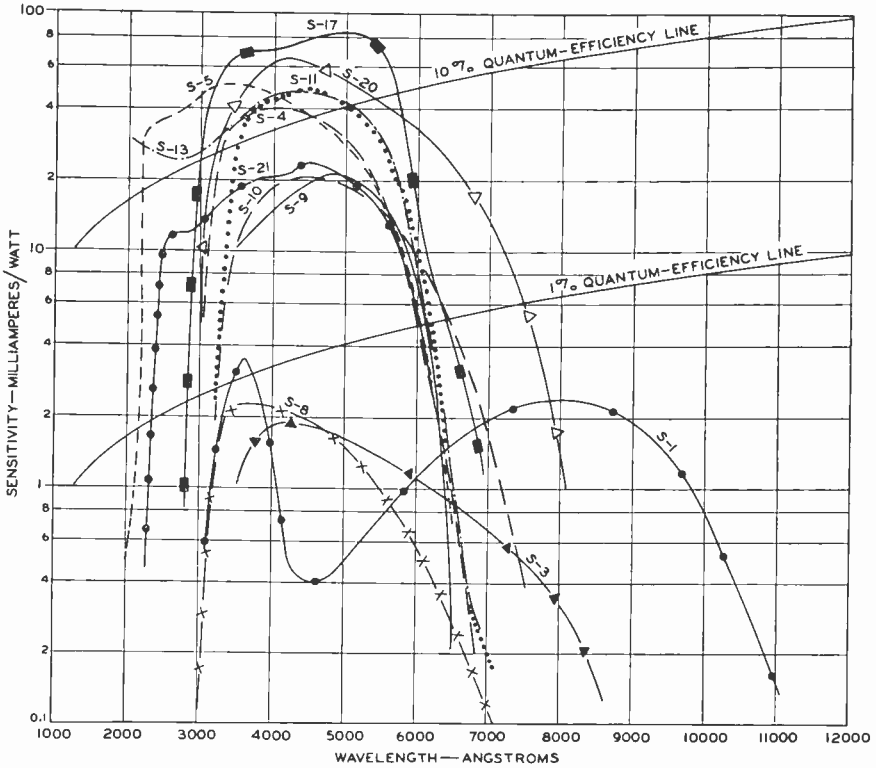

Fig. 2—Absolute spectral characteristics showing various photocathode responses as modified by the window transmission of the particular device. Lines of constant quantum efficiency are indicated. The S-5 curve shown is suspected to be in error (see footnote to Table I).

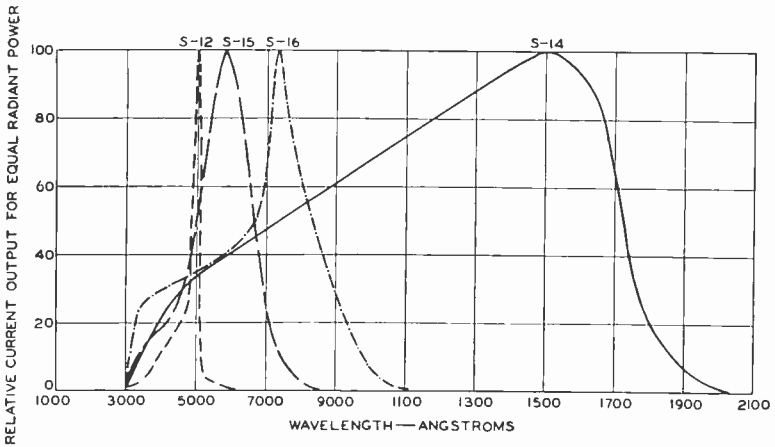

Fig. 3—Relative spectral responses for devices employing photoconductive sensors.

Table I—Spectral Responses for Devices with Related Photocathode Characteristic Values

Device S-Number[1]	Photocathode Type and Envelope	Conversion Factor[2] (k) (lumens/watt)	Typical Luminous Sensitivity[3] (s_{typ}) (μa/lumen)	Maximum Luminous Sensitivity[4] (s_{max}) (μa/lumen)	λ_{max} (angstroms)	Typical Radiant Sensitivity[5] (σ_{typ}) (ma/w)	Typical Quantum Efficiency[6] (per cent)	Typical Photocathode Dark Emission[7] at 25° C (amperes/cm^2)
S-1	Ag-O-Cs Lime-glass bulb	93.9	25	60	8000	2.35	0.36	$900. \times 10^{-15}$
S-3	Ag-O-Rb Lime-glass bulb	286	6.5	20	4200	1.86	0.55	——
S-4	Cs-Sb Lime-glass bulb	977	40	110	4000	39.1	12	0.2×10^{-15}
S-5†	Cs-Sb 9741 glass bulb	1252	40	80	3400	50.1†	18†	0.3×10^{-15}
S-8	Cs-Bi Lime-glass bulb	755	3	20	3650	2.26	0.77	0.13×10^{-15}
S-9	Cs-Sb Semi-Transparent, Lime-glass bulb	683	30	110	4800	20.5	5.3	——
S-10	Ag-Bi-O-Cs Semi-Transparent, Lime-glass bulb	508	40	100	4500	20.3	5.6	70×10^{-15}
S-11	Cs-Sb Semi-Transparent, Lime-glass bulb	804	60	110	4400	48.2	14	3×10^{-15}
S-13	Cs-Sb Semi-Transparent, Fused-silica bulb	795	60	80	4400	47.7	13	4×10^{-15}
S-17	Cs-Sb Lime-glass bulb, Reflecting substrate	664	125	160	4900	83	21	1.2×10^{-15}
S-19	Cs-Sb Fused-silica bulb	——*	40	70	——*	22*	11*	0.3×10^{-15}
S-20	Sb-K-Na-Cs (Multialkali) Semi-Transparent Lime-glass bulb	428	150	250	4200	64.2	18	0.3×10^{-15}
S-21	Cs-Sb Semi-Transparent, 9741 glass bulb	779	30	60	4400	23.4	6.6	——

[1] The S-number is the designation of the spectral-response characteristic of the device and includes the transmission of the device envelope.

[2] k is the conversion factor from amperes/lumen to amperes/watt at the wavelength of peak sensitivity.

[3] s is the luminous sensitivity for the photocathode for 2870°K color temperature test lamp. In the case of a multiplier phototube, output sensitivity is μs, where μ is the amplification of the multiplier phototube.

[4] Care must be used in converting s_{max} to a σ_{max} figure. Photocathodes having maximum lumen sensitivity frequently have more red sensitivity than normal, and the formula cannot be applied without re-evaluation of the spectral response for the particular maximum sensitivity device.

[5] σ is the radiant sensitivity at the wavelength of maximum response.

[6] 100 per cent quantum efficiency implies one photoelectron per incident quantum, or $e/h\nu = \lambda/12{,}395$, where λ is expressed in angstrom units. Quantum efficiency at λ_{max} is computed by comparing the radiant sensitivity at λ_{max} with the 100 per cent quantum efficiency expression above.

[7] Most of these data are obtained from multiplier phototube characteristics. For tubes capable of operating at very high gain factors, the dark emission at the photocathode is taken as the output dark current divided by the gain (or the equivalent minimum anode dark current input multiplied by cathode sensitivity). On tubes where other d-c dark-current sources are predominant, the dark *noise* figure may be used. In this case, if all the noise originates from the photocathode emission, it may be shown that the photocathode dark emission in amperes is approximately $0.4 \times 10^{18} \times$ (equivalent noise input in lumens times cathode sensitivity in amperes per lumen)[2]. The data shown are all given per unit area of the photocathode.

* No value for k or λ_{max} is given because the spectral response data are in question. The values quoted for σ and *typical quantum efficiency* are only typical of measurements made at the specific wavelength 2537 angstroms and not at the wavelength of peak sensitivity as for the other data.

† The S-5 spectral response is suspected to be in error. The data tabulated conform to the published curve, which is maximum at 3400 angstroms. Present indications are that the peak value should agree with that of the S-4 curve (4000 angstroms). Typical radiant sensitivity and quantum efficiency would then agree with those for S-4 response.

absolute scale. It is hoped that these data will prove useful in providing a quick comparison of the advantages of various photocathodes.

Calculations of absolute radiant-sensitivity figures from luminous-sensitivity figures included consideration of the transmission of the lamp bulb and of experimental values for tungsten emissivity. The significance of these corrections relative to previous calculations,[1] which assumed a black-body equivalence for the test lamp, can be seen in the difference of calculated k values. The previous values of k for

Table II

Device S-Number	Photosensitive Material	Conversion Factor (k) (lumens/watt)	λ_{max} (angstroms)
S-12	CdS (Crystal)	4070	5020
S-14	Ge (p-n junction)	42.1	15000
S-15	CdS (Sintered)	352	5800
S-16	CdSe (Sintered)	160	7300

the S-1 and S-4 spectral characteristics were 89.1 and 1010 amperes per watt, respectively. The corresponding new values are 93.9 and 977 amperes per watt.

The procedure outlined in this paper is a simple method for computing absolute radiant-sensitivity figures from luminous-sensitivity data. It is recommended that the method at least be used as a check on other methods to ensure consistency. Luminous standards are common, simple, and readily maintained. Direct measurement of radiant sensitivity requires more elaborate instrumentation. For example, a radiant standard lamp may be used to calibrate a radiation thermocouple which, in turn, may be used to calibrate the radiation from a monochromator. Radiant sensitivities measured by means of a calibrated monochromatic source have been found to be in fairly good agreement with the calculated values shown in this paper.

A LOW-WATTAGE PLANAR CATHODE*

By

T. N. Chin†

Summary—*A new type of cathode assembly developed for use in electron-beam tubes, such as camera tubes, kinescopes and traveling-wave tubes is described, and a brief record of its development is given. The thermal losses in a cathode structure are analyzed. Both analytical and experimental evidence indicates that the conduction loss dominates over the radiation loss in oxide-coated cathodes. For a 6.3-volt heater, 0.6 watt of power input is adequate to maintain the emitting surface of the new type cathode at a temperature of 1050°K, as against 4 watts for a similar cathode of conventional construction.*

Introduction

THE THERMIONIC cathode of almost all cathode-ray tubes, as T. Soller[1] summarizes it, is a nickel cylinder or cup indirectly heated by an internal heater that is electrically insulated from the cathode by a ceramic covering. The emitting portion of the cathode is a small area, on the surface of the closed end of this cylinder, which is coated with barium and strontium oxides. The emitting surface is usually on a plane perpendicular to the axis of the cup. The input power to the heater is customarily 4 watts, and most heaters are designed for operation at 6.3 volts.

There are two principal reasons which make a reduction of the heater power desirable. First, power consumption may be an important consideration in certain applications of the tube, for instance, airborne equipment or portable sets. Second, the heat dissipation may become a major problem. In this case, the temperature increase may deteriorate the performance of elements in the tube or of components in the vicinity of the tube.

This paper describes a new and improved cathode structure suitable for production at low cost and large volume. The thermal losses of this cathode assembly are discussed and compared with the experimental results. It is demonstrated that the heater power can be reduced by a factor of six.

* Manuscript received January 6, 1960.

† Formerly, RCA Electron Tube Division, Lancaster, Pa., now, RCA Laboratories, Princeton, New Jersey.

[1] T. Soller, M. A. Starr, and G. E. Valley, Jr., *Cathode-Ray Tube Display*, McGraw-Hill Book Co., Inc., New York, 1948, p. 58.

Considerations of Heating Power for Thermionic Cathodes

In a vacuum tube, the heat loss from the cathode due to convection is very small and can be neglected. To maintain a constant cathode temperature, therefore, the heater power must supply the loss due to thermal radiation and heat conduction through the cathode supports. The heater power which must be supplied per cm^2 of the total cathode surface is called specific heater power, and low values of specific heater power indicate that the cathode assembly has good thermal efficiency.[2] It is clear that the most efficient cathode will have the smallest radiant emissivity and the lowest heat conduction loss.

The radiation loss from a surface of emissivity ϵ_1 at uniform absolute temperature T_1 to another surface of emissivity ϵ_2 at absolute temperature T_2 can be derived by applying Kirchoff's law,[3]

$$P = K\epsilon\,(T_1^4 - T_2^4), \tag{1}$$

where P is the radiated power in watts per cm^2, K is the Stefan–Boltzmann constant (5.73×10^{-12} watt per cm^2 per degree), and ϵ is the emissivity factor defined by

$$\epsilon = \frac{1}{\frac{1}{\epsilon_1} + \frac{1}{\epsilon_2} - 1}.$$

The radiant emissivity ϵ of the cathode depends upon the type and surface of the materials used, and on the density and particle size of the oxide coating. Variations in the radiant emissivity are not too great, the largest being 50 per cent. For oxide-coated cathodes, the thermal radiation loss depends more upon the cathode configuration than upon its radiant emissivity.

For a practical cathode structure, the cathode body is often partially enclosed, and a part of the thermal radiation is reflected back in the enclosed structure. It is rather difficult, therefore, to give an accurate estimate of the heat loss due to thermal radiation.

The heat loss through the cathode supports may be estimated according to the law of heat conduction. For a homogeneous solid the

---

[2] G. Herzman and P. S. Wagener, *The Oxide-Coated Cathode*, pp. 80-83, Chapman and Hall, Ltd., London, 1951.

[3] Max Jakob, *Heat Transfer*, Vol. II, p. 3, John Wiley and Sons, Inc., New York, 1957.

heat-flow equation[4] in the steady state can be written:

$$Q = \sigma A \frac{dT}{dz} \tag{2}$$

where Q is the rate of heat flow at a point in calories per second, z denotes the coordinate units in the direction of heat flow in centimeters, dT/dz is the temperature gradient in the direction of the heat flow, A is the cross-sectional area in cm^2 normal to the direction of heat flow, and σ is the thermal conductivity of the material.

For the heat flow where the thermal-current flow Q is the same through the whole circuit, it is more convenient to deal with Equation (2) in the form

$$\frac{Q}{\sigma}\int_{z_1}^{z_2}\frac{dz}{A} = -\int_{T_1}^{T_2} dT. \tag{3}$$

In analyzing the thermal circuit, the extent of heat flow may be represented by the factor

$$\frac{1}{\sigma}\int_{z_1}^{z_2}\frac{dz}{A}, \tag{4}$$

which is often called the thermal resistance of a particular body.

Fortunately, although heat radiation and conduction occur together, one or the other often dominates in practical cases. Therefore, separate laws governing each kind of heat transfer may be used. Also, superposition of these laws is often possible.

Description of Cathode Assembly

The cathode assembly for the ½-inch Vidicon tube is shown in Figure 1. The cathode unit consists of four parts—cup, sleeve, support, and shield. Since the planar structure described here is fabricated of concentric self-jigging parts, it can readily be assembled in a few steps. This cathode assembly is simple to manufacture and should be suitable for production at a low cost.

In this arrangement the cathode support will compensate somewhat for the thermal expansion of the cathode sleeve. It is intended to

[4] Max Jakob, *Heat Transfer*, Vol. I, p. 9, John Wiley and Sons, Inc., New York, 1949.

maintain the emitting surface of the cathode substantially fixed in position not only when the cathode is cold but also when it is hot. The cathode support used in this structure acts as a heat shield and provides a long thermal conduction path. The heater power is further reduced by using materials of low thermal conductivity such as nickel-cobalt-iron alloy.

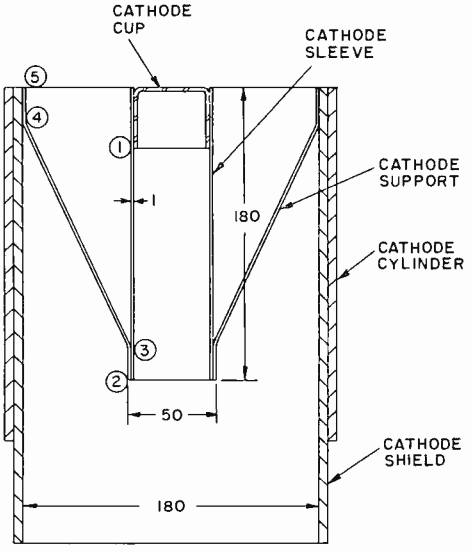

Fig. 1—A cathode assembly as used in developmental half-inch Vidicon (all dimensions are in mils).

Thermal Losses in a Cathode Assembly

For an oxide-coated cathode, the operating temperature usually ranges from 1000 to 1100°K. In the following computation, the cathode cup is assumed to be at 1050°K and the cathode shield at 293°K (room temperature).

First, the conduction loss alone in this structure is computed. The conduction path as shown in Figure 1 is divided into four sections, 1-2, 2-3, 3-4, and 4-5. The last point denotes the joint of cathode support and the cathode shield. The thermal contact resistances between the cathode cup and sleeve and between the cathode sleeve and support are neglected.

All four sections of the conduction path are composed of the same nickel-cobalt-iron alloy with a thermal conductivity of 0.19 watt/cm/°K; the thermal resistance of each section is given in Table

I. The total conduction loss, as calculated from Equation (3), amounts to 0.32 watt.

Next, the thermal radiation from different parts of the cathode assembly is estimated. For cathode coatings of normal thickness sprayed on nickel cores, the mean value[2] of the total radiant emissivity is approximately 0.3. Although the emissivity[5] for Kovar* varies from 0.05 to 0.1 in this temperature range, a mean value of 0.075 is used. The temperature of the cathode cup is considered uniform; between the cup and the end of the cathode support the temperature drops off gradually in proportion to the thermal resistances. The power loss due to thermal radiation from the cathode cup, side wall, and cathode sleeve are 0.022, 0.027, and 0.059 watt, respectively.

Table I — Thermal Resistance in the Conduction Path

Section	Thermal Resistance (°K/watt)
1-2	1790
2-3	128
3-4	400
4-5	35
Total	2353

As mentioned before, part of this radiant energy may be reflected back to the cathode. If all of this radiation is not recovered, the total radiant power may amount to 0.108 watt. In this conservative estimate, the cathode structure may reach a total heat loss of 0.44 watt.

Experimental Results

For the cathode assemblies in the initial tests, 0.5 to 0.8 watt of heater power was required for a cathode temperature in the range of 1050 to 1100°K. Some data were obtained on the variations of the cathode assembly. The oxide coating sprayed on the cathode cup was prepared in the same manner in each case, and the same type of heater was used in all test assemblies. The variations made during the development were as follows:

---

* Registered trade mark.

[5] Max Jakob, *Heat Transfer*, Vol. I, p. 125, John Wiley and Sons, Inc., New York, 1949.

A. For Kovar cathode sleeve,
   1. Use of .001-inch wall thickness seamless tubing.
   2. Use of .0005-inch thick wrapped and welded tubing.

B. For cathode support materials,
   1. Use of Kovar.
   2. Use of nickel.

Some of the test data obtained with these variations are shown in Figure 2. Test assembly #5 used 0.001-inch seamless tubing and

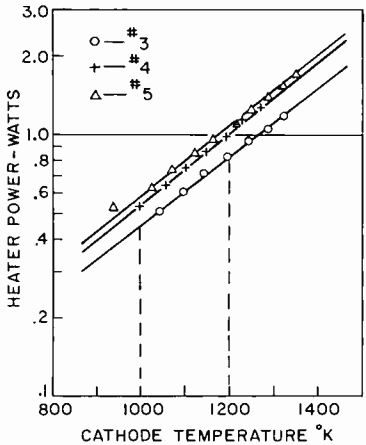

Fig. 2—Heater power as a function of cathode temperature.

a Kovar support. Test assembly #4 used a 0.0005-inch wrapped cathode sleeve and a nickel cathode support. Test assembly #3 used a 0.0005-inch wrapped cathode sleeve and a Kovar support. It can be seen that the variation of cathode sleeve causes the greatest change in the heater power required. This is expected from the estimate of heat losses.

The estimate made for the idealized conditions shows that the conduction loss exceeds the radiation loss. The evidence obtained from these tests seems to agree with this estimate. The discrepancy between the computed and experimental results may be explained by errors in the thickness measurement or the conductivity value used in the calculation.

As shown in Figure 2, the #3 assembly required the least heater power. For structural rigidity, seamless tubing was adapted for this

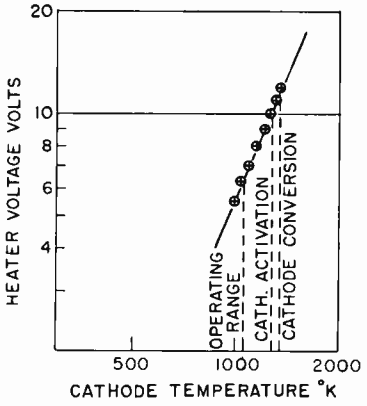

Fig. 3—Relationship between heater voltage and cathode temperature in developmental half-inch Vidicon.

design. A type of double-coil heater was, therefore, optimized for the structure using Kovar support and the 0.001-inch seamless tubing. The final results from three identical cathode assemblies are summarized in Figures 3, 4, and 5. In brief, the operating conditions are:

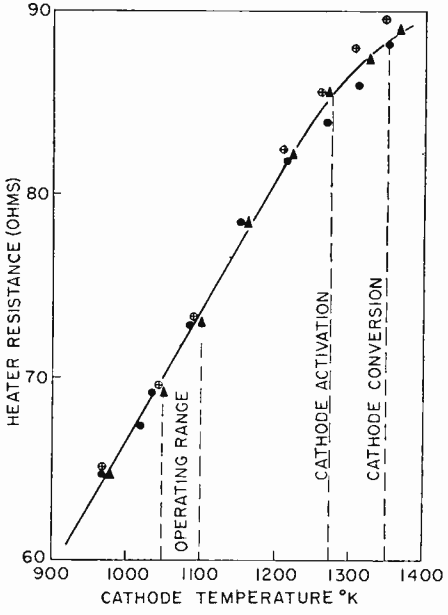

Fig. 4—Relationship between heater resistance and cathode temperature in developmental half-inch Vidicon.

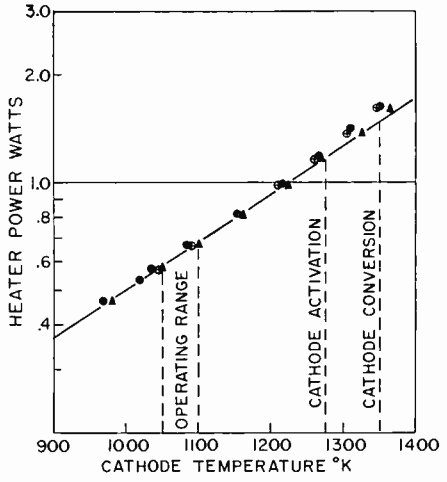

Fig. 5—Relationship between heater power and cathode temperature in developmental half-inch Vidicon.

cathode temperature	1050-1075	°K
heater voltage	6.3	volts
heater current	95	ma
heater power	0.6	watt.

The thermal efficiency of the planar cathode is much lower than that of the cylindrical type.[2] For instance, the cathode used in the one-inch Vidicon has a specific heater power of 50 watts/cm^2. Based on the 0.6-watt heater power, this cathode assembly has a specific heater power of 56 watts/cm^2. The corresponding specific heater power for the cylindrical type cathodes is usually 2 to 3 watts/cm^2.

It may be of interest to mention the warm-up period as determined from tests on 6 cathode assemblies. After the application of heater voltage, 5 to 10 seconds is required for the cathode to reach 90 per cent of its emission.

The observed thermal expansion of the cathode cup towards grid No. 1 is about one mil when heated from the room temperature to the operating temperature. During cathode activation, the total net elongation may reach one and one-half mils.

ACKNOWLEDGMENT

The writer would like to thank J. Kuehne, R. R. Reidenbach, and G. W. Rineer for their assistance in many phases of this work. He is also indebted to F. S. Veith and R. G. Neuhauser for their interest and helpful discussions.

MICROMINIATURE MULTICHANNEL PULSE-POSITION-MODULATION SYSTEM INCORPORATING TRANSISTOR-MAGNETIC-CORE CIRCUITRY*

By

H. Kihn,† R. J. Klensch,# and A. H. Simon#

Summary—An experimental five-channel time-division multiplex system has been built incorporating a microminiature transistor–core ring counter for both the transmitter modulator and receiver sampler. The pulse-position modulation of the transmitter modulator results from the variable time triggering of a transistor–core pulse generator by the variation of either the transistor input voltage or ferrite-core coercive-force thresholds.

The sampling rate used in the system is 15 kilocycles with an upper limit set only by the transistor and core high-frequency cutoff. Channel cross talk as low as —40 decibels may be obtained by suitable adjustment of operating parameters. Increased isolation can be obtained by reduction of repetition rate and use of a faster transistor such as the 2N139 or equivalent. Power consumption is approximately 200 milliwatts at the 15-kilocycle rate. Linearity is adequate (of the order of several per cent) for voice communication, but could be improved by optimization of drive and by trigger-current shaping to compensate for hysteresis-loop curvature.

Introduction

THE requirements in modern communications for a large number of channels, high speed, low power consumption, and adequate noise immunity has necessitated a re-evaluation of the more conventional multiplexing systems and techniques. This is particularly true for airborne and space communications systems where miniaturized components and low power consumption would allow the incorporation of truly complex data systems in limited volumes.

Multiplex systems fall into one of two general categories, frequency-division multiplex and time-division multiplex, both of which have been discussed extensively in the literature. Frequency-division multiplex uses a separate subcarrier for each channel with adequate frequency separation to prevent overlapping of modulation sidebands.

* Manuscript received March 24, 1960.

† Engineering staff, Vice President of Engineering.

RCA Laboratories, Princeton, N. J.

The modulated subcarriers are then added in a linear mixer and fed to the transmitter. In this arrangement, shown in Figure 1, all channels are sampled at the subcarrier rate and transmitted simultaneously. The receiver separates, by means of bandpass filters tuned

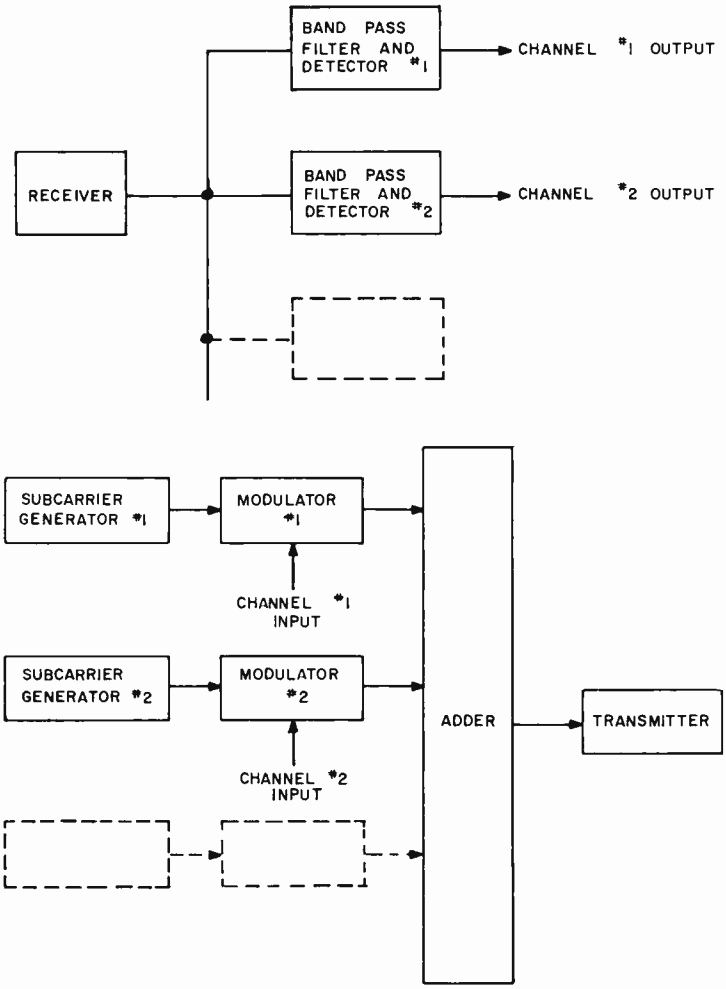

Fig. 1—Frequency-division multiplex system.

to the subcarrier frequencies, and then detects each of the modulated subcarriers.

In time-division multiplex systems, the information channels are sampled sequentially by a recurrent pulse train, and the instantaneous

amplitude of each information signal determines the amplitude (PAM), the duration (PDM), or the position (PPM) of a particular pulse in the pulse train. Thus, each pulse in the train refers to a particular information channel. Pulse waveforms representing these three types of modulation are shown in Figure 2.

For economy of bandwidth, it is also possible to subcommutate some of the channels in both frequency-division and time-division multiplex systems. In frequency division, one or more of the subcarriers may be time-division multiplexed to allow transmission of a number of narrow-band channels over a single subcarrier, while the wide-band channels continue to modulate the remaining subcarriers directly. In the case of time-division multiplex, a number of low-information-rate channels can be multiplexed to sequentially modulate a particular pulse in the recurrent output pulse train.

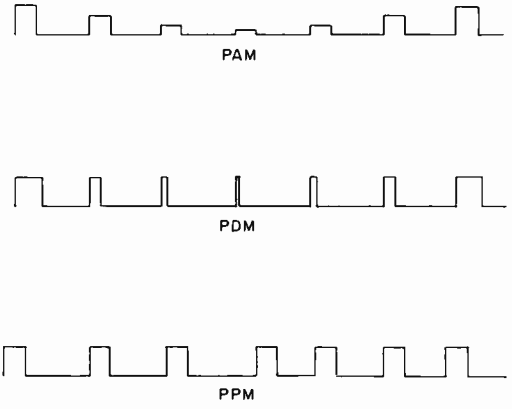

Fig. 2—Comparison of waveforms for PAM, PDM, and PPM systems.

Figure 3 illustrates a rudimentary time-division multiplex system which utilizes a mechanical sampling switch whose rotational speed determines the sampling rate of the system. Mechanical switches have been largely supplanted by electron-tube or transistor circuitry (except for telemetry use). Figure 4 shows, as an example, a system using an electronic ring counter commutator which may incorporate either a two-transistor or double-triode flip flop per stage.

Even transistorized systems require considerable power because of the continuous current required in their operation. A more desirable ring counter, as far as power consumption is concerned, is one where no holding current is required to maintain the two states of the flip

flop. Saturable magnetic cores offer this advantage, since the only power required is that needed to switch from one saturated state to another.

The system described here uses a transistor–magnetic-core ring counter which accomplishes both the sampling and modulating functions. The ring-counter stages are directly modulated by the information waveform and produce pulse-position-modulation output. This

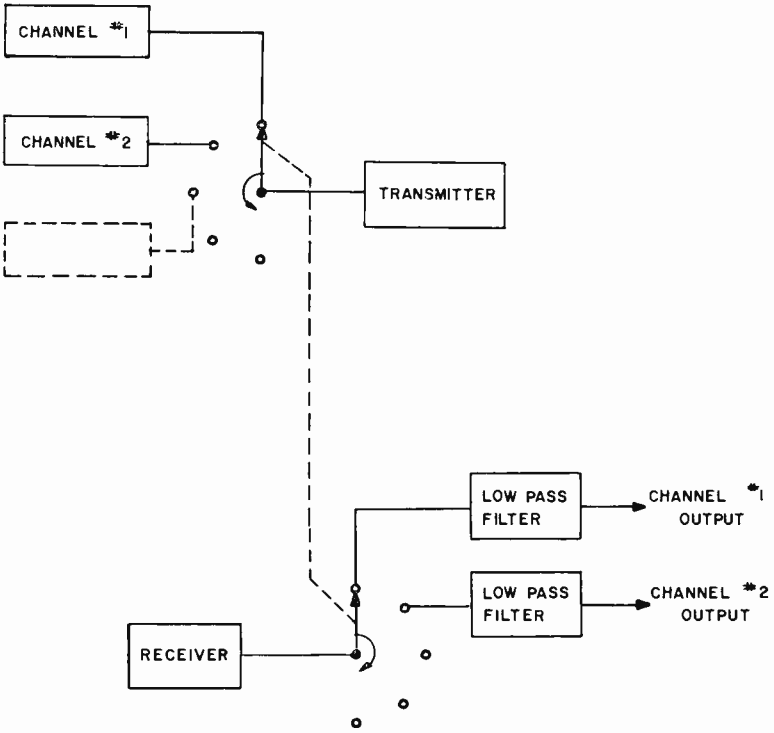

Fig. 3—Time-division multiplex system using mechanical switching.

output can, of course, be used to amplitude or frequency modulate an r-f transmitter. Synchronization between transmitter modulator and receiver demodulator is achieved by introducing one unmodulated reversed-polarity pulse in each sampling cycle. Additional sync pulses can be transmitted if required.

By the use of a sequential-sampling device the power required for subcarrier generation is eliminated. Since the entire commutator and associated drive circuit is composed of solid-state devices only, the required operating voltage and power is further reduced.

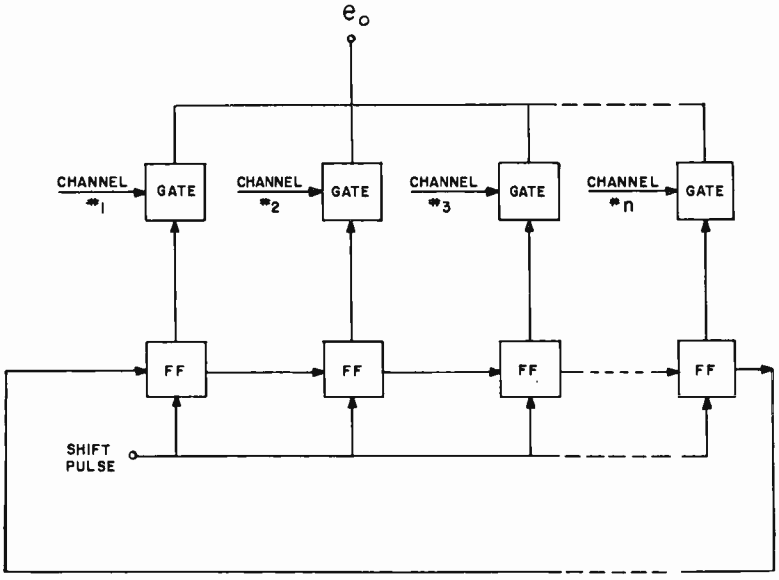

Fig. 4—Time-division multiplex system using bistable elements.

Transistor–Core Ring-Counter Sampling Devices

The basic element of the PPM system described here is the transistor–magnetic-core ring counter, shown in Figure 5. The interleaved-trigger or shift-pulse lines are used to provide a delay between the triggering of one stage and the triggering of the following stage. To clarify the principles of operation, it is advantageous to discuss first the two-state magnetic characteristic of a ferrite core.

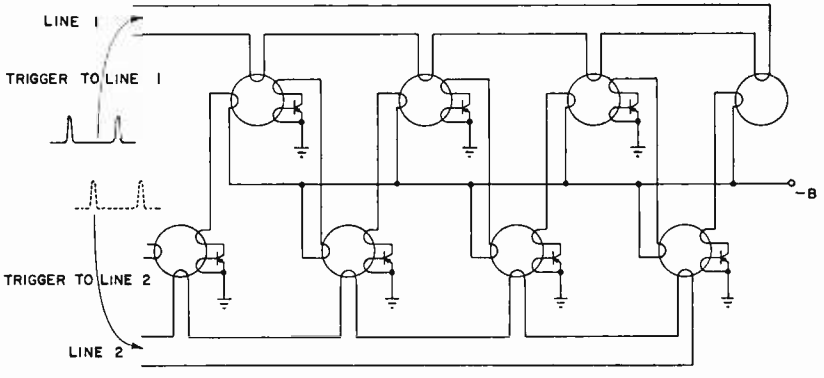

Fig. 5—Two-core-per-bit shift register.

A typical hysteresis loop of the ferrite cores used in the ring counter is shown in Figure 6. The two possible states of saturation are arbitrarily labelled "1" and "0," and the trigger-current pulses are always applied in a direction to drive the core toward the "0" state. If the core happens to be in the "0" state, the application of a trigger pulse will produce no output voltage on any of the other core windings. This may be explained by reference to Figure 6. The slope dB/dH of the hysteresis curve is defined as the core permeability. It

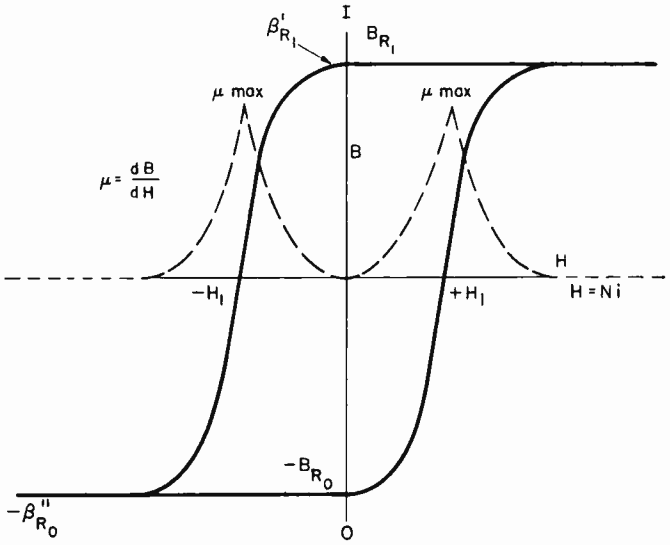

Fig. 6—Hysteresis loop diagram.

is evident that, under the "0"-state condition, the coupling between windings is minimal. If, however, the core is in the "1" state at the time of triggering, there will be a transition from the "1" to the "0" state, passing through a region of high permeability, and voltages will be induced on all windings.

As shown in Figure 5, the transistor base winding is connected so that the base is driven negative with respect to ground, causing collector current to flow through a feedback winding. The collector winding is connected to produce positive feedback to the base, thus producing an oscillatory half-cycle increase in current which serves to switch the core from a "1" to "0" state. The feedback is reduced to zero once the core is saturated thus cutting off the collector current. Because of the transistor feedback circuit, the trigger-current pulse

is only required to initiate the feedback action and, therefore, can be quite small. The transistor collector is also in series with the input winding of the following core and the B supply. Current flow in this collector circuit will cause a "1" to be set in this core because of the polarity of the input winding. This state persists until the next trigger-current pulse is applied to this core. In this fashion a "1" is propagated from core to core in synchronism with the trigger-current pulses. The transistors supply only the core-switching current; no holding current is required.

The interleaved configuration also protects against the initiation of multiple firings by a single trigger pulse. That is, in the course of one trigger-current pulse, a "1" might be shifted out of one core into the next core and so on until the trigger pulse stops. Another

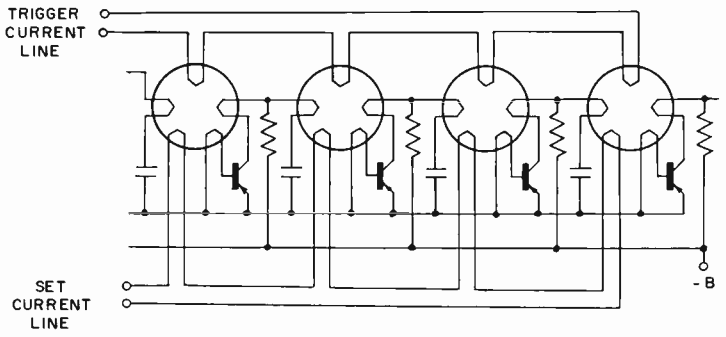

Fig. 7—One-core-per-bit shift register.

way to eliminate the possibility of multiple shifts is by the use of the circuit[1] shown in Figure 7. Here, a common trigger-current line is used, but an RC network is added to provide a delay between the triggering of one stage and the setting of the next. The charge on the capacitor supplies the collector current of the stage being triggered, and the recharge of the capacitor through the resistor provides the set current for the following stage. The only requirement on the trigger-current duration for proper shifting is that it does not exceed the switching or "on" time of the transistor being triggered. If this requirement is not fulfilled, the capacitor will start to recharge and, consequently, start to set the following core. The presence of a trigger

[1] H. Kihn and W. E. Barnette, "The Megacoder — A High-Speed, Large-Capacity Microminiature Decoder for Selective Communication," *RCA Review*, Vol. XX, p. 153, March, 1959.

pulse and a set pulse simultaneously may either (1) not set the core or (2) set and trigger the core. Trigger-current pulses less than 10 microseconds in width are sufficiently narrow to provide satisfactory operation.

As far as maximum shift or sampling rate is concerned, the interleaved system offers approximately a two-to-one advantage. Figure 8 illustrates the inherent higher speed capability of the interleaved system which requires no delay for the setting function. The removal of a resistor and capacitor per stage is also advantageous for circuit simplification.

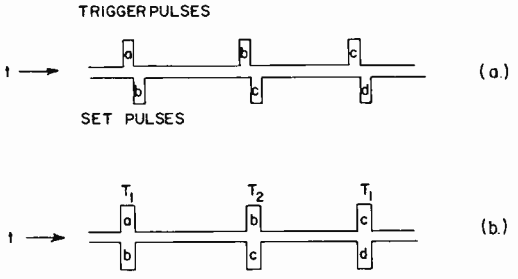

Fig. 8—Comparison of two-core and one-core-per-bit shift registers.

When used as a shift register, however, where a number of "1's" and "0's" are to be shifted simultaneously for each trigger pulse, the price paid for the removal of an RC network is the addition of a core and transistor to perform the required storage. For this reason the interleaved circuit is called a "two-core-per-bit" shift register.

Modulation Techniques

As mentioned in the previous section, the switching of the core is initiated by the trigger-current pulse and aided by regeneration due to positive feedback in the transistor circuitry. Because a minimum transistor base-to-emitter voltage must be exceeded for transistor conduction, there is a delay between the start of the trigger-current pulse and the time at which the transistor conducts and switches the core. The base-to-emitter voltage prior to transistor conduction as a function of time is

$$E_{BE} = E + \frac{d(LI)}{dt}$$

where I is the trigger current and L is the mutual inductance, both

expressed as functions of time. Since the base–emitter voltage must reach a certain minimum negative threshold voltage before regeneration occurs, the delay time will be a function of $d(LI)/dt$ and the base–emitter bias, E. Therefore, any change or modulation of L, I, or E will cause a change in the delay time and, consequently, will produce a variation of the transistor firing time which constitutes a form of PPM.

Figure 9 illustrates two methods for producing such PPM. In Figure 9a, the modulating source is a high-impedance current generator connected to an auxiliary core winding. The flux produced by

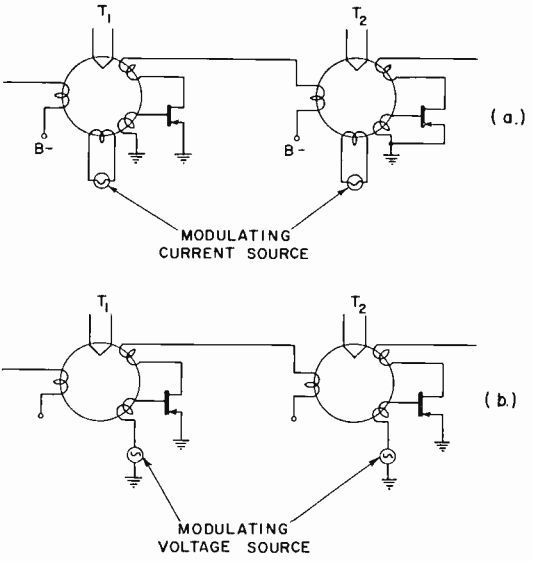

Fig. 9—Modulation techniques.

this current flow will either aid or oppose the flux produced by the trigger-current pulse and will modulate the firing time of the regenerative transistor–core circuit. This constitutes a variation of I in the $d(LI)/dt$ term. The method of introducing base-bias modulation is shown in Figure 9b. In this case, the modulating source is a low-impedance voltage generator. Here, the variation is in E_{BE}. Another method of modulation consists of changing the core characteristics at the modulation rate, thus varying L. Although this could be done by heating or stressing the core at the modulation rate, L is obviously not a practical parameter to modulate. In fact, variation in core

characteristics by environmental conditions may constitute a source of nonlinearity.

A detailed comparison of the above two forms of modulation will now be made. For this discussion, the trigger-current wave shape will be assumed to be a sawtooth, as illustrated in Figure 10a. The voltage produced across any core winding is then $d(LI)/dt$ which, for this case, has the shape of dB/dH, as shown later. The feedback is adjusted so that the transistor regenerates when point o in Figure 10a is reached, which point is referred to as the quiescent firing point. If the modulation is introduced as in Figure 9a, the time at which

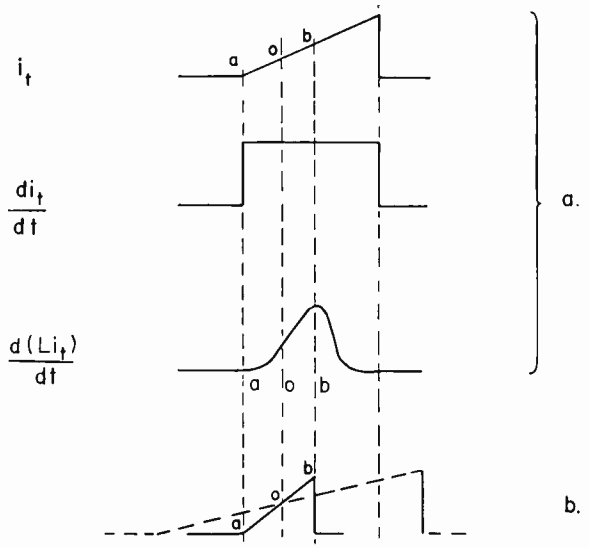

Fig. 10—Coupling characteristics of square-loop core.

the critical inductance on the B versus H curve is reached will depend on the magnitude and direction of the modulating flux. The output linearity will depend on the linearity of the sawtooth trigger-current pulse, and the maximum time deviation will be a function of the slope of the trigger-current sawtooth. In Figure 10b the reduced slope of the dashed curve will allow approximately 3½ times the maximum deviation of a sawtooth with the slope of the solid curve. The peak-to-peak modulation-flux amplitude for full deviation is equal to the maximum flux generated by the trigger-current pulse.

The bias-voltage modulation technique consists of introducing a modulation voltage between the base and emitter of the transistor as illustrated in Figure 9b. In this system, the transistor conducts

when the regeneration threshold voltage is reached and therefore the conduction delay is a function of the shape of the hysteresis loop. Referring to the $d(LI)/dt$ curve of Figure 10a, point o is the time during the triggering cycle at which transistor regeneration begins. Point a represents the time for incidence of regeneration for a large negative modulating voltage and, similarly, point b is the firing point for a large positive modulating voltage. The region between a and b can be made linear by properly shaping the trigger-current pulse. The relationship necessary between trigger current and the B versus H characteristic to produce a linear voltage on the base winding can be found from the equation

$$e_t = \frac{dB}{dt},$$

where e_t is the voltage per turn induced in the base winding and B is the flux as a function of time. Since $B = \mu H$ and $H \propto I$, the trigger circuit current, the assumed general equation of the B versus H curve from 0 to $+H_1$, as shown in Figure 6, is

$$B = a_0 + a_1 I + a_2 I^2 + a_3 I^3 + \cdots a_n I^n$$

The current I is a function of time and, in the general case, is given by

$$I = b_0 + b_1 t + b_2 t^2 + \cdots b_q t^q.$$

By substitution,

$$B = a_0 + a_1(b_0 + b_1 t + \cdots b_q t^q) +$$
$$a_2(b_0 + b_1 t + \cdots b_q t^q)^2 + \cdots$$
$$a_n(b_0 + b_1 t + \cdots b_q t^q)^n$$

and the derivative of B will be the induced voltage as a function of time. Since the induced voltage e_t should be linear, $e_t = Kt$, the b coefficients of t can be found, thus giving the required trigger current shape. A practical approximation is to assume B versus H to be a simple power function $B = AI^n$. The solution for this case is

$$e_t = \frac{dB}{dt} = \frac{d(AI^n)}{dt}.$$

Therefore,

$$Kt = \frac{d(AI^n)}{dt}.$$

By integration,

$$K_0 + \frac{Kt^2}{2} = AI^n,$$

where the constant of integration, K_0, is equal to zero because of the initial conditions. Solving for I,

$$I = \left[\frac{Kt^2}{2A}\right]^{1/n},$$

$$I = \left[\frac{K}{2A}\right]^{1/n} t^{2/n},$$

$$I \propto t^q$$

where $q = 2/n$.

This solution is valid when the B versus H curve has the form $B = H^n$. The required exponent of the trigger current versus time function, q, will then be related to n by $q = 2/n$. Therefore, if the B versus H curve is *parabolic*, the trigger current should be a *sawtooth*. The general expression for B and I mentioned previously leads to greater mathematical complexity than is warranted in B versus H curves normally encountered in this application. The slight amount of distortion resulting from the simplifying assumption, even for large modulating signals, may be compensated for by use of inverse nonlinearity in the detecting device.

Microminiature PPM Modulator

Figure 11a shows the basic block diagram and composite output signal of the PPM modulator. The three primary elements of the system are (1) the multivibrator clock, (2) the trigger and sync generator, and (3) the ring counter. The clock determines the rate at which the trigger-current pulses are produced by the trigger generator. Negative sync pulses are also derived from the trigger-generator unit, and the ring-counter output is added to the negative sync pulses to produce the composite output signal. One stage of the ring counter is unmodulated and its output is inverted for receiver synchronization.

The circuit of the PPM modulator, shown in Figure 12, is similar

to the basic ring-counter circuit of Figure 5. Base-bias modulation is used. The addition of an RC network and diode per stage allows the use of a common load resistor, R_0, without any interaction between stages.

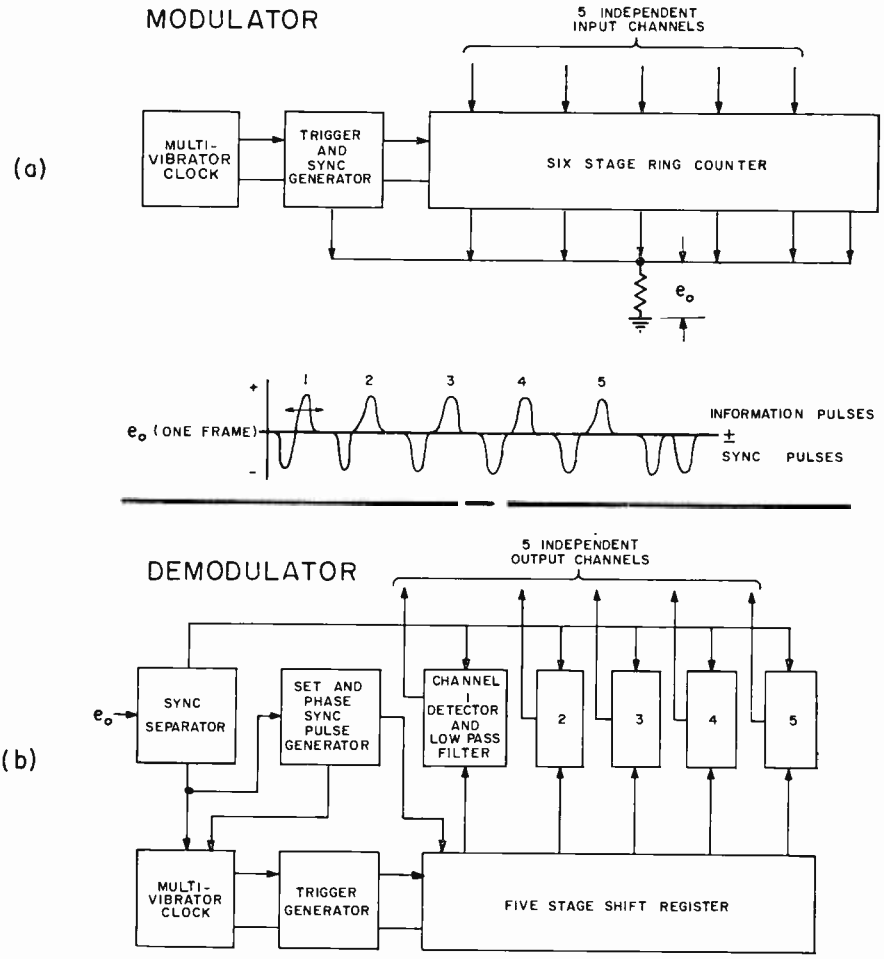

Fig. 11—Block diagram of microminiature PPM system.

The collector-voltage waveform is shown in Figure 13a with the trigger-current pulses used as a time reference. The collector is driven positive only when conduction occurs; a negative voltage results when either the preceding or succeeding stage fires. The small "noise" pulses at the collector are caused by trigger-current pulses and would

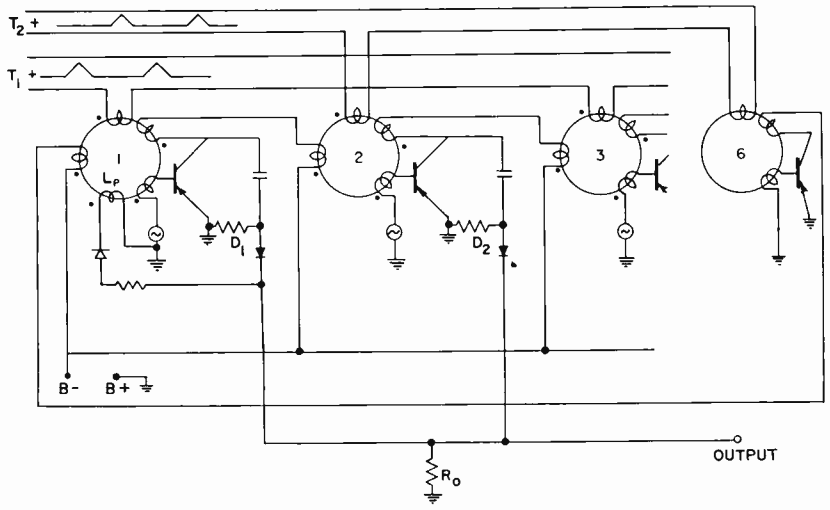

Fig. 12—Modulator ring counter.

be minimized if the B versus H curve of the core material had zero slope when saturated. The addition of a diode connected to the collector prevents the unwanted negative pulses from appearing across R_0. The waveform at R_0 is shown in Figure 13b, where each positive pulse represents the triggering of a different stage. Each pulse is

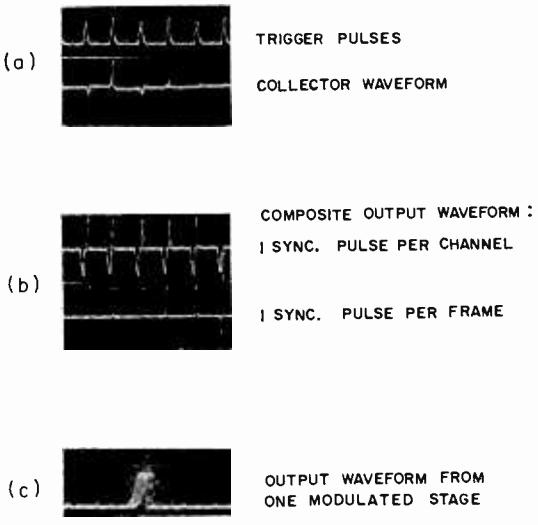

Fig. 13—Modulator-ring-counter waveforms.

approximately 3 microseconds in width. When modulation is applied to one of the stages, the output is as shown in Figure 13c.

The other components of the modulator circuit consist of a novel combination multivibrator clock and trigger-current-pulse generator, shown in Figure 14. The collector current of each transistor in the multivibrator flows through a separate winding on the trigger-generator square-loop core. Two pairs of windings so connected to the trigger-generator transistors as to produce positive feedback are also wound in this core. When multivibrator transistor Tx_1 conducts,

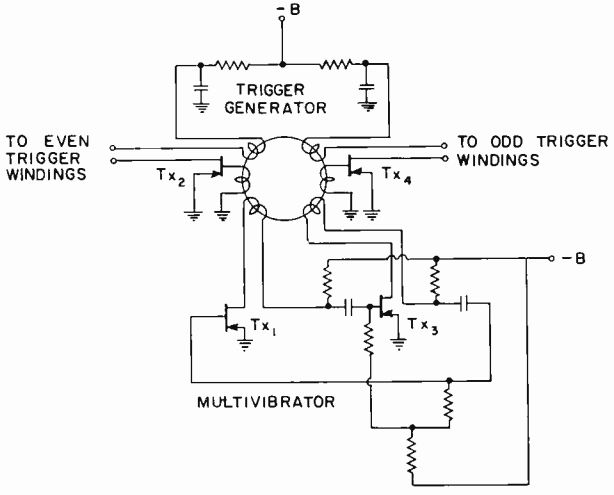

Fig. 14—Multivibrator clock and trigger generator.

switching of the core is initiated, causing transient conduction of the trigger generator transistor Tx_2 which produces core saturation. The collector current Tx_2 flows through the trigger windings of all the even stages of the ring counter. When the multivibrator switches (Tx_3 conducting), Tx_4 generates a trigger-current pulse for the odd stages of the ring counter. Figure 15c shows the trigger generator with two diodes inserted to obtain negative sync pulses. The output of the diodes is fed through a small isolation resistor to R_0. Since the base voltage has a faster rise time than the collector current, the sync pulses lead the information pulses as shown in Figure 11a.

As mentioned earlier, a negative pulse in the signal waveform serves as a synchronizing pulse. This pulse also is used in the resetting of the receiver shift register. The method of deriving this pulse

from the triggering of stage *six* is shown in Figure 15a. Although the required negative pulse could be obtained from the set winding of core *six*, use of the set winding of core *one* provides greater immunity from the deleterious effect of the positive information pulses which are present at the common output junction. Positive pulses at the common output point, shown in Figure 15a, produce current pulses through the set winding of core *one*, driving the core

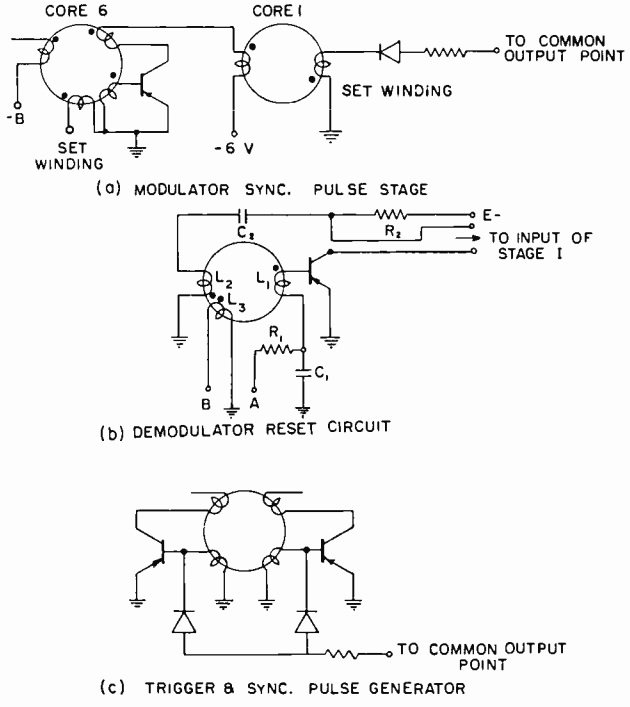

Fig. 15—Synchronization circuits.

toward the "0" magnetic state. Since the core has previously been triggered to the "0" state, this additional current flow is unobjectionable. If, however, the set winding of core *six* were used to generate the negative sync pulse, the polarity of this winding would be reversed, allowing the insertion of extraneous "1" magnetic states by the positive information pulses. The transformer "dot" notation, which indicates the polarity of the various windings, is used to clarify the circuit operation.

PPM Demodulator

The demodulator consists of a multivibrator clock, a trigger generator, and a shift register similar to the corresponding elements in the modulator, and also includes synchronizing and detector circuitry. The receiver block diagram, shown in Figure 11b, outlines the detection process. The circuit consists of a shift register which is used to generate detector gating pulses. These gating pulses occur sequentially at the sync-pulse recurrence frequency and are compared in the detectors with the information pulses to recover the modulation. The double negative pulse produced by stage *six* in the transmitter is detected by integration and provides (1) phase locking of the receiver multivibrator and (2) resetting of the receiver shift register.

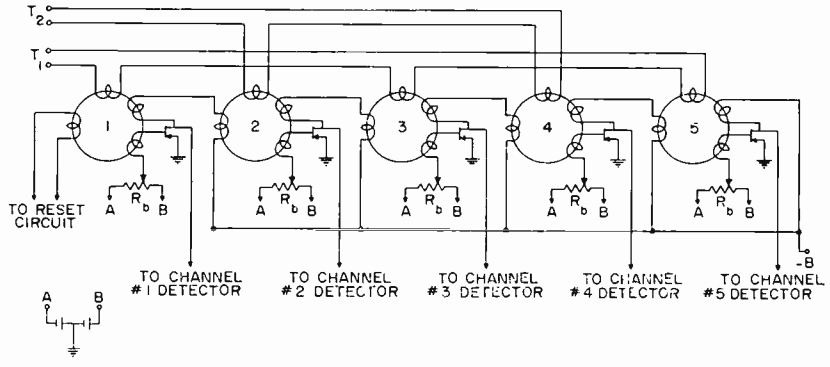

Fig. 16—Receiver shift register.

Receiver Shift Register

As can be seen from the circuit diagram in Figure 16, the receiver shift register deviates from the transmitter modulator in that it has one stage less than the transmitter register, independent outputs from each stage fed to detector circuits, individual bias-control potentiometers, and no feedback from the last to the first stage.

If a "1" is set in core *one*, it is apparent that this magnetic state will be shifted out of the register after five consecutive trigger-current pulses, leaving the register inoperable until stage *one* is again reset. The resetting of stage *one* is performed by the reset circuit shown in Figure 15b, providing there is a signal having a certain well-defined waveform applied between A and ground. The reset circuit is basically a transistor–core monostable flip flop requiring no holding current. When the supply voltage, E, is applied, capacitor C_2 is charged

through R_2 and L_2. This charging current will set a "1" in the core, because of the polarity of L_2, regardless of the initial state of saturation. The circuit will remain in this state until the base of the transistor is triggered with a negative voltage of sufficient amplitude to initiate regeneration. The collector current, supplied by C_2, flows through L_2 (the positive-feedback winding) and the set winding of core *one* of the receiver shift register. This causes the state of the core in the reset circuit of Figure 15b to be switched from a "1" to a "0" state, and core *one* of the register from a "0" to a "1". This action eliminates the positive feedback, explained earlier, thus causing the collector current to return to zero. The discharged capacitor C_2 now recharges through R_2 and L_2 returning the core in the reset circuit to the stable "1" state.

When a signal is applied between A and ground, the integral of the signal will appear across C_1. If the signal is the output of the transmitter modulator (Figure 11a), the voltage from C_1 to ground in Figure 15b will reach its largest negative value when stage *six* in the modulator produces its negative output pulse. By maintaining a constant input signal level (for example, by the use of limiters), the circuit can be adjusted to cause regeneration only when two successive negative pulses are applied. For greater noise immunity, the duration of the pulse generated by stage *six* should be lengthened, with an accompanying increase in the R_1C_1 time constant shown in Figure 15(b).

The operation of the receiver shift register in the presence of a signal, then, can be described as follows. The reset circuit regenerates and sets a "1" in stage *one* of the receiver register when stage *six* in the transmitter produces an output pulse. At this time the "even" trigger current generator in the receiver is "on", driving stages *two* and *four* only. (Since no trigger is applied to stage *one*, no difficulty in the setting of this stage is encountered.) When, following the above sequence, stage *one* of the transmitter fires, the "odd" trigger current generator in the receiver is "on" and triggers stage *one* in the receiver. Thus, if the transmitter and receiver "clocks" are in synchronism, the registers will also be in stage-to-stage synchronism. The clock synchronizing problem is discussed later as is the function of the third winding, L_3, on the core of the reset circuit.

Slope Detection

As has been stated, each stage of the receiver shift register is used to independently gate "on" an appropriate detector, as illustrated in Figure 17. Recovery of the original modulation can be accomplished

in a number of ways, the simplest of which is by integration. Because of the low duty cycle, however, detection by integration produces a very small output signal and, furthermore, does not respond to static variations in pulse position. A method which provides a larger output signal is peak detection and filtering. This is the method used here, and it is achieved by means of slope detection.

Another detector also capable of large signal output and having d-c response is the coincidence gate. The PPM signal is converted to a PDM (pulse duration modulation) signal by applying an unmodulated pulse to one element of a transistor and the PPM pulse to the other. Since bias is adjusted so that both signals must be present to produce collector current, the width of the output pulse will be a function of the degree of coincidence between the two input signals. The output is integrated to convert to AM and further filtered to remove the carrier signal.

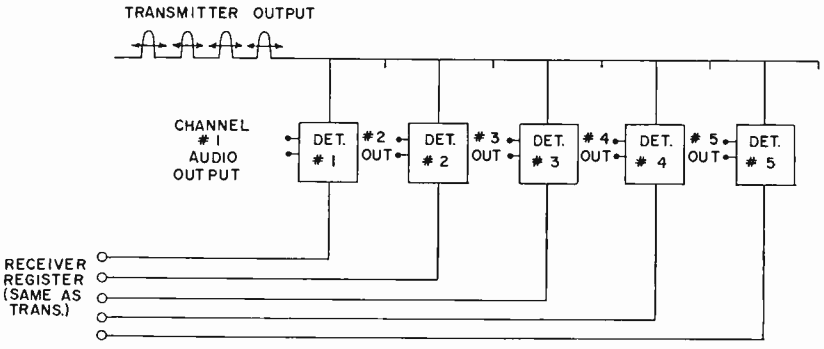

Fig. 17—Detector system.

As stated above, slope detection was used in the experimental demodulator described here. This method has advantages similar to the coincidence gate detector, and was used because of its simplicity. The circuit used for slope detection is shown in Figure 18. The collector terminal of the receiver shift register, which is not shown in Figure 18, is connected to the input terminal of the slope detector. The modulated positive pulses are removed from the composite transmitted signal by a diode clipper in the sync separator (Figure 11b) and fed to the terminal marked "positive transmitter pulses" on all of the detector circuits. The low-impedance demodulated and filtered output voltage is fed to the output terminal via an emitter follower. To clarify the operation of the detector, a more detailed explanation is given below.

The voltage waveform on the collector of a transistor in the receiver shift register is identical to its counterpart in the transmitter and is shown in Figure 13a. This signal, when applied to the input of the detector, is clipped by diode D_1, attenuated by a resistive network, integrated, and then inverted by transistor Tx_1. This produces a negative-going sawtooth at the base of transistor Tx_2. Transistor Tx_1 is a 2N105, and, because of its high input capacitance, produces the desired sawtooth when driven by a rectangular pulse. Transistor Tx_2 is biased beyond cutoff and requires both the negative sawtooth voltage at its base and the positive modulated pulse at the emitter to produce collector conduction. The magnitude of collector current is,

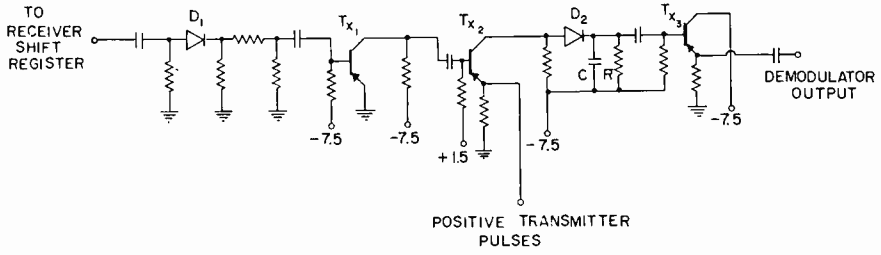

Fig. 18—Detector circuit.

therefore, dependent on the position of this pulse along the sawtooth. Figure 19a illustrates this process showing that output occurs only for one particular channel (channel two in this case). Figure 19b depicts the collector output current pulse for a number of consecutive samples or frames. These current pulses charge capacitor C (Figure 18) through the low-impedance diode D_2 with resistor R serving as the discharge path for C. The waveform across RC is shown in Figure 19c. The emitter follower Tx_3 serves to isolate the RC circuit from output loading. A low-pass filter with a cutoff frequency just below the sampling frequency may be used to further reduce the carrier amplitude. The sampling frequency in this system is 15 kilocycles, thus allowing transmission of intelligence up to a maximum rate of 7.5 kilocycles. A two-section constant-K filter (not shown), whose cutoff was 10 kilocycles, reduced the carrier amplitude by 45 decibels in the experimental system described herein.

The function of the bias potentiometer, R_b, in Figure 16, is to position the sawtooth waveform relative to the modulated pulse. Since the firing or regeneration time of the transistor in the shift register is a function of its base bias, the sawtooth can be positioned so that

the quiescent position of the pulse occurs half way up the leading slope of the sawtooth. This allows maximum deviation with minimum distortion. Any distortion resulting from the modulation process may be compensated by introducing inverse nonlinearity in the sawtooth used in detection.

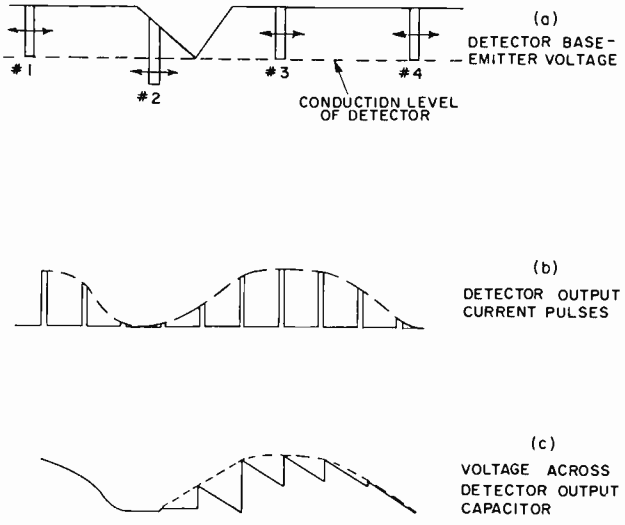

Fig. 19—Detector waveforms.

SYNCHRONIZATION

For an accurate reproduction of the original modulating signal at the output of the receiver, it is mandatory that synchronous operation between transmitter and receiver be achieved. Both frequency and phase locking are necessary since frequency synchronism alone does not necessarily prevent channel *one* of the transmitter from appearing at the output of channel *two* in the receiver, and so forth. If the receiver multivibrator clock is in perfect frequency synchronism with the transmitter clock, there is a 50 per cent probability of proper phase synchronism. Correct phase synchronism requires that the even-trigger generator in the receiver be activated when an even-numbered channel in the transmitter fires. The odd-numbered channels must correspond in a similar fashion.

The phase ambiguity is removed by the addition of a tertiary winding, L_3, on the core of the reset circuit in Figure 15b and an

emitter follower connected as shown in Figure 20b. The polarity of L_3 is chosen so that a negative voltage is applied to the base of the emitter follower when regeneration occurs in the reset circuit. The negative output of the emitter follower is capacitively coupled to the base of a transistor in the multivibrator clock driving it to conduction irrespective of its initial state. Thus, once per frame, the reset circuit both inserts a "1" in the receiver register and phase locks the multivibrator. An emitter follower with a large emitter resistor is used to prevent loading of the multivibrator by L_3. The

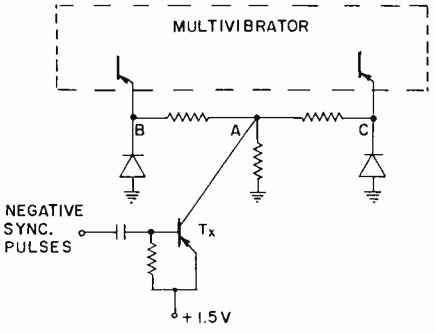

(a) FREQUENCY SYNCHRONIZATION CIRCUIT

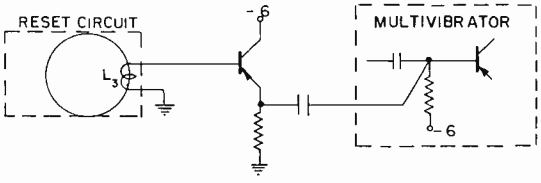

(b) PHASE SYNCHRONIZATION CIRCUIT

Fig. 20—Receiver synchronization circuits.

output impedance of the emitter follower when conduction occurs is low, however, making it possible to rephase the multivibrator by allowing rapid change of capacitor charge.

Frequency synchronization between the transmitter and receiver clocks is accomplished by driving the receiver multivibrator with the negative sync pulse generated at the transmitter. Figure 20a shows a method of triggering a free-running multivibrator having a natural frequency of oscillation not too far removed from the sync pulse rate. When the negative sync pulses are applied to the base of the normally cut-off driver transistor Tx, point A is driven to plus 1.5 volts. The

emitter-to-ground potential of the nonconducting stage in the multivibrator will also be driven to 1.5 volts, but the emitter of the conducting stage will remain practically unchanged because of the diode clamp. The net effect, therefore, is a change of state in the multivibrator. The function of the diodes is to allow a low-impedance path for the conducting transistor in the multivibrator and, consequently, to "steer" the sync pulse to the emitter of the nonconducting transistor. The receiver trigger generator and the portion of multivibrator not shown in Figure 20a are identical to the units used in the transmitter (Figure 14).

Other methods of synchronization, such as fly-wheel synchronization, could of course be used. This would allow the transmission of fewer sync pulses (perhaps one per frame); however, the redundancy in the transmitted signal and, to a certain extent, the reliability of operation is reduced. If, for example, a crystal-controlled oscillator was used as the transmitter clock, a stable LC oscillator requiring only periodic synchronization could be used in the receiver. By comparing the incoming sync signal to the locally generated signal in a phase detector and using the error signal to control the receiver clock, a well-synchronized system may be obtained.

Performance of Microminiature PPM System

By means of a breadboard model of the PPM system, the operating characteristics and performance have been determined. Such factors as crosstalk, noise, maximum sampling rate, stability as a function of supply voltage, and temperature were measured, and methods for increasing reliability were investigated.

The complete circuit of the modulator unit, including all interconnections and battery power supply, is shown schematically in Figure 21 and photographically in Figure 22. The five miniature shorting jacks on the front panel provide a convenient means for introducing modulation voltages to the ring counter. Figure 23 shows a microminiature version of a multivibrator clock and a 3-stage ring counter including three cores, three 2N105 transistors, four 1N192 diodes, three 0.3-microfarad capacitors, and four 0.1-watt resistors. The addition of another 3-stage ring counter and a trigger generator would complete the microminiaturization of the circuit shown in Figure 21 in a volume of less than one cubic inch.

The experimental core used in the ring counter described requires approximately 2 microseconds to switch its state, and the 2N105 transistor requires 10 microseconds for its current to drop to 10 per cent of its conduction value after cutoff. By using faster transistors and

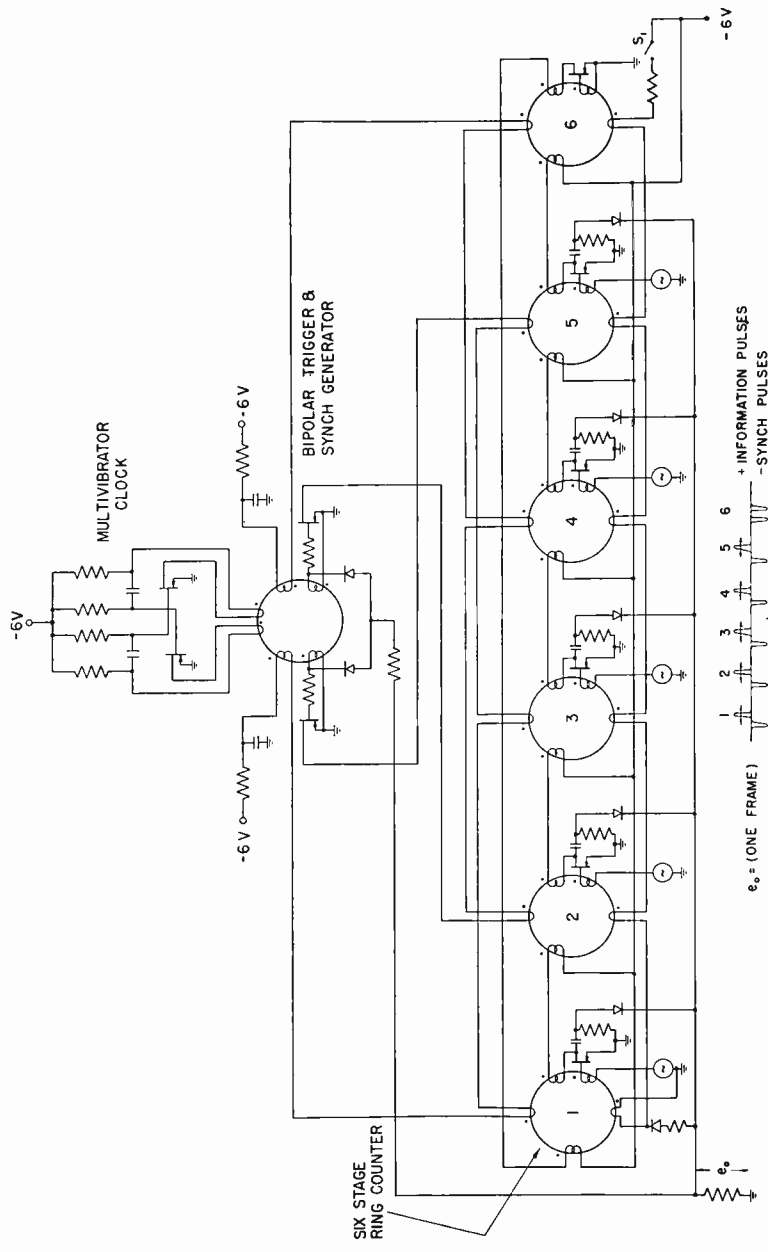

Fig. 21—Microminiature six-channel PPM system.

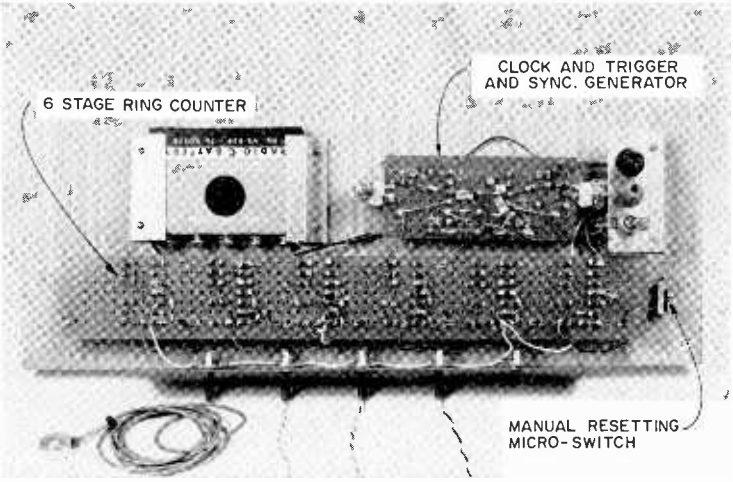

Fig. 22—Breadboard model of PPM system.

greater core switching current, the total switching time can be reduced to less than one microsecond. The trigger-current pulse spacing in the experimental PPM system is 11 microseconds and represents the minimum spacing consistent with acceptable values of adjacent-channel crosstalk.

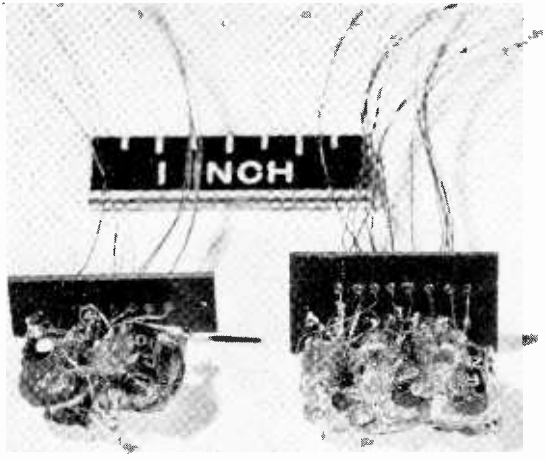

Fig. 23—Microminiature model of PPM system.

One form of crosstalk ("transistor-holdover-current crosstalk") is caused by transistor collector current of one stage flowing through the input winding of the following core at the time of triggering. The crosstalk, therefore, is produced by modulation of the core magnetic field. If the collector current were zero when the following stage was being triggered, this crosstalk would be eliminated. The only measurable crosstalk with 11-microsecond trigger separation is from one stage to the stage immediately following, and measured values between —30 and —50 decibels have been obtained. To minimize this type of crosstalk, the number of turns on the interstage coupling or input winding should be the minimum required for adequate core setting by the collector current of the transistor of the previous stage.

The inadequate core setting resulting from too few turns on the input winding may also cause crosstalk, however, but in a different manner. In Figure 6 the permeability, μ_0, of a core which has not been completely saturated is higher than that of the saturated core. Consequently a core incompletely saturated will require a trigger-current pulse of smaller magnitude than a saturated core to produce transistor regeneration. The degree of saturation of a core will determine, at least to a small extent, the time at which regeneration occurs with respect to the trigger-current pulse. Since the degree of saturation of a core depends on the transistor collector current of the previous stage, any amplitude variations in this current will be converted to pulse-position variations in the output pulse of the stage being discussed. Amplitude variations proportional to the amplitude of the modulating signal, as well as the desired position variations, are present in the collector-current pulses of a modulated stage and are capable of producing crosstalk in the following stage by the process described above. The collector-current amplitude modulation can be explained as follows. When the modulating signal applied to the base of the transistor is a positive voltage, the instant of oscillatory conduction is retarded until the trigger-current pulse drives the associated core well into the region of high permeability, where switching occurs. Even before the collector current had risen to its maximum value, the core is completely switched. When the modulating signal is negative, the instant of oscillatory conduction is advanced, allowing the collector current to rise to a slightly greater value than in the previous case before the core is completely switched. This is designated "core-setting modulation crosstalk".

The conditions for minimizing the above two types of crosstalk are incompatible. For the core and the 2N105 transistor used in the experimental PPM system, the crosstalk is minimized when eight turns

are used on the input winding of the core. From an analysis of these two types of crosstalk, it is evident that "transistor-holdover-current crosstalk" produces in-phase crosstalk while "set-modulation crosstalk" produces out-of-phase crosstalk. By increasing the number of turns on the input winding to insure complete core saturation and by using transistors with sharp current-cutoff characteristics, the crosstalk will be greatly reduced even at high-speed operation.

Noise generation appears as pulse-position jitter and is caused by transistor noise and the Barkhausen effect in the cores. The measured signal-to-noise voltage ratio for maximum signal output is approximately 200 (noise 46 decibels below signal). This represents the total noise generated in the modulator and demodulator in a bandwidth of 10 kilocycles. A reduction in noise could be realized by the use of lower-noise transistors in the ring counters.

The breadboard PPM system functions properly from a battery-supply voltage ranging from 3 to 15 volts, although a somewhat higher voltage may be used. The only adjustment required over this voltage range is the maintenance of adequate trigger-current amplitude. Obviously, if the peak trigger current becomes too small, triggering of the ring-counter stages will not take place. An 8-turn trigger winding (the input and set winding are also 8 turns for convenience of construction) is used in the PPM modulator and requires approximately 10 milliamperes peak trigger current for optimum ring-counter operation.

As explained in the discussion of modulation techniques, the maximum obtainable pulse deviation is dependent on the rise time of the trigger-current pulse. The trigger-current pulse generated in this system has a rise time of 5 microseconds and, therefore, allows a peak deviation of ± 2.5 microseconds, or approximately one output voltage pulse width. The modulation drive requirement to produce maximum deviation is only .05 volt r-m-s from a low-impedance source. A source impedance of 200 ohms or less can be used without significant reduction in base current.

Temperature dependence of the microminiature PPM system is primarily a function of the temperature dependence of the transistor and cores used in the ring-counter circuits. The use of a high-Curie-temperature core insures a minimum variation of hysteresis-loop characteristic with temperatures in the vicinity of ambient. Although the cores used in the system have a relatively low Curie temperature, other cores have been made in experimental batches which exhibit excellent temperature stability. The effect of increasing the temperature of a core is to reduce the width of the hysteresis loop and increase

its steepness (maximum permeability), thus causing transistor regeneration to occur at a lower trigger current level. This results in advancing the firing time of the transistor–core regenerative circuit. The miniature 2N105 transistor, which was used primarily for its size, is not the ideal solution to the temperature problem. A 2N139 or equivalent transistor provides greater temperature stability, particularly when used with a high-Curie-point core.

If an excessively large positive modulating voltage is applied to any stage of the modulator ring counter, this stage will not be triggered, because the conduction threshold voltage will not be reached. This will render the ring counter inoperative until both the modulating signal is reduced in amplitude and the ring counter is reset. Resetting of the ring counter is accomplished by the insertion of a "1" magnetic state in core one and a "0" magnetic state in the remaining cores. The reset microswitch, S_1, shown in Figure 21 is used for this purpose (the series resistor limits the current in the circuit).

Although the transistors in the ring counter develop peak collector currents as high as 150 milliamperes when triggering occurs, the low duty cycle of the system results in low average power requirements. The power consumption of the entire modulator, when operated from a 4.5-volt battery at a shift rate of 90 kilocycles, is approximately 200 milliwatts. At this shift rate, the sampling rate for six channels is 15 kilocycles per channel, thus allowing a maximum theoretical bandwidth per channel of 7.5 kilocycles. The measured distortion introduced by the modulation process was 3 per cent or less for pulse deviations of ± one pulse width.

Conclusion

An experimental five-channel time-division-multiplex system has been conceived and built incorporating a microminiature transistor–core ring counter for both the transmitter modulator and the receiver sampler. The pulse position modulation results from the variable time triggering of a transistor–core pulse generator by the variation of either the transistor input voltage or ferrite-core coercive-force thresholds. The sampling rate used in the system is 15 kilocycles with an upper limit set only by the transistor and core high-frequency cutoff.

The number of channels and the sampling rate can be increased to meet the requirements of a particular application with a proportionate increase in operating power if the sampling rate per channel is maintained constant. If the clock rate remains constant with an

increase in the number of channels used, no increase in power consumption will result.

Channel cross talk attenuation of 40 decibels may be obtained by suitable adjustment of operating parameters. Increased isolation can be obtained by reduction of repetition rate and use of a faster transistor such as the 2N139 or equivalent. Power consumption is approximately 200 milliwatts at the 15-kilocycle rate. Linearity is adequate for voice communication, of the order of several per cent, but could be improved by optimization of drive, and trigger current shaping to compensate for hysteresis-loop curvature.

The time deviation of the pulse from its quiescent position is dependent on slope of the trigger current sawtooth waveform. The deviation obtained in the modulator described herein is approximately ±2.5 microseconds. Deviations of ±5 microseconds are possible by suitable alterations in the trigger-generator circuitry.

The electronic pulse position modulation system is capable of extreme miniaturization, requires low operating power and allows high-speed operation. These characteristics makes feasible the use of such a PPM system as a telemetry link between guided missile and ground station as well as a multichannel low-power ground or airborne communication system.

PARAMETRIC AMPLIFICATION, POWER CONTROL, AND FREQUENCY MULTIPLICATION AT MICROWAVE FREQUENCIES USING CYCLOTRON-FREQUENCY DEVICES*

BY

C. LOUIS CUCCIA

RCA Electron Tube Division,
Harrison, N. J.

Summary—*If an electron beam is projected through an axial magnetic field and acted upon by a transverse alternating-current electric field having a frequency approximately equal to the characteristic cyclotron frequency of the magnetic field, a rope-like bunch of electrons will circulate about the beam axis with the cyclotron angular frequency. This electron bunch will have a radius of angular motion corresponding to the power absorbed from the transverse field. Power control, frequency multiplication, and low-noise amplification can be achieved by passing the bunched circulating beam through appropriate structures. This paper describes basic structures for providing these functions and their principles of operation.*

INTRODUCTION

FOR MANY years, the classical form of traveling-wave tube dominated most of the thinking about noise figures obtainable from traveling-wave-type amplifiers, and minimum noise figures of 5 to 6 decibels were widely accepted. However, lower noise figures were being achieved. Commercially available 6861 low-noise S-band traveling-wave tubes yielded noise figures as low as 4.1 decibels, and noise figures as low as 2.9 decibels were reported for backward-wave amplifiers. Nevertheless, the electron-beam type of microwave amplifier, with its hot cathode, was not expected to compete with the maser, the new low-temperature molecular-resonance amplifier which was providing noise figures of less than 1 decibel.

In October 1958, however, Robert Adler[1,2] announced the achievement of a noise figure of 1.4 decibels with an electron-beam parametric

* Manuscript received April 21, 1960.

[1] R. Adler, "Parametric Amplification of the Fast Electron Wave," *Proc. I.R.E.*, Vol. 46, p. 1300, June, 1958.

[2] R. Adler, G. Hrbek, and G. Wade, "A Low Noise Electron-Beam Parametric Amplifier," *Proc. I.R.E.*, Vol. 46, p. 1756, October, 1958; and R. Adler, G. Hrbek, and G. Wade, "The Quadripole Amplifier, A Low Noise Parametric Device," *Proc. I.R.E.*, Vol. 47, p. 1713, October, 1959.

amplifier. Until the disclosure of Adler's results, the noise-figure gap between the electron-beam microwave tube and the maser had been tacitly assigned to the solid-state parametric amplifier.

The electron-beam parametric amplifier is not merely another version of the traveling-wave tube; it is different from any amplifier presently in use. It is a microwave amplifier using a crossed-field type of operation that was first employed in the late 1940's in a research tube called the electron coupler.[3]

This paper explains the principles of operation of not only the electron-beam parametric amplifier, but also of the electron-coupler power-control tube, and the electron-coupler frequency multiplier, all of which fall into a new group of microwave devices using transverse electric fields and axial cyclotron-frequency magnetic fields.

Electron-Bunching Processes

The electron-coupler and parametric-amplifier types of devices make use of a unique type of electron "bunching." This bunching is produced by an electron beam projected along a path parallel to a magnetic field and subjected to a transverse electric field. The magnitude of the magnetic field corresponds to a "cyclotron" frequency, and the electric field alternates at, or in the vicinity of, the cyclotron frequency.

Figure 1(a) represents a typical interaction region. The electrons pass between a pair of pole faces which are energized by a generator to develop a transverse alternating electric field. The beam is transferred through the plates by a beam voltage V_b. A magnetic field H_c, parallel to the axis of movement of the electron beam, defines a characteristic cyclotron frequency f_c where

$$H_c = f_c \frac{2\pi m}{|e|}.$$

e and m are the electron charge and mass, respectively. In practical units, the cyclotron frequency is related to the axial magnetic field by

$$f_c = 2.794 \times 10^6 H_c \text{ cycles per second,}$$

where H_c is in gausses. Table I gives cyclotron frequencies characteristic of various magnetic fields.

---

[3] C. L. Cuccia, "The Electron Coupler—A Developmental Tube for Amplitude Modulation and Power Control at the Ultra High Frequencies, Part I, Physical Theory," *RCA Review*, Vol. 10, p. 270, June, 1949; "Part II, Engineering Aspects," *RCA Review*, Vol. 14, p. 72, March, 1953.

Table I

Magnetic Field H_c (gausses)	Cyclotron Frequency f_c (megacycles)
200	558.8
500	1397
1000	2794
2000	5588
3000	8382
4000	11176

If the transverse alternating electric field has a frequency substantially equal to f_c, each electron spirals with increasing radius as is moves past the pole faces. At any instant in time, all electrons have the same phase and the electron beam describes the directrix of a cone, as shown in Figure 1(a), rotating about the central-beam axis at the cyclotron frequency.

Thus, the action of the transverse alternating electric field produces a unique effect. All the electrons form a long rope-like "bunch"

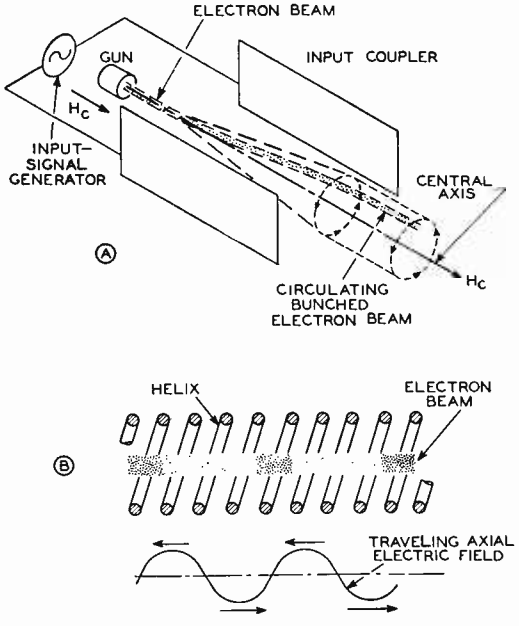

Fig. 1—(A) Circulating bunched electron beam developed in an input coupler, and (B) electron bunching in a traveling-wave tube.

that circulates, or revolves, in space, in full constraint, and in an azimuthal position determined only by the phase and timing of the transverse field.

The rope-like bunching shown in Figure 1(a) differs somewhat from the bunching that takes place in a traveling-wave tube. As indicated in Figure 1(b), the electron beam of a traveling-wave tube interacts with radial and axial electric fields developed by the helix, and produces bunching in an axial direction. This bunching is not clear cut. The beam space is filled with space charge at all times, but the space charge varies in density as a function of axial distance.

Microwave Devices Using Cyclotron-Frequency Electron Bunching

Figure 2 shows the basic structures of several varieties of microwave devices that use electron beams in axial cyclotron-frequency magnetic fields and transverse electric fields, and take advantage of the unique electron-bunching process illustrated in Figure 1(a).

Figure 2(a) shows an electron beam passing through an input coupler, a device basic as an input circuit to all the devices illustrated in Figure 2. The structure of Figure 1(a) is basically an input coupler in which a transverse alternating electric field developed by an input-signal source interacts with an electron beam passing through the transverse field while constrained by a parallel cyclotron-frequency magnetic field. The input coupler presents a resistance to the input-signal source which is directly proportional to the intensity of the electron beam.

Figure 2(b) shows the structure of the electron coupler, an input coupler driving an output coupler. The output coupler is a structure that extracts the power in the circulating or spiralling motion of each electron and delivers this extracted power to an output load.

Figure 2(c) shows an electron coupler frequency multiplier. It comprises an input coupler driving a harmonic-frequency output coupler. The output coupler develops a harmonic of the input signal in response to the bunched circulating electron beam.

Figure 2(d) shows a basic structure of the electron-beam parametric amplifier. This consists of an input coupler, a pump coupler, and an output coupler. The electron beam passes in succession through the three couplers. The pump coupler is driven by a "pump" generator, and increases the energy of the bunched electron beam by increasing the radius of the circular motion.

The Input Coupler

The input coupler comprises the transverse-field interaction space illustrated in Figure 1(a) and is the first interaction circuit through which the electron beam passes. In this coupler, the input signal develops a transverse alternating-current electric field between the pole faces, and the electron beam interacts with this transverse electric field and the axial magnetic field to produce the circulating rope-like bunch shown.

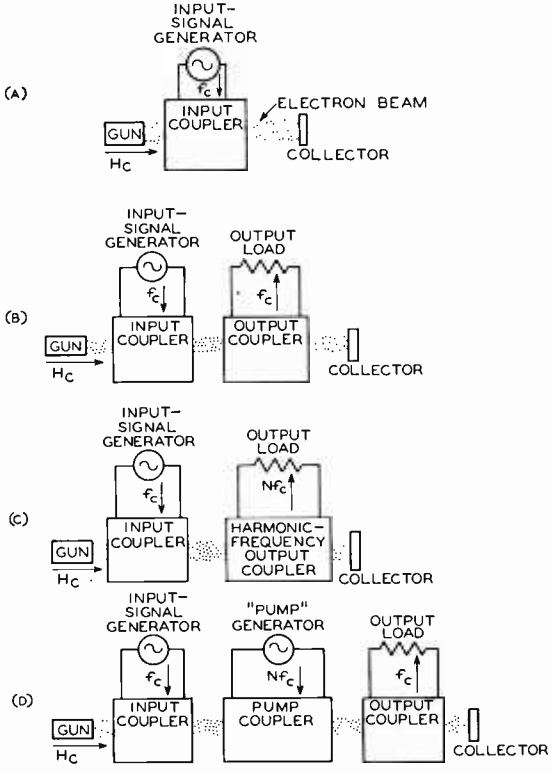

Fig. 2—Basic configuration of (A) input-coupler resistance device, (B) electron coupler, (C) frequency multiplier, and (D) electron-beam parametric amplifier.

The expressions given below describe the final radius x of the circulating electron beam and the actual power P absorbed by the beam. (This energy is quite separate from the energy given to the electron beam by the beam voltage which transfers the electron beam

from the cathode through the tube.)

$$x = 2.36 \frac{E_1 L_1}{V_b^{1/2} f_c} \text{ centimeters,}$$

$$P = 1.122 \times 10^{-2} f_c^2 x^2 I_0 \text{ watts,}$$

where I_0 is the beam current, in amperes,

f_c is the frequency, in megacycles,

L_1 is the length of the path traversed by the electron in the input coupler, in centimeters,

V_b is the beam voltage, in volts, and

E_1 is the peak value of the transverse electric field, in volts per centimeter.

The equation for P describes the power-handling capability of the input coupler as a function of frequency. Some indication of the use

Table II

	f_c (mc)	V_b (volts)	L (cm)	E_1 (volt/cm)	I_0 (ma)	x (cm)	P (watts)
High-Power Tube	800	800	6	1000	90	1.25	1010
Low-Power Tube	1000	100	1	1	10	2.36×10^{-4}	0.0264

of these equations can be obtained from the examples shown in Table II. As can be seen, the electron beam is capable of acting as a carrier of very large powers, as represented by the circulation energy of the electrons, even though the beam power due to the beam voltage may be very small.

The action of the electron beam in setting up the rotating beam in response to an input signal results in an electronic resistance.[3,4] This

[4] J. S. Donal, Jr. and R. R. Bush, "A Spiral-Beam Method for Amplitude Modulation of Magnetrons," *Proc. I.R.E.*, Vol. 37, p. 375, April, 1949.

resistance, presented to the transverse-field pole faces of the input coupler, is given by

$$R = 8\frac{V_b}{I_0}\left[\frac{d}{L_1}\right]^2$$

where R is in ohms, d is the width of the transverse-field boundary in centimeters, and L_1 is the length of the field boundary in centimeters. This concept of beam resistance is important to the understanding of the output coupler.

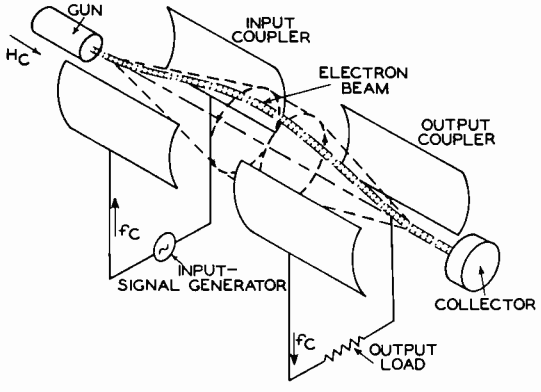

Fig. 3—Basic electron-coupler structure, comprising an input coupler driving an output coupler.

The Output Coupler

If the electron beam, which has been subjected to a transverse electric field in a cyclotron-frequency magnetic field, is transferred directly to a collector, both the beam power (represented by the product of the beam voltage and the beam current) and the power represented by the azimuthal motion of the electrons are dissipated in the collector in the form of heat.

When the rotating electron beam is passed through a pair of transverse-field pole faces across which a load is connected, the circulating electron beam induces a current in the load resistance. This current develops a transverse electric field between the pole faces, and the power represented by the azimuthal electron motion is developed in the output load. This pair of pole faces and the shunt load R comprise the output coupler, as shown in Figure 3.

If the field-forming pole faces of the output coupler are identical to the corresponding pole faces of the input coupler and the beam voltage is the same in both couplers, all energy represented by the azimuthal motion of the electron beam passing through the output coupler is dissipated in the output load, provided the resistance of the output load is equal to the beam resistance of the input cavity. Under this condition, the cone formed by the bunched beam in the output coupler is a mirror image of the beam cone formed in the input coupler.

Figure 4 illustrates the phase relationships representative of the transverse fields in the input coupler and in the output coupler while the coupling beam is passing through them. Figure 4(a) shows that

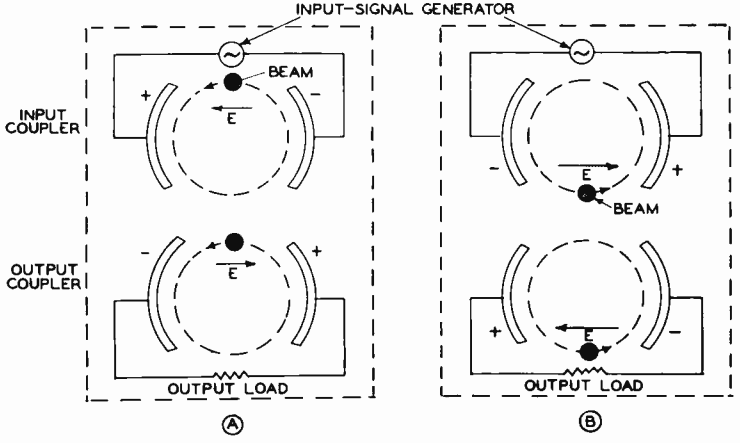

Fig. 4—Phase relationships between electron beam and transverse electric fields in input and output couplers (A) at one instant in time and (B) one-half cycle later.

the transverse electric field in the input coupler is in the direction of the left-hand pole face as the electron beam approaches that pole face and thus produces an accelerating electric field that gives up energy to the electron beam. In the output coupler, shown in Figure 4(a), the electric field is 180° out of phase with the electric field in the input coupler, and is in the direction to decelerate the electron beam and extract the energy of circulatory motion from the electron beam.

Figure 4(b) shows the relationship between the electron motion and the transverse fields in the input and output couplers a half-cycle later than the condition shown in Figure 4(a). The electron beam has traversed half of the circular path and is approaching the right-

hand pole faces. However, the electric fields have reversed phase so that the transverse electric field in the input coupler continues to accelerate the electron beam, and the transverse electric field in the output coupler continues to decelerate the electron beam.

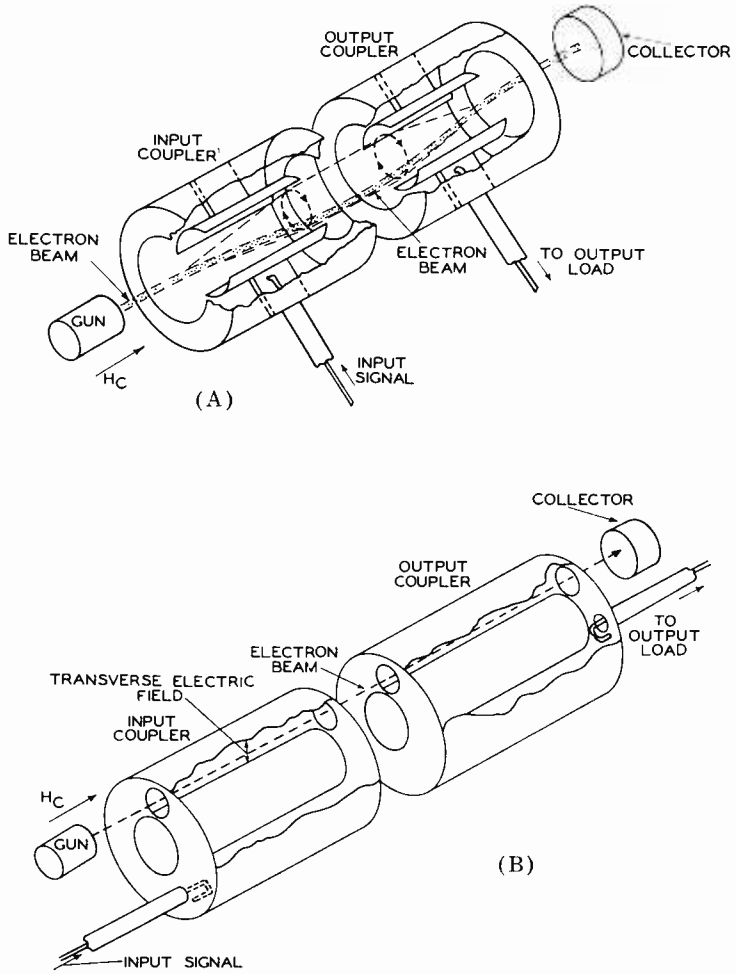

Fig. 5—(A) Electron-coupler structure using two-vane resonators to develop transverse electric fields, (B) electron-coupler structure using coaxial resonators to develop transverse electric fields.

The Electron Coupler

The electron coupler which is a nonamplifying version of the electron-beam parametric amplifier, comprises an input coupler driving an output coupler. It is particularly useful as a power-control device,

as a unilateral impedance between a driving circuit and an output circuit, and as a device for controlling the power to an output circuit when high power (such as that provided by a magnetron) is available and power amplification is not required.

The structural elements of the input and output couplers may take many forms. Figure 5 shows two different transverse-field structures arranged as input and output couplers. A coupling beam couples the signal energy from the input coupler to the output coupler.

Figure 5(a) illustrates the use of cavity structures[5] that develop transverse electric fields. Each structure is of the two-vane magnetron type. Figure 5(b) illustrates the use of resonant coaxial cavities[6] that develop radial electric fields, the intensities of which vary sinusoidally in the axial direction.

Electron couplers using these structures have been employed successfully to control the output power of a 1-kilowatt UHF magnetron. These tubes are described here to illustrate pertinent operating principles associated with the electron-beam parametric amplifier and cyclotron-frequency devices in general.

Figure 6 is a photograph of an experimental electron coupler[5] designed to permit independent control of the potentials of the input and output couplers. The input-coupler cavity and the electron gun are shown in Figure 7, together with the tuning plunger and the coupling loop. In this tube, the curved pole faces are one inch apart and two inches long. A 100-milliampere electron beam having a diameter of $\frac{5}{8}$ inch passes through the cavities. The input-coupler voltage is 800 volts.

The tube shown in Figure 7 successfully controlled almost a full kilowatt of UHF power; power-transfer efficiencies as high as 70 per cent were measured. The output power was controlled from maximum to substantially zero by varying the potential between the output coupler and input coupler from 0 volts to 800 volts (no current was collected by the output coupler).

Figure 8 shows a coaxial-resonator type of electron coupler[6] using a structure similar to that of Figure 5(b), and Figure 9 shows the components. This tube, which is designed to provide uniform transverse-field spaces for a pair of coupling beams, is 18 inches long and 6 inches in diameter. Five modulating electron beams are projected

---

[5] C. L. Cuccia and J. S. Donal, Jr., "The Electron Coupler, A Spiral Beam UHF Modulator," *Electronics*, p. 80, March, 1950.

[6] C. L. Cuccia, "Spiral Beam Tube Modulates 1-Kilowatt at Ultra High Frequencies," *Electronics*, p. 130, April, 1953.

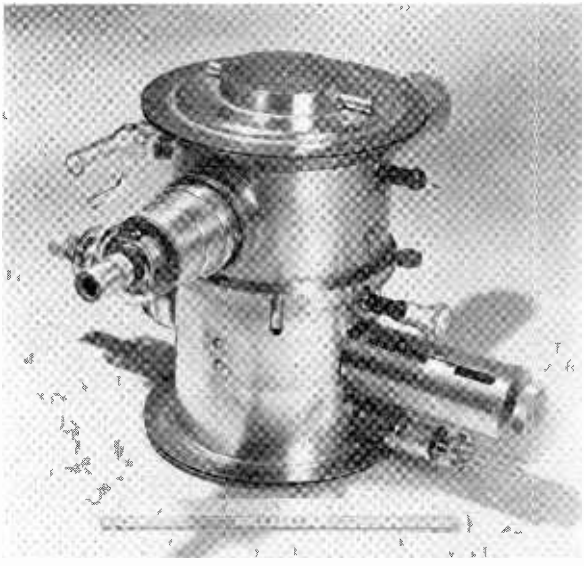

Fig. 6—Experimental electron coupler using output-coupler voltage control for power-output modulation.

through the output coupler; grid control of these beams provides a controllable resistance to shunt the output load. These modulating

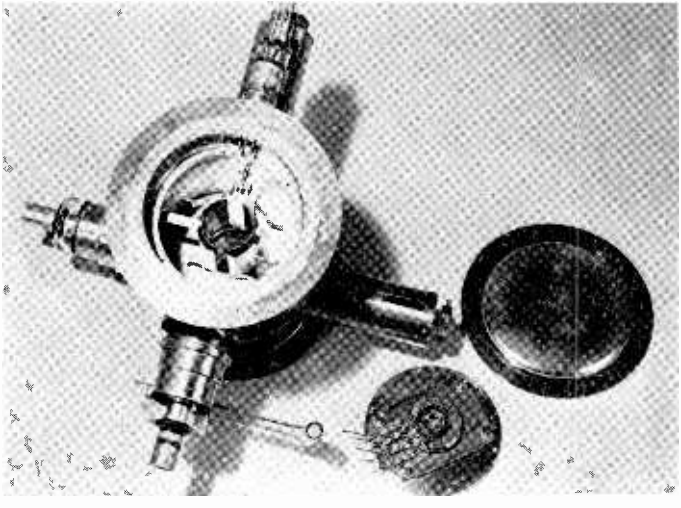

Fig. 7—Input coupler and electron gun of transit-time-controlled electron coupler.

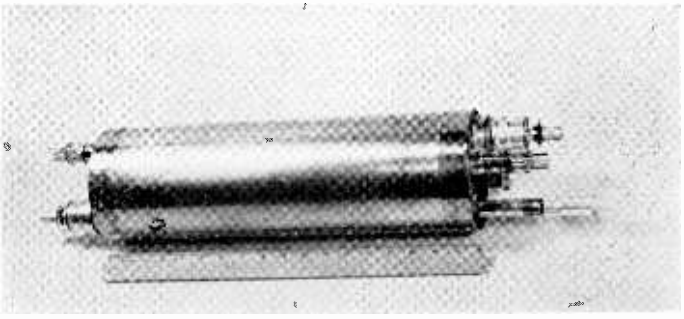

Fig. 8—Experimental electron coupler using coaxial cavities and five modulating electron beams in the output cavity.

electron beams are capable of producing power modulation in excess of 98 per cent with less than 50 volts of grid swing. A high-definition television picture was translated to a monitor by use of a modulated signal provided by the tube.

Electron-Coupler Frequency Multiplier[3,7]

The structure shown in Figure 10 consists of an input coupler adjacent to a magnetron-cavity type of structure. The latter structure

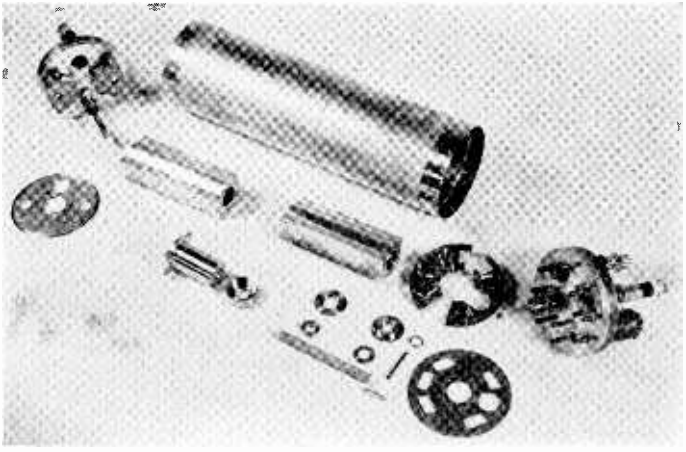

Fig. 9—Component parts of the coaxial-cavity electron coupler shown in Figure 8.

---

[7] C. L. Cuccia and Harwick Johnson, "Spiral Beam Frequency Multipliers," presented at *I.R.E. Electron Tube Conference*, Syracuse University, June, 1947.

is coupled to a resistive load. An electron beam is projected through both structures parallel to a cyclotron-frequency magnetic field. The magnetron type of structure is representative of a class of structures that produce an azimuthal traveling electric field, as distinguished from the transverse electric field developed by the input coupler or output coupler.

Figures 11(a) through 11(d) are diagrams of the fringe electric fields developed by four-pole and six-pole structures in response to alternating-current voltages developed between adjacent poles. These figures also include the circular paths traversed by a bunched electron beam about a central axis during one cycle of the cyclotron frequency.

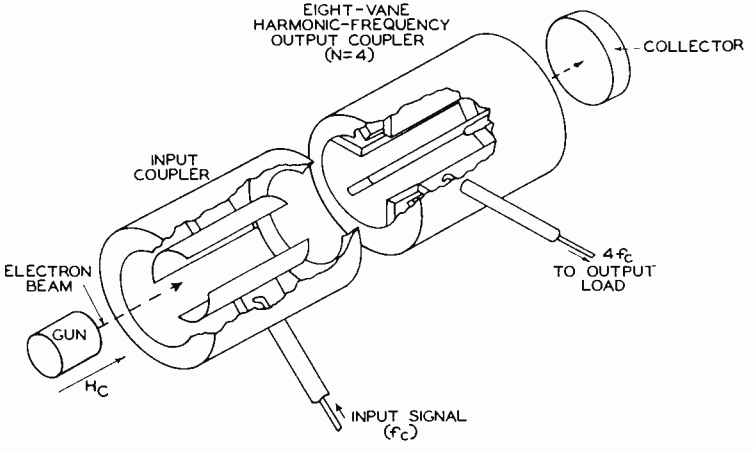

Fig. 10—Diagram of an input-coupler structure coupled to an azimuthal-electric-field structure to produce frequency multiplication.

Figures 11(a) and 11(b) show the traversing of a quadrant during a quarter-cycle of the cyclotron frequency by an electron bunch. During this quarter-cycle, the fringe fields reverse polarity, and the electron bunch experiences a continuous decelerating electric field. Voltages will therefore be developed between adjacent pole faces of the structures of Figures 11(a) and 11(b) by the azimuthally moving electron beam at a frequency equal to twice the cyclotron frequency as a consequence of currents induced in the resistive load by the motion of the electron beam.

Figures 11(c) and 11(d) show a six-pole structure in which the bunched electron beams circulate about the interaction space defined by the six pole faces. A complete circular transit of the electron bunch takes place during one cycle of the cyclotron frequency, and a

voltage is developed between adjacent pole faces at three times the cyclotron frequency as a consequence of the electron bunch experiencing a continuously decelerating electric field.

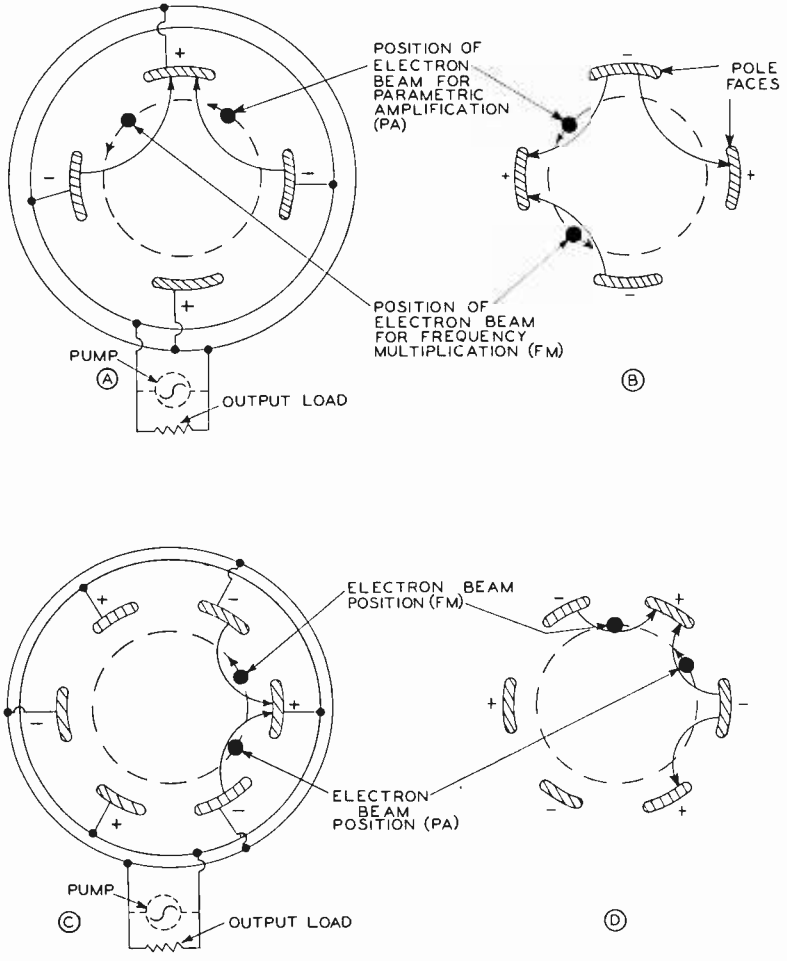

Fig. 11—Electric-field configurations and bunched-electron-beam position at two instants in time in the output coupler of the frequency multiplier and in the pump coupler of the parametric amplifier. (A and B) A four-pole azimuthal electric-field structure, (C and D) a six-pole azimuthal electric-field structure.

Any power dissipated in the resistive load results in a corresponding decrease in the radius of circulation of the bunched electron beam. In general, when a bunched coupling beam is passed through a concentric array of 2N pole faces in which an output load is coupled be-

tween adjacent pole faces, the coupling beam develops a signal having a frequency equal to N times the input-signal frequency of the input coupler, and the beam radius decreases to an extent corresponding to the energy dissipated in the output load.

Figure 12 is a photograph of an electron-coupler frequency-multiplier that was constructed to study the action of an azimuthal-traveling-wave device on a bunched coupling electron beam emerging from an input cavity. The basic structure is similar to that shown in

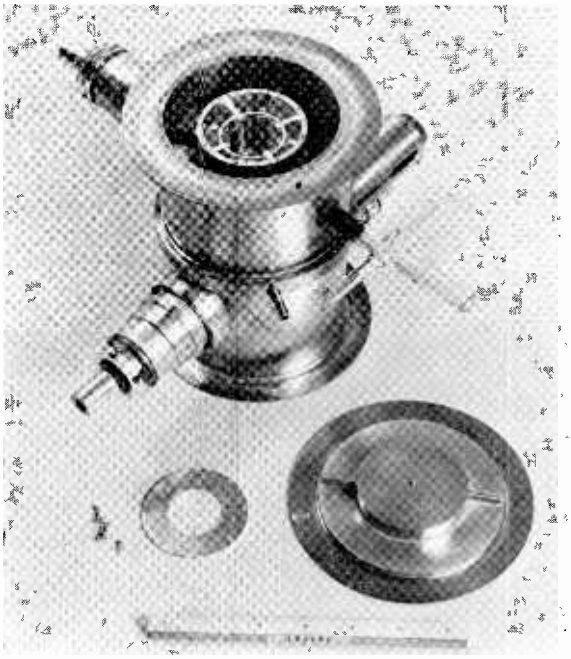

Fig. 12—Electron-coupler frequency multiplier with azimuthal-electric-field output-coupler structure.

Figure 10. An eight-vane cavity used as the frequency-multiplying coupler is tuned to π-mode resonance at 3200 megacycles, four times the frequency of the 800-megacycle input coupler. The interaction space defined by the vane tips is one inch in diameter and two inches long. An electron beam having a diameter of 0.050 inch is used as a coupling beam. This tube provided an output power of almost 5 watts at 3200 megacycles with power input to the input coupler of 100 watts at 800 megacycles. No 800-megacycle energy was observed at the output of the 3200-megacycle cavity.

The Electron-Beam Parametric Amplifier

Figure 13 shows a parametric amplifier in which a pump coupler is introduced between the input and output couplers. The pump coupler is a four-pole structure (basic to the "quadripole" structure of Adler and his colleagues).

As the coupling electron beam passes through the input coupler, it is bunched to form a rope-like beam having a radius which increases with increasing distance from the cathode, and having a final radius which is proportional to the signal strength of the input signal. The circulating bunched electron beam enters the pump coupler. A pump generator develops a twice-frequency voltage between adjacent faces

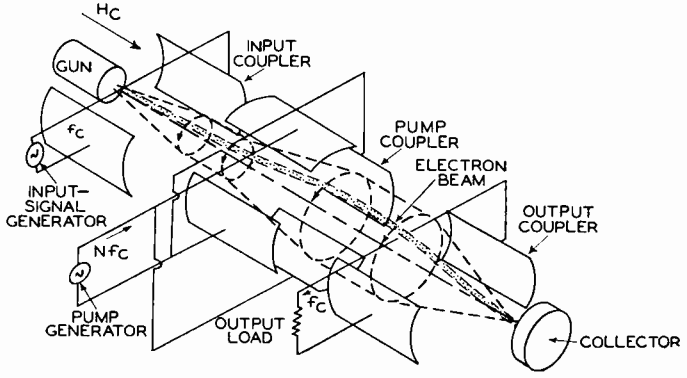

Fig. 13—Diagram of a parametric amplifier showing a four-pole pump-coupler structure between the input coupler and output coupler.

of an array of pole faces which are positioned to develop an azimuthal traveling electric field that has the angular velocity of the circulating bunched electron beam as shown in Figure 11. The electric field accelerates the electrons in the bunched beam so that the radius of the circulating motion increases. The energy corresponding to the increase in radius is supplied by the pump.

The bunched electron beam having a radius of circulation increased by the pump coupler leaves the pump region and enters the output coupler, where a matched load causes transfer of the circulating power to the output load. The electrons emerging from the output coupler have substantially zero-radius azimuthal motion for an ideal case.

The electron-beam parametric amplifier is capable of very-low-noise operation as a result of the nature of the input and output couplers. The output coupler is responsive only to bunched electrons circulating about the beam axis. The axially directed noise velocities of the electron beam, which are amplified in a traveling-wave tube

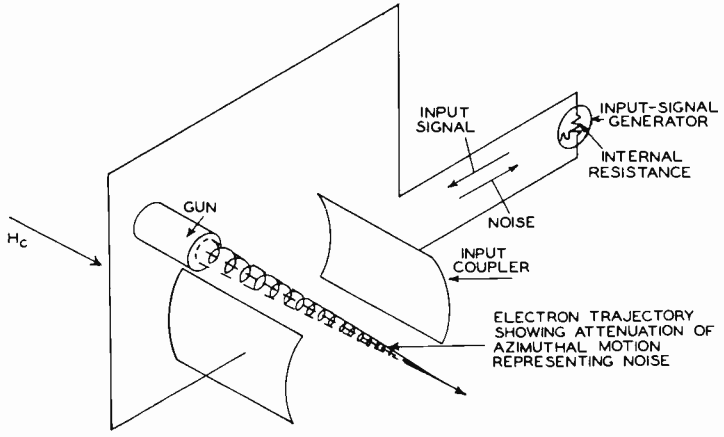

Fig. 14—Noise suppression of the cyclotron-frequency azimuthal noise velocities of an electron passing through the input coupler cavity.

by the normal electron beam and traveling-wave reaction, do not excite either the input or output couplers, nor are they amplified by the pump.

The input coupler performs an important noise-suppressing function in the manner shown in Figure 14. If any electrons enter the input coupler with circulatory motion representing noise energies that could excite the output coupler, the input coupler, which is loaded down by the driving signal generator, causes the circulating motion of the electrons entering the input coupler to induce noise voltage between the pole faces which, in turn, dissipates the noise energy in the driving-signal generator. Therefore, the radius of the circulatory motion of each electron (representing noise) decreases as the electron passes through the input coupler.

Adler, Hrbek, and Wade[2] reported a noise figure of 1.3 decibels, of which 0.4 decibel represents input-coupler loss, with a parametric amplifier designed to operate at 560 megacycles. The tube used a beam current of 35 milliamperes with a beam voltage of 6 volts. Gains in excess of 20 decibels were achieved with a few milliwatts of pump power. The magnetic field, which had the characteristic cyclotron frequency of 560 megacycles, was 200 gausses.

DETERMINATION OF THE IMPURITY DISTRIBUTION IN JUNCTION DIODES FROM CAPACITANCE-VOLTAGE MEASUREMENTS*

By

J. Hilibrand and R. D. Gold

RCA Laboratories,
Princeton, N.J.

Summary—*Reliable information on the impurity distribution in completed semiconductor junction devices is of value to the understanding of the device operation and in control of the fabrication processes. To be useful, the impurity density* level *should be accurate to better than twenty per cent and the impurity* profile *should be even more accurate. A method for the measurement of impurity distributions to the required degree of accuracy is described.*

Introduction

In 1942 Schottky pointed out that the impurity distribution could be determined from the dependence of transition capacitance on junction voltage.[1] The use of the proportionality of $1/C^2$ and the applied voltage for abrupt junctions[2] and of $1/C^3$ and the applied voltage in linearly graded junctions[3,4] has been described. Unless the shape of the doping profile (e.g., constant, linearly graded) is known in advance, however, differentiation of the raw capacitance–voltage data is necessary. If the impurity density varies rapidly, points which are closely spaced in capacitance are needed to minimize averaging of the calculated impurity distribution. On the other hand, with closely spaced points, differentiation of the experimental data results in very poor accuracy. The emphasis, then, must be on taking pains to obtain very precise capacitance and voltage data.

---

* Manuscript received April 13, 1960.

[1] W. Schottky, "Vereinfacht und erweiterte Theorie der Randschicht-gleichrichter," *Zeitschrift für Physik*, Vol. 118, p. 539, February, 1942.

[2] B. Goldstein, "Electron Mobility in the Germanium-Silicon Alloys," *RCA Review*, Vol. 18, p. 458, December, 1957.

[3] K. B. McAfee, W. Schockley, and M. Sparks, "Measurement of Diffusion in Semiconductors by a Capacitance Method," *Phys. Rev.*, Vol. 86, p. 137, April, 1952.

[4] L. S. Greenberg, Z. A. Martowska, and W. W. Happ, "A Method of Determining Impurity Diffusion Coefficients and Surface Concentrations of Drift Transistors," *Trans. I.R.E. PGED*, Vol. ED-3, p. 97, April, 1956.

The impurity distribution profile in outdiffused, alloy-junction germanium diodes[5] has been determined by the use of high-precision capacitance and voltage measurements. The raw data was smoothed and reduced to final form on a digital computer. The areas of these junctions were measured to an accuracy of ten per cent by means of etching to reveal the recrystallized region and microscopic examination. The estimated absolute accuracy for the determination of impurity concentration is about twenty per cent, with the error attributable mostly to inaccuracies in junction area determination. It should be noted, however, that the impurity *profile* is accurate to about ten per cent, since only the exact *level* of the calculated impurity concentration is affected by the area measurement.

Theory

The dependence of the variation of the junction depletion layer width on the ionized impurity concentration at the edge of the depletion layer is the basis for determining the impurity distribution. The desired relation is obtained from a double integration of Poisson's equation. Although the analysis which follows applies to a specific junction model, the "one-sided" junction, the results for other types of junctions are similar and extension is straightforward.* It is assumed that (1) the junction is planar; (2) the impurity concentration is much higher on one side of the junction than on the other so that the depletion layer extends only into the more lightly doped base material; (3) the impurity atoms are completely ionized, as is essentially the case for nondegenerately doped germanium at room temperature; and (4) the applied potential appears entirely across the junction.

Figure 1 shows the space charge, the field, and the potential profiles for a junction with arbitrary impurity distribution in the base. (The concentration on the other side of the junction is much greater than in the base region, as indicated.) Increasing the applied potential by dV_T results in an increase in depletion layer width by dw, and a corresponding change in the field and potential profiles, as shown. The differential change in field is obtained by integrating Poisson's equation graphically for the width w and for $w + dw$. The field is increased by the additional charge entering the depletion layer.

---

[5] C. W. Mueller, C. F. Stocker, J. Hilibrand, and R. D. Gold, "Parametric Diodes for Ultra-High Speed Computers," Paper presented at I.R.E. PGED Meeting, Washington, D.C., October 29-30, 1959.

* For example, the result for a symmetrically doped junction differs from that for an alloy junction only by a factor of two. Diffused junctions are treated later in this section.

$$dE = \frac{e}{\epsilon} N(w)\, dw, \tag{1}$$

where e is the electronic charge, ϵ the semiconductor permittivity, and $N(w)$ the *net* impurity concentration at the edge of the depletion layer. The differential voltage is again obtained from a graphical

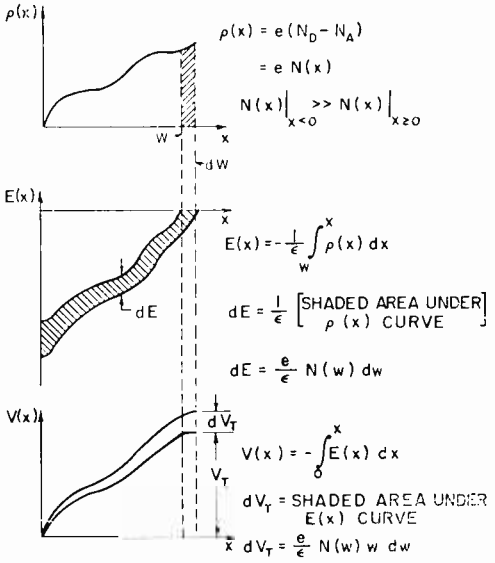

Fig. 1—Space charge, field, and potential for a one-sided junction.

integration and is given by the additional area under the $E(x)$ curve:

$$dV_T = \frac{e}{\epsilon} N(w)\; w\, dw = \frac{e}{2\epsilon} N(w)\; d(w^2). \tag{2}$$

Substitution of the capacitance expression

$$C = \frac{\epsilon A}{w}, \tag{3}$$

where A is the junction area, leads to the desired expression:

$$A^2 N(w) = \frac{2}{e\epsilon} \left(\frac{d\left(\frac{1}{C^2}\right)}{dV_T} \right)^{-1} \tag{4}$$

The impurity profile, $N(x)$, is obtained from a series of measurements, each of which yields an impurity concentration value using Equation (4). It should be noted in Equation (4) that errors in determining the area will lead to errors in $N(x)$, but that the shape of $N(x)$ is independent of the area.

The assumption of a one-sided junction may not be accurate for diffused junctions. The impurity distribution in the vicinity of such junctions can usually be approximated by

$$N(x) = N_B \, (\epsilon^{-bx} - 1), \tag{5}$$

where $N(x)$ is the net impurity concentration at a distance x from the metallurgical junction, N_B is the impurity concentration of the bulk semiconductor before diffusion, and b is a constant. The constant b can be determined in terms of the location of either edge of the depletion layer by imposing the requirement of net space-charge neutrality. It can be shown that the impurity concentrations at the opposite edges of the depletion layer are related to the equivalent impurity concentration for a one-sided junction by

$$\frac{1}{N_1} + \frac{1}{N_2} = \frac{1}{N_t}. \tag{6}$$

Here, N_1 and N_2 are the concentrations at the depletion layer edges for a specified junction voltage, and N_t is the concentration given by Equation (4) for the "one-sided" junction with the same voltage.

The use of these relations directly would require the evaluation of the constant b. It is usually simpler, however, to use curves developed by Lawrence and Warner[6] for the division of the depletion layer width, a_t, between the widths of the two sides, a_1 and a_2, in a diffused junction and to apply this result in Equations (5) and (6). This results in the curves of N_1/N_T and N_2/N_T as functions of a_1/a_t in Figure 2. When little is known about the nature of the actual diffusion process, of course, it is necessary to resort to a careful interpretation of the values of N_T obtained for a range of voltages in order to establish a value for the constant b.

---

[6] H. Lawrence and R. M. Warner, Jr., "Diffused Junction Depletion Layer Calculations," *Bell Sys. Tech. Jour.*, Vol. 39, p. 389, March, 1960.

Experimental Procedure

Capacitance was measured using a Boonton Electronics Corp. type 75A capacitance bridge. This is a fixed-frequency (1-megacycle) bridge which reads to 0.0002 micromicrofarad with an accuracy of ± 0.25 per cent in the absence of any shunt conductance. It is

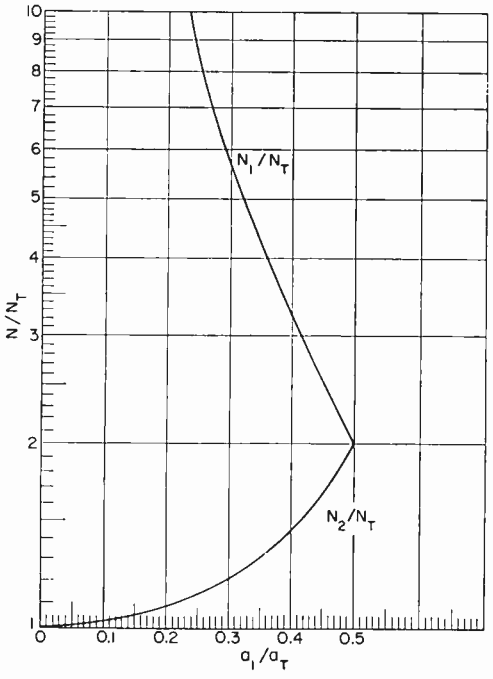

Fig. 2—Correction factors for diffused junctions.

reasonable to expect that the fluctuations of the error over a five or ten per cent range in capacitance are considerably less than the ± 0.25 per cent accuracy of the bridge. Measurements can be made with shunt resistances down to 1000 ohms, and capacitances up to 1000 micromicrofarads. The bridge signal amplitude was decreased to less than 10 millivolts r-m-s by means of a 20-decibel attenuator in the line from the oscillator to the bridge and by the use of the signal-amplitude control of the instrument. The panel null indicator of the bridge was replaced by a more sensitive microammeter to increase sensitivity to the null at balance. A bias supply was used which permitted precise measurement of the applied diode voltage with a

potentiometer. With these instruments, data could be taken to four significant figures.†

In order to obtain a series of impurity concentration values for several depletion layer widths, a series of "clusters" of six voltage–capacitance points at one to two per cent intervals in capacitance was taken. For the range covered by each cluster, it was assumed that the capacitance could be given by

$$C = \frac{K}{(V+\phi)^n}, \tag{7}$$

where K, ϕ, and n are constant within each cluster. These constants were evaluated to give a best "least squares" fit to the logarithm of Equation (7). The impurity concentration was then calculated in terms of these constants:

$$A^2N(w) = \frac{K^2}{ne\epsilon}(V+\phi)^{1-2n}. \tag{8}$$

The location of the edge of the depletion layer, w, is given by

$$\frac{w}{A} = \frac{\epsilon}{C_a}, \tag{9}$$

where C_a is the capacitance obtained from Equation (7) for the average voltage of the "cluster."

The concentration and depletion-layer width were obtained from the capacitance–voltage data using a computer. A computer program has been written so that, for each "cluster" of capacitance–voltage points, a best "least squares" fit to the data is obtained from

$$\log C = \log K - n \log (V+\phi). \tag{10}$$

The best fit is made to $\log K$ and n for each of a series of selected ϕ values. This has two advantages over obtaining a least-squares fit directly from Equation (7). First, Equation (10) gives equal weight to all the points in the cluster for the best fit, whereas Equation (7) would favor the higher capacitance points in the cluster. Second, since (10) is linear in $\log K$ and n, the best values for these constants are

† For diodes with large shunt conductance, capacitance could be read to only three significant figures.

obtained explicitly for each chosen value of ϕ. Obtaining a least-squares fit for an equation which is not linear (or a polynomial), on the other hand, involves a series expansion and possible difficulty with convergence.

To determine the junction area, the diode case was disassembled and the alloy dot removed by an HCl etch. This revealed the recrystallized region (which is not attacked by HCl), and the area was photographed through a microscope and measured with a planimeter. The area is estimated to be accurate to within 10 per cent. A typical photomicrograph is shown in Figure 3. The accuracy of this technique

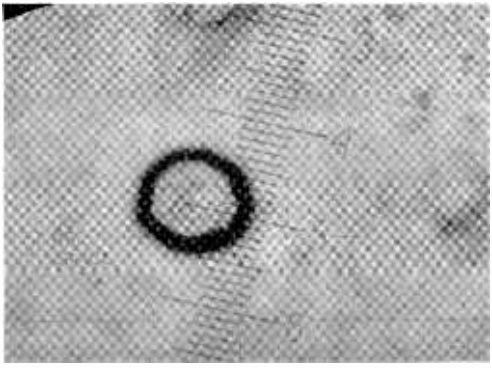

Fig. 3—Typical photomicrograph of recrystallized region (junction area, A, is 7.7×10^{-6} cm^2).

was checked by measurements on diodes with known uniform base-material impurity density. The result for a typical diode is shown in Figure 4. The known doping as derived from a precise four-point probe measurement on the crystal is indicated. It is seen that very good agreement is obtained. The impurity profile for a parametric diode supplied by C. W. Mueller of RCA Laboratories is also shown. The usefulness of this technique is emphasized by the appreciable impurity density variation in the vicinity of the junction.

Table I shows the values of the normalized sum of residual squared, R, for each $N(x)$ point of a particular diode.

$$R = \sum_{i=1}^{6} \left(\frac{C_{ci} - C_{mi}}{C_{mi}} \right)^2 \tag{11}$$

where C_{mi} represents the six measured capacitance values for each cluster and C_{ci} represents the six calculated capacitance values for

Table I—Normalized Sum of Residual Squared (R) for Each $N(x)$ Point of Diode #771.

$N(x)$	R
2.7×10^{17}	.000059
2.1×10^{17}	.000018
2.0×10^{17}	.0000013
1.6×10^{17}	.0000009
1.4×10^{17}	.0000010
1.1×10^{17}	.0000042
1.0×10^{17}	.000057

each cluster. It is seen that the measured data for each cluster fits the logarithm of Equation (7) to better than one per cent.

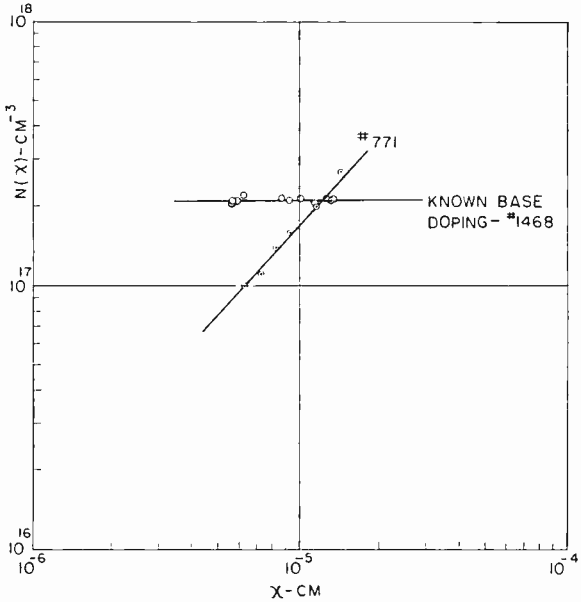

Fig. 4—$N(x)$ versus x for outdiffused junction diode (#771) and abrupt junction diode (#1468).

Conclusions

The impurity distribution in fabricated junction devices can be determined by capacitance–voltage measurements. Instruments of sufficient precision are now available. The accuracy of the impurity level determination is limited primarily by the junction area measurement and is better than 20 per cent. The shape of the impurity profile can be determined to 10 per cent. The quantities of interest can be calculated on a computer directly from the measured data.

SINE-SQUARED PULSES IN TELEVISION SYSTEM ANALYSIS*

By

R. Kennedy

National Broadcasting Company, Inc.,
New York, N. Y.

Summary—The development of sine-squared pulse testing as it has occurred in Europe is traced, followed by a comparison of Heaviside step versus sine-squared pulse spectra and their effect on a system. The methods of pulse generation are next presented. The methods of testing various portions of system bandwidths by use of shaped bars, T, and 2T pulses are discussed. Rating factors, time-series computations, envelope delay, and linearity testing are also considered.

Introduction

DELINEATION of suitable signals for accurate appraisal of the performance of a particular transmission system always offers a challenge. This is particularly true of wideband systems such as radar, microwave, computers, and television. Furthermore, the greater the number of criteria used to judge a system, the greater the complexity of a test signal or, alternatively, the greater the number of individual test signals which must be used.[1] Evaluation of over-all system performance while the circuit is in use[2] is still more difficult.

The nature of television signals is such that the system must meet the most rigorous of standards, especially when color-television signals are being transmitted.[3] Among the various distortions which can affect a color signal are amplitude and phase versus frequency, linearity of amplification versus signal level, differential gain and phase, and transient response. Suitable signals have been available for testing the amplitude-versus-frequency response by means of multiburst, linearity by means of stair steps, and differential gain and phase by means of modulated stair steps. Recently, use of the sine-squared

* Manuscript received April 24, 1960.

[1] Howard C. Gronberg, "Routine Tests and Alignment Procedures for Amplifiers and Circuits Used for Color T.V.," Paper Presented at NARTB Engineering Conference, Chicago, May, 1954.

[2] Ralph C. Kennedy, "A Dynamic Standard Signal for Black-And-White and Color Television Systems," *IRE National Convention Record*, Part 7, p. 17, March 18-21, 1957.

[3] R. C. Kennedy, "Color Television — System Performance Requirements," *Amer. Inst. of Elec. Eng.*, Part I, Communications and Electronics, Vol. 75, p. 653, January, 1957.

pulse has begun to be accepted here in the United States.[4] This signal offers some interesting possibilities not only in transient evaluation of television systems but also in the areas of envelope delay and linearity testing.

The pioneer work on all the techniques described here have long been known to investigators in England and on the Continent.[5-9] In fact, Eurovision broadcasting has benefited greatly by sine-squared pulse testing techniques. The magnitude of the problems encountered in Europe may be appreciated when one considers the fact that scanning rates of 405 lines, 625 lines, and 819 lines are all currently in use in Europe.

Theory of Waveform Choice

The sine-squared pulse supplements and augments rather than replaces other test signals. Initially, the sine-squared pulse was intended to fulfill a very specific need as a transient test tool. As such, it appears to be particularly well chosen, since it permits an accurate evaluation of the performance of a system by subjecting the system to the same form of data as that encountered during actual picture transmission. Cooper[10] has shown that horizontal scanning across a vertical black-to-white transition by a conventional camera tube whose beam has a finite diameter does not result in an abrupt change in output-signal voltage. Instead the change is somewhat "S" shaped having sharp knees at the bottom and top with reverse curvature in the middle. The whole transition closely resembles the peak-to-peak excursion of a sinusoid, as shown in Figure 1.

Further investigation shows that the frequency of the sine wave is limited by and equal to the system bandwidth for conventional camera tubes. Actually, the period of the sine wave from the camera

---

[4] R. C. Kennedy, "Sine-Squared Pulses Test Color-TV Systems," *Electronic*, p. 138, December, 1954.

[5] Comité Consultatif International Téléphonique. 16th Plenary Assembly, Florence, 1951.

[6] I. F. Macdiarmid, "A Testing Pulse for Television Links," *Proc. British I. E. E.*, Vol. 99, Part III A, p. 436, May, 1952.

[7] N. W. Lewis, "Waveform Computations by the Time-Series Method," *Proc. British I.E.E.*, Vol. 99, Part III, p. 294, September, 1952.

[8] N. W. Lewis, "Waveform Responses of Television Links," *Proc. British I.E.E.*, Vol. 101, Part III, p. 258, July, 1954.

[9] Hans E. Froling, *Das Prüfzeitenverfahren beim Fernsehen*, Funkschau, 1958, 2, Marz-Heft 6.S.135, 137.

[10] V. J. Cooper, "High Power Television–Transmitter Technique, With Particular Reference to the Transmitter at Holme Moss," *Proc. British I.E.E.*, Vol. 99, Part IIIA, p. 231, April, 1952.

tube is equal to twice the period represented by the beam diameter. This period represents the maximum resolution of the camera tube, which is somewhat higher than that possible in the conventional 4-megacycle system. The pulse suitable for testing such a system has a frequency of 4 megacycles. It is common practice to define the test

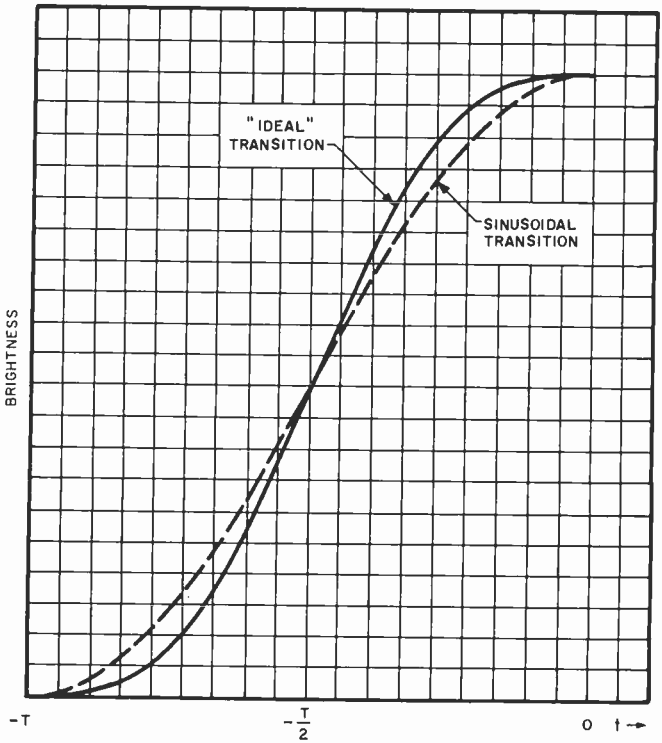

Fig. 1—Brightness versus time of a spot of light crossing a black-to-white transition.

pulse in terms of its half amplitude duration (h.a.d.), T, as shown in Figure 2. The relationship between system bandwidth, f, and T is given by

$$f = \frac{1}{2T}.$$

For a 4-megacycle system, T is 0.125 microsecond. It is also common practice to set the pulse on the conventional synchronizing waveform. Thus, the pulse has a repetition rate equal to line frequency.

Pulse Spectrum

Fourier analysis of such a waveform shows that there are components in its spectrum spaced every 15,750 cycles extending up to a frequency $f = 1/T$. The general shape of the spectrum amplitude closely approximates the response of a low-pass filter. At $f = 1/(2T)$, the amplitude of the component is down 6 decibels in power from the fundamental amplitude. At $f = 1/T$, the spectrum amplitude is zero and remains at least 35 decibels down from the fundamental amplitude for all higher frequency components (see Figure 3). Thus, the test

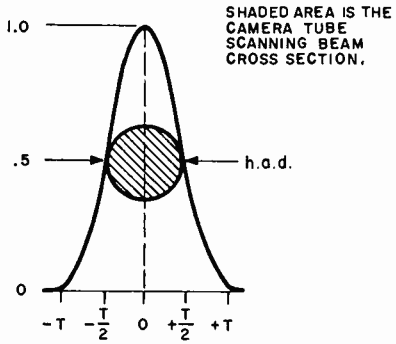

Fig. 2—Relationships existing between beam diameter, maximum frequency of resolution, and the half amplitude duration.

pulse has accurately predictable and controllable components which test the system in the frequency range of normal use. This is one essential difference between sine-squared pulse testing and the usual square-wave test signal. The square wave has components which extend far beyond the bandwidth required. These components cause overshoot, ringing, and phase shift which do not normally occur in the video. As a result, the transient response will appear much worse than it really is; the system bandwidth would have to be vastly and unnecessarily extended to make the square-wave response appear satisfactory.

Not only does the sine-squared pulse test the system in the proper frequency range, but it also does so more rigorously. As is well known, the ideal bandwidth limiting of a perfect system results in a Heaviside step having a Gibb's overshoot of 8.9 per cent. The same system causes 13 per cent overshoot in a sine-square pulse as it becomes $\sin x/x$ in shape (see Figure 4). As a result, the sine-squared pulse makes a more sensitive test means than the square wave.

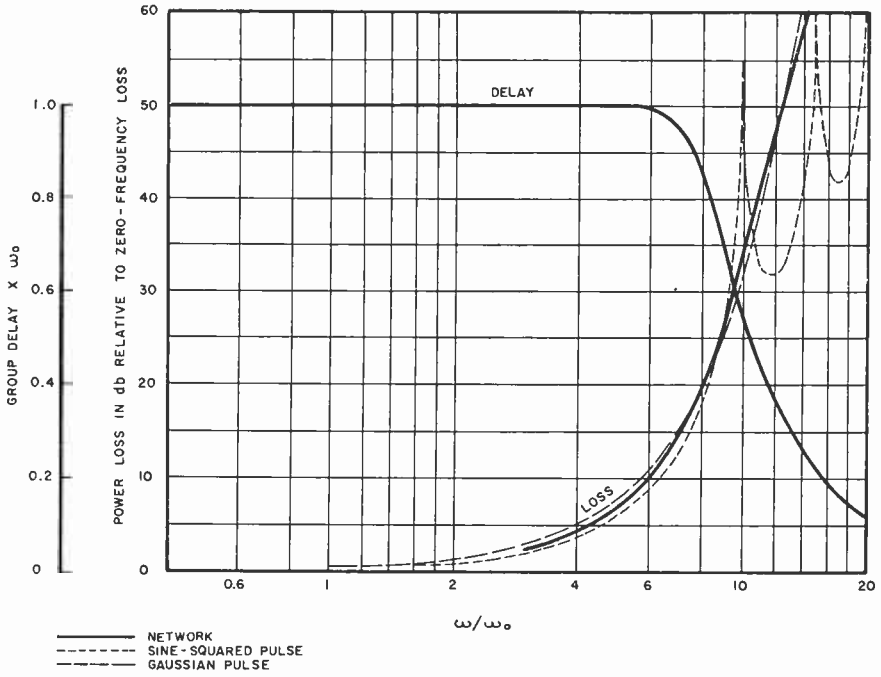

Fig. 3—Normalized spectra of pulse-shaping network, a sine-squared pulse, and a gaussian pulse and the group delay of the network.

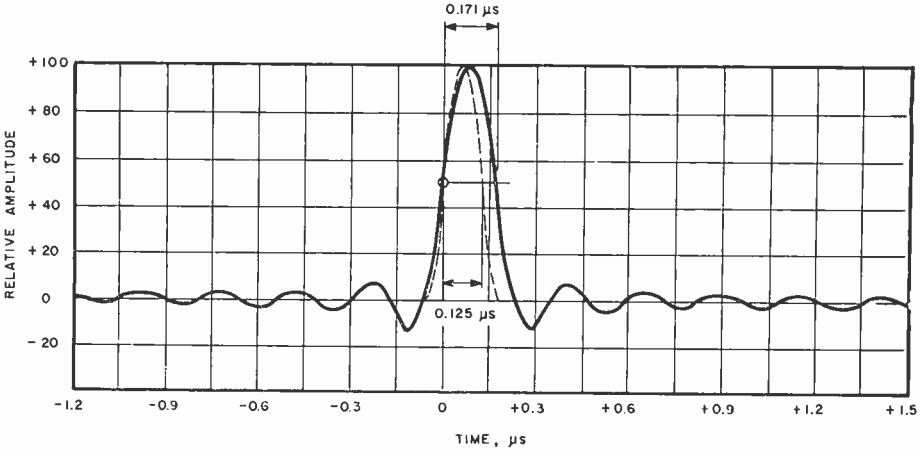

Fig. 4—The response to 0.125 μsec sine-squared pulse by ideal 4-megacycle per second low-pass filter.

Further, the group delay characteristic of the pulse is constant to a frequency well above $1/(2T)$. Thus, extremely precise symmetry around the pulse maximum-amplitude axis exists. This makes the pulse particularly sensitive to phase distortion. Moreover, the type of phase shift occurring in a system is clearly shown by the pulse. If high-frequency delay is less than for low frequencies, a ripple occurs on the leading side of the pulse, as shown in Figure 5. If the opposite type of delay exists, the ripple follows the pulse.

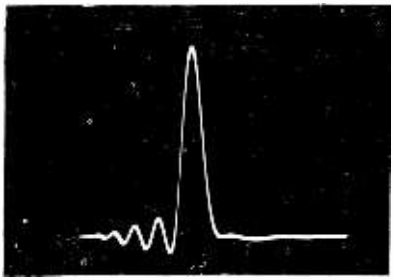

Fig. 5—The response to a sine-squared pulse by a filter having decreasing delay versus frequency.

Reproducibility of Pulse

A further advantage of the sine-squared pulse is the fact that pulse generators can easily be built to generate pulses whose actual shape deviates less than 1 per cent from the true mathematical sine-squared pulse shape (see Figures 6 and 7). Thus, good uniformity of test pulses is possible.[6,11,12] Furthermore, the essential active element is a blocking oscillator whose output wave shape closely approximates the legs of an isosceles triangle. This impulse is shaped into a sine-squared pulse by means of a passive network. Once the filter elements have been properly measured and assembled, the desired pulse shape will be assured for wide variations in tube characteristics. It should be noted that this is in marked contrast to square-wave generators, whose waveforms do not have constant shapes during tube aging nor the same shape for a group of generators.

Testing Techniques

Transient testing of wideband systems creates the demand for

[11] W. E. Thomson, "Networks with Maximally-Flat Delay," *Wireless Engineer*, Vol. 29, p. 256, October, 1952.

[12] W. E. Thomson, "Delay Networks having Maximally Flat Frequency Characteristics," *Proc. British I.E.E.*, Vol. 96, Part III, p. 487, November, 1949.

several test pulses each of which is sensitive to distortions occurring in different portions of the system bandwidth. To assure proper transmission of the vertical component, a test signal must be capable of revealing frequency response and, particularly, the phase response

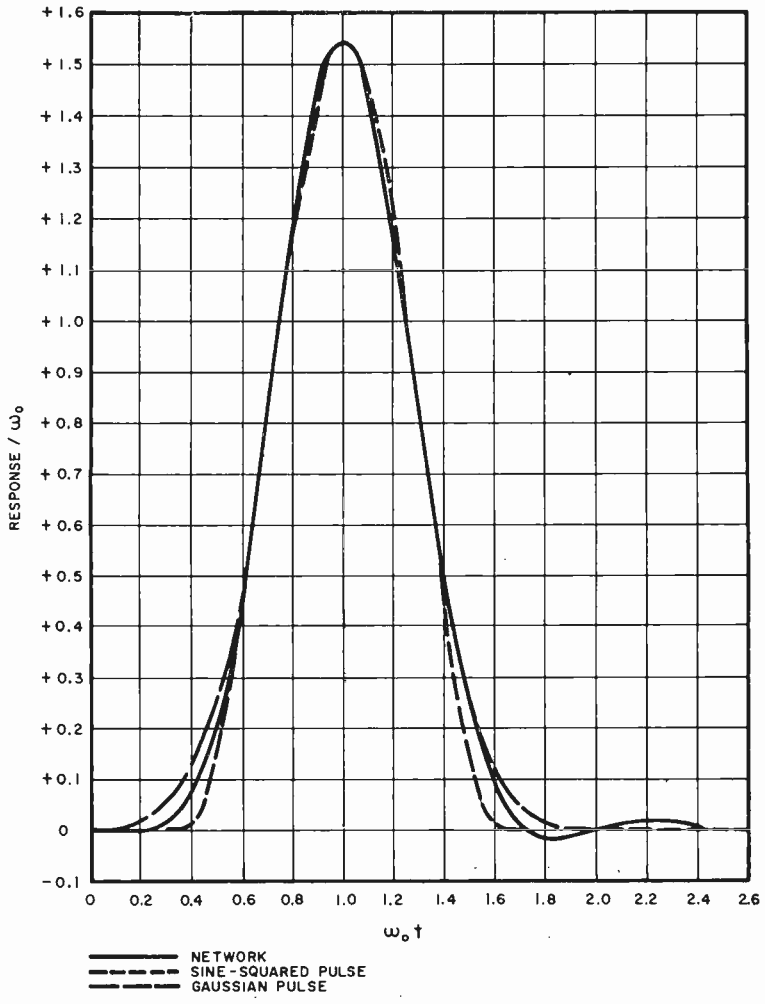

Fig. 6—Distortion present in response of pulse shaping network versus sine-squared and gaussian pulses (calculated).

of the region around 60 cycles. Proper performance of clamper amplifiers is also essential. It is highly desirable to have some test means for evaluating pulse tilt at line frequency so as to be able to test such

amplifiers. It is also necessary to test the system in both its midband and upper-frequency portions.

It has become common practice, therefore, to utilize four test signals. First, the common 60-cycle square wave and submultiples are used to determine the performance of systems components which do not have clampers in them. The amount of tolerable tilt is engraved on a scope graticule so that one may quickly judge the acceptability of a component.

The second test waveform is a shaped-bar type of signal commonly called "window" in this country. The bar has a duration of approximately one half line. The rise and fall edges of the bar are given a

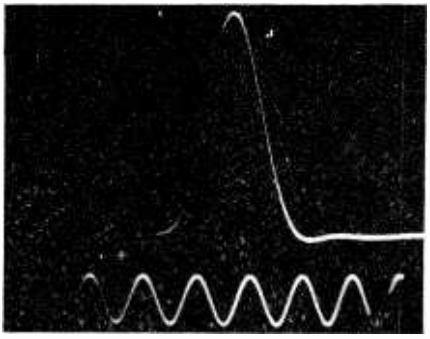

Fig. 7—Sine-squared pulse at shaping network output. (Compare with Figure 6.) An 8-megacycle timing wave appears below the pulse.

sine-squared shape corresponding to the $2T$ pulse. Thus, there are no components in the bar spectrum having frequencies above 4 megacycles and no ringing can appear on the bar. This signal is particularly sensitive to distortions from line frequency up to several hundred kilocycles. As a result, malfunctioning of clampers which cause smear or streaking in a picture may be observed and properly corrected.

The third test signal is the $2T$ sine-squared pulse. It, like the shaped bar, contains no data above 4 megacycles. It has an h.a.d. of 0.25 microsecond for a 4-megacycle-bandwidth system. It is particularly sensitive to distortions occurring in the spectrum between about 0.5 and 2 megacycles. As such it is well suited for routine adjustments of a system where it is not possible or desirable to make a detailed system analysis.

The fourth, or T pulse, is reserved for the upper region of the spectrum. It has an h.a.d. of 0.125 microsecond for the 4-megacycle system. Its spectrum is 6 decibels down in power at 4 megacycles and is zero at 8 megacycles. It therefore contains sufficient data to permit

evaluation of the transient conditions in the region of cutoff in the sideband filter of the transmitter where excessive phase shifts may occur.

It is conventional to transmit the shaped bar during the last half of a horizontal line and to precede it with either the T or $2T$ pulse on the same pedestal (see Figure 8). The generator usually has a switch for selecting the desired pulse.

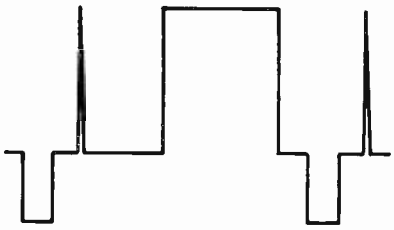

Fig. 8—Combined pulse and bar test signal for system testing.

Rating Factor

It was recognized quite early in the investigations in Europe that little correlation existed between transient and steady-state testing, since time and frequency domains are mathematically related by transforms (e.g., LaPlace, Heaviside, Fourier, Mellin). Thus, for example, no assurance could be given that doubling the system bandwidth would produce improvement in picture quality. Further, a broad dip of about 2 decibels at, for example, 50 kilocycles will cause far more waveform distortion than a very sharp hole of 5 or 10 decibels at 500 kilocycles.

In order to develop a means of correlating picture quality with system characteristics, the British Post Office Department and the BBC conducted a series of interesting tests. A group of about twenty television engineers were chosen as subjective observers. A scanner and monitors were set up and a sequence of different test slides was chosen. The circuit between the scanner and the monitors was distorted in a particular manner. The slides were viewed on the monitors and evaluated on a scale of five. A sine-squared pulse was then fed through the circuit and its waveform photographed. Numerous forms of distortion were introduced and individually treated in the same manner. Separate steady-state measurements were also made.

With these data it was possible to evolve what is termed a rating factor for the system. The rating factor is a number assigned to a

system based upon the quality of sine-squared pulse transmission. For certain forms of distortion, a 5 per cent rating factor may produce a totally useless picture. A 3 per cent rating factor is usually acceptable for remote circuits or complete systems. Some of the newer circuits in England have rating factors of 0.25 per cent.

One virtue of the rating factor is that two different methods of evaluating circuit performance are possible. The "routine-test" method permits evaluations of remote circuits and daily tests of transmission equipment. It consists of a few simple measurements using a standard oscilloscope and the ratings given in Table I.

Table I

Per Cent Distortion	Maximum half-amplitude duration (μsec)	Minimum Ringing Frequency (mc)	First Lobe (negative) Leading or trailing (%)	Second Lobe (positive) Leading or trailing (%)
1	.185	4	10	6
2	.190	4	12	8
3	.195	4	14	9
4	.200	4	16	10
5	.205	4	18	11
6	.210	4	20	12

The second method of circuit evaluation is by the "acceptance test." Photographs of the system output waveforms are taken and include an 8-megacycle sine wave as a time base. The waveform is divided into intervals of 0.125 microsecond starting with the axis of maximum pulse amplitude as zero. A comparator microscope is used to measure the waveform ordinates at each time interval. All ordinates are normalized using the maximum pulse amplitude as unity. A time series is then formed from these data. It is the realization of the time-series that makes the sine-squared pulse such a powerful tool both for analysis and synthesis. With it, one is able to answer such questions as:

1. Given the individual time-series (responses) of each of a chain of different circuits to a specified signal, what would be the over-all response of the chain to the same signal? (Thus, if we know the time-series for New York to Chicago, Chicago to Denver, and Denver to Los Angeles, individually, we can compute the New York to Los Angeles response.)

2. Given the waveform responses of the whole and one part of a chain of networks to a specified signal, what response would the remaining part have to the same signal? (This is essentially a statement of the equalizer problem. If the desired response is known as well as the response of the circuit alone, it is possible to determine the response which an equalizer must have to correct for the circuit deficiencies.)

EQUALIZERS

Considerable work has been done on the design of equalizers which will provide a wide range of equalization for correcting waveform responses. One type[13] which is particularly suitable for correcting remote circuits or other temporary applications makes use of the echoes occurring on tapped delay lines. This is a manually adjustable device, and optimum equalization is obtained by visual inspection of the equalizer output as adjustments are made.

Another equalizer has also been developed which permits manually optimizing the response. The various adjustable components are calibrated. From the readings, it is possible to design a fixed equalizer having the same time response, and this equalizer may then be substituted for the adjustable equalizer.

VERTICAL INTERVAL TESTING

The American Electronics Industries Association (EIA) in making recommendations for vertical interval test signal transmissio suggested that such signals be confined to the last 12 microsecond of line 17 and all of lines 18, 19, and 20 of the vertical blankin interval. Line 1 of field 1 begins with the first equalizing pulse. Li 1 of field 2 begins ½ line after the first equalizing pulse.

In addition to uses already discussed, it should be pointed out t the sine-squared pulse and bar signal may be transmitted during l 18, 19, and 20 of the vertical blanking interval so as to prov a constant means of evaluating system performance. This technique had its origins in Germany[14] in 1952 and has become widely used in Europe and here.

---

[13] J. M. Linke, "A Variable Time-Equalizer for Video-Frequency Waveform Correction," *Proc. British I.E.E.*, Vol. 99, Part IIIA, p. 427, May, 1952.

[14] Hans E. Froling, German patent No. 949,350. Process of Checking Transmission Properties in Television. Issued October 4, 1953.

Envelope Delay in Color Systems

There is another area where it appears that the sine-squared pulse may have some application. The FCC standards for color television include an envelope-delay specification. The intent is to assure the same time delay for the luminance as for the chrominance component of the signal. A very simple technique for determining the delays has been proposed[15] wherein a T-pulse (h.a.d. of 1 microsecond) or a $2T$ pulse (h.a.d. of 2 microseconds) for Q-channel testing is modulated by the subcarrier sine wave during alternate lines. Thus, the T pulse has a duration of 3.58 cycles of subcarrier and the $2T$ pulse a duration of 7.16 cycles. Since lines having the sine-squared pulse alternate with lines having the modulation, it is possible to superimpose the two waveforms by proper adjustment of the oscilloscope. If the time delay for the pulse (luminance component) is different from the modulation (chrominance component), they will not register and the difference in delay may be easily determined. Further, this same presentation shows whether the frequency response of the system is flat, since complete registry should occur.

Linearity Testing

As indicated earlier, the sine-squared technique may be used for linearity testing. The conventional signal used for testing linearity is the stair step. Usually ten steps are used. For the proposed test, the number of steps is first reduced to five and the signal is introduced into the system. At the output, the signal is differentiated so that spikes all having a common base result. This signal is fed into a sine-squared pulse-shaping filter so as to bandwidth limit the noise and is then presented on an oscilloscope. It is a simple matter to see whether all five pulses have identical amplitude (the case for perfect linearity).

The shaping filter should be such as to produce a 2.75 microsecond h.a.d. pulse in the conventional manner. The response is 6 decibels down at 182 kilocycles and zero at 364 kilocycles. If more steps are used, it becomes necessary to use narrower pulses which, in turn, have greater bandwidth and consequently introduce more noise and error.

Conclusions

A survey of the uses of the sine-squared pulse has been presented.

---

[15] I. F. Macdiarmid and B. Phillips, "A Pulse-and-Bar Waveform Generator for Testing Television Links," *Proc. British I.E.E.*, Vol. 105, Part B, p. 440, September, 1958.

Areas wherein the use of sine-squared pulses offers advantages over conventional test signals for evaluating circuits and its application in establishing techniques for general picture enhancement have been discussed.[16] The equipment for some uses is complex, while for others it is relatively simple.

ACKNOWLEDGMENT

It would be very difficult indeed to give credit to all the various workers who have made contributions to this broad subject. However, the following people have shown me work being pursued in their laboratories while I was in Europe in 1955 and 1958.

Dr. A. R. A. Rendall, Mr. S. N. Watson and Mr. Geoffrey G. Gouriett of the BBC; Drs. N. W. Lewis and J. M. Linke and Mr. I. F. Macdiarmid of the Post Office Research Station at Dollis Hills, London; Dr. R. Jacob of Sender Freies, Berlin; and Mr. P. Denis of Radiodiffusion et Télévision Française, Paris.

I should also like to express appreciation to A. L. Hammerschmidt and to George M. Nixon of NBC for valuable suggestions during the preparation of this paper.

[16] I. F. Macdiarmid and B. Phillips, "Waveform Distortion in Television Links," *The Post Office Electrical Engineers Jour.* (British), Vol. 52, Parts 2 and 3, July and October, 1959.

A NEW MINIATURE BEAM-DEFLECTION TUBE*

By

M. B. Knight

RCA Electron Tube Division,
Harrison, N. J.

Summary—A new method for beam-deflection control of plate current has been developed and applied to a tube design that uses beam-deflection control in addition to conventional grid control. The new tube, the 7360, is a nine-pin miniature type especially suitable for use in modulators, demodulators, and converters. It has an "electron gun" that comprises a cathode, a control grid, and a screen grid; a deflection structure that includes two grid-like deflecting electrodes; and two plates. Beam currents of several milliamperes can be deflected from one plate to the other by means of a potential difference of a few volts between deflecting electrodes.

Introduction

Beam deflection has been used in the past for sensitive control of current in high-frequency tubes. Although excellent performance has been obtained, it is very difficult to achieve sensitive control of beam currents higher than a fraction of a milliampere, and beam deflection has not been economically competitive with conventional grid control. It has been recognized, however, that beam deflection is more desirable than grid-No.3 control as the "outer control" means in product-modulator tubes.[1]

In pentodes and pentagrid tubes, the space current is determined by the voltages on grid No. 1 (control grid) and grid No. 2 (screen grid); the fraction of the space current passed on to the plate is controlled by the potential at grid No. 3. As a first approximation, therefore, the plate current is a function of the mathematical product of grid-No.1 and grid-No.3 voltages. Errors in the approximation arise from nonlinear characteristics of both grids, and from the fact that grid-No.3 voltage affects cathode current. This effect on cathode current is due, in a small degree, to the penetration of the field of grid No. 3 through the screen and control grids. The most serious cause, however, is that the electrons turned back from grid No. 3 reach the grid-No.1–cathode region and alter the space charge. Other effects

* Manuscript received February 8, 1960.

[1] R. Adler and C. Heuer, "Color Decoder Simplifications Based on a Beam-Deflection Tube," *Trans. I.R.E. PGBTR*, p. 64, January, 1954.

of the returned electrons are undesired coupling from grid No. 3 to grid No. 1 and variations of input loading of grid No. 1. The degree of influence of grid-No.3 voltage upon cathode current is a good indicator of the magnitude of these adverse effects. In conventional pentodes, such as the 6AS6, grid No. 3 has about one-third the control over cathode current that it has over plate current. The effect is reduced to about one-twentieth in pentagrid converters, which are designed to return electrons along different paths as much as practical.

In the beam-deflection tube, the electrons always move away from the cathode; thus, the major cause of interaction with the control grid is eliminated. Furthermore, balanced operation of the deflecting electrodes minimizes the influence of the deflecting-electrode signal voltage on the electric field near the cathode, and tends to neutralize capacitance coupling between deflecting electrodes and control grid. Another advantage is that both plates may be used for output signals in push-pull. Although output may be obtained from the screen grid of tubes having grid-No.3 control, the resultant feedback is usually not tolerable. The beam-deflection tube design described in this paper has further advantages of quite linear and almost exactly symmetrical deflection characteristics. It has transconductance about equal to that of good pentagrid converters, although its plate resistance is much lower. Its transconductance falls a little short of that of the best suppressor-grid-control pentodes.

Design of Beam-Deflection Tubes

The principle of beam deflection leads conventionally to a structure resembling that of a cathode-ray tube except that the electrodes are designed to produce a ribbon-like beam rather than a circular beam and to move the beam from one plate to the other. The tube cross section shown in Figure 1 illustrates this principle as applied to one experimental design.

Both the sharpness of beam focus and the distance the beam travels after deflection influence deflection transconductance. However, as the distance is increased to obtain higher deflection sensitivity, the beam tends to spread due to space charge; the net result is that the length of beam travel is of secondary importance. The velocity of electrons passing the deflecting electrodes also has a secondary effect on deflection transconductance in that low velocity increases deflection sensitivity, but beam focus suffers.

The most important factors in the design are the length of the deflecting electrodes and the spacing between them. For best deflec-

tion transconductance, the deflecting electrodes must be placed as close as possible to the beam throughout their length. However, the spacing must be sufficient to permit the beam to be deflected from one plate to the other without striking the deflecting electrodes. Design for minimum spacing leads to appreciable current collection by the deflecting electrodes because practical beams do not have sharp edges. Another fault of design for minimum spacing is that a part of the beam

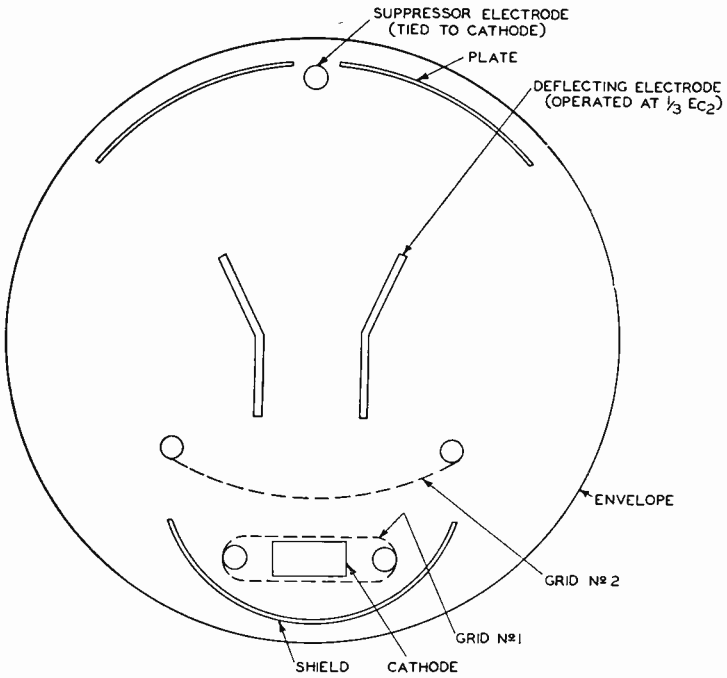

Fig. 1—Cross section of experimental tube using conventional beam-deflection principles.

current is collected by the deflecting electrodes as soon as the deflection exceeds the amount required to just switch the beam. With further increase in deflection, the amount of current collected by the deflecting electrodes increases until almost all of the current is collected by the deflecting electrodes. Even if the tube is designed so that the deflecting electrodes operate with negative bias, the instantaneous voltage is necessarily positive on the electrode that is approached by the beam. Any practical design is compromised by this factor of deflecting-electrode current.

Design of Type 7360

The beam-deflection structure used in the 7360 circumvents several of the problems associated with conventional structures. The major innovation is the use of porous deflecting electrodes. The beam passes through these electrodes to plates situated alongside them. This structure is shown in cross section in Figure 2. The deflecting electrodes operate at an average voltage which is only slightly positive with

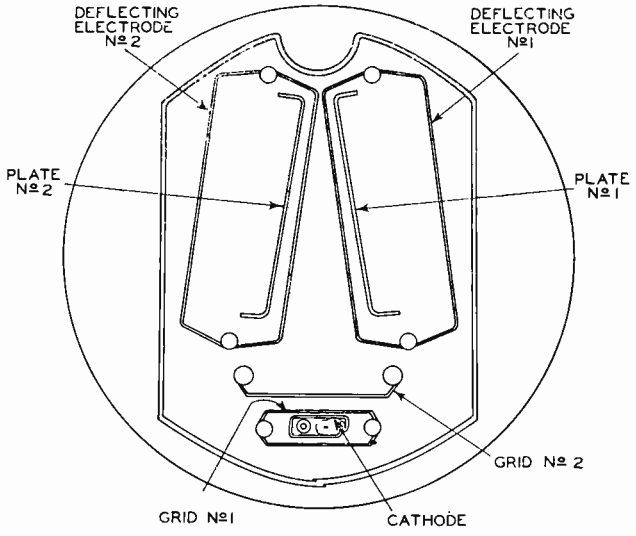

Fig. 2—Cross section of 7360 beam-deflection tube.

respect to cathode and, therefore, intercept only a small fraction of the beam current regardless of whether the beam is deflected not at all or far beyond the point at which all the current flows to one plate. Thus, the deflecting electrodes may be placed very close to the beam for most of the length of beam travel. This arrangement results in high deflection transconductance without abnormal deflecting-electrode current.

The porous deflecting-electrode construction also eliminates the need for the extremely sharp electron-beam focus that is required when solid deflecting-electrode construction is used. Although it is very important that the electrons be directed along the proper converging paths, sharp focus, a condition opposed by space charge, is not required.

The control grid and screen grid form an almost parallel electron beam and control its intensity. Because the beam emerging from the screen grid diverges somewhat in this simple "electron gun," more complex gun structures were tried in the early stages of design in an attempt to approximate a "Pierce gun"[2] and to mask the beam. The approximation was so poor in designs considered practical for manufacture, however, that these tubes had poorer performance than the 7360.

The electron beam is focused by the electron lens formed between the screen grid and the deflecting electrodes. The strength of the lens is a function of the spacing between the deflecting electrodes, the distance between the screen grid and the deflecting electrodes, and the potentials of the screen grid and the deflecting electrodes.

The spacing of the deflecting electrodes is made just large enough to accept the beam width. Wider spacing reduces deflection sensitivity; narrower spacing increases the amount of stray plate current (current not effectively controlled by the deflecting electrodes).

The potential of the screen grid must be at a level that will permit the desired beam current in the gun; the deflecting electrodes must be positive enough to permit passage of the current to the plates. As a result of the limitations on deflecting-electrode spacing and on the potentials of the screen grid and the deflecting electrodes, the distance from screen grid to deflecting electrodes is governed by the strength required of the electron lens.

It is interesting to note that, because of the effect of the deflecting-electrode potential on the electron lens, the axis of the electron lens will be skewed when there is a potential difference between the electrodes. This effect causes some deflection of the beam before it reaches the deflecting electrodes.

The space between deflecting electrodes is tapered away from the cathode to follow the contour of the converging beam so that deflection sensitivity and, hence, deflection transconductance are high. The gap at the far end of the deflecting electrodes is made as small as practical tube manufacture permits in order to achieve maximum deflection transconductance and to minimize the amount of beam current which passes through the gap. Although most of the electrons which do pass through the gap return to the plates, the percentage collected by the deflecting-electrode wires and side rods is higher than when the electrons pass through the deflecting electrodes in the normal fashion.

---

[2] J. R. Pierce, "Rectilinear Electron Flow in Beams," *Jour. App. Phys.*, Vol. 11, p. 548, August, 1940.

The spacing between the deflecting electrodes and between the plates is also tapered away from the cathode. This feature decreases the deflecting-electrode-to-plate amplification factor toward the far end and provides a slight accelerating field to inhibit the return of electrons toward the gun. The plates extend as close to the far end of the deflecting electrodes as practical to collect effectively the electrons which pass through the gap between deflecting electrodes. The plates do not extend close to the near end of the deflecting electrodes so that the deflecting-electrode potentials are more effective in focusing and deflecting the beam in the electron-lens region. The folded-over ends of the plates are used primarily for mechanical strength, although they do tend to collect some electrons which might otherwise graze the plate edge and follow long orbits before actually striking the plate. Experimental designs used half-grids for the control grid and the deflecting electrodes to eliminate the capacitance of the unused grid halves. Full grids, however, have been found to give a great advantage in the rigidity and reproducibility of the tubes.

The internal shield around the cage provides electrostatic shielding to reduce undesired coupling capacitances as well as to provide a small amount of shielding from external magnetic fields. The shield also prevents electron bombardment of the glass bulb and resulting gas evolution and bulb charges. The indentation in the shield is very important in returning the electrons that pass through the gap between deflecting electrodes directly to the plates. Without such a shield near the gap, the deflecting-electrode current and input-impedance characteristics are impaired.

Tube Characteristics

The characteristics of the electron gun of the 7360 are best shown by plate-characteristics curves for the triode-connected tube, as shown in Figure 3. The curves of Figure 3 are useful in estimating cathode current with normal electrode connections because cathode current is normally almost independent of deflecting-electrode voltage or plate voltage. The screen grid normally intercepts about 20 per cent of the cathode current and the deflecting electrode intercepts about one per cent. Therefore, the beam current, or sum of both plate currents, is about 79 per cent of the current shown in Figure 3.

Although the mean* potential of the deflecting electrodes is chosen

* To avoid cumbersome descriptions later in the paper, the term "mean" will refer to the instantaneous mean of the two electrode quantities in question; "average" will refer to a time-average current or voltage; and "differential" will imply measurement of one electrode quantity with respect to the other, irrespective of another reference point.

primarily on the basis of best deflection characteristics, some limitations are imposed by other characteristics. If the mean deflecting-electrode voltage is less than about 10 volts, appreciable beam current may be turned back to the screen grid at low plate voltages; in effect, the tube will be "oversuppressed." Inasmuch as normal mean deflecting-electrode voltage is about 20 to 30 volts, the oversuppressed condition would be reached only if single-ended signals of large amplitude were applied to one deflecting electrode. If very large signals are to

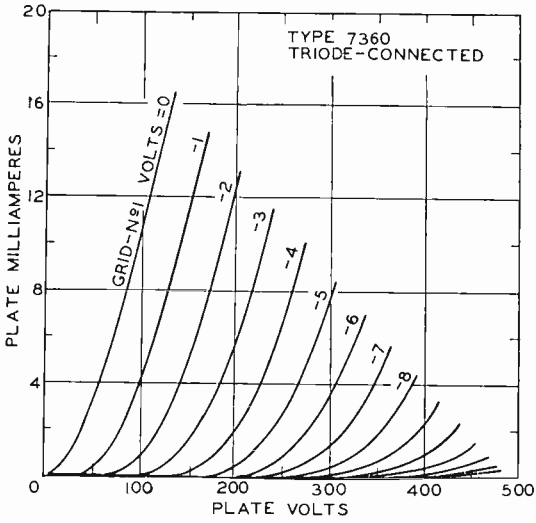

Fig. 3—Plate characteristics of triode-connected 7360 (deflecting electrodes and plates tied to Grid No. 2).

be encountered, therefore, push-pull operation of the deflecting electrodes is recommended so that the mean deflecting-electrode voltage will remain constant.

The effects of the mean plate voltage are apparent in the plate-characteristics curves of a "pentode-connected" tube shown in Figure 4. These curves are applicable for the values indicated for mean plate voltage and mean deflecting-electrode voltage even though a differential voltage may exist between plates or between deflecting electrodes. Plate voltage affects deflecting-electrode current appreciably; deflecting-electrode current is about one per cent of the beam current at plate voltages of 150 volts. It drops to about 0.5 per cent at 300 volts and rises to about 5 per cent at 50 volts.

Figure 5 shows the deflection characteristics obtained for one set

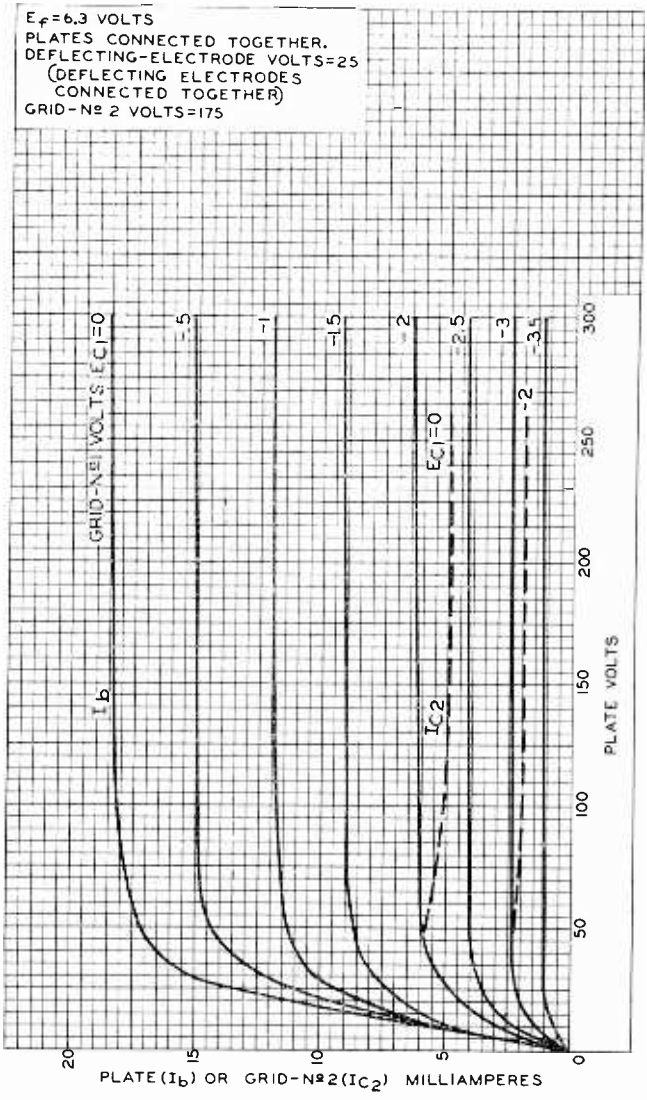

Fig. 4—Plate characteristics of 7360 used as pentode.

of conditions of control-grid, screen-grid, plate, and mean deflecting-electrode voltages. The transconductance and amplification-factor values are measured from deflecting electrode No. 1 to plate No. 1 or from deflecting electrode No. 2 to plate No. 2; the same values, though negative in sense, are obtained from deflecting electrode No. 1 to plate No. 2 or from deflecting electrode No. 2 to plate No. 1. The mean

deflecting-electrode voltage may be reduced to about 11 volts or raised to 35 volts before the plate-current curves are noticeably affected. Similarly, the plate voltage is not critical over a range of 50 to 300 volts.

The value of the amplification factor (μ) is rather low, and, as a result, the values of *differential* plate resistance are rather low; *parallel* plate resistance is very high, as can be seen in the curves of Figure 4. This low-μ characteristic appears to be a result of the construction in which the plates lie alongside the deflecting electrodes.

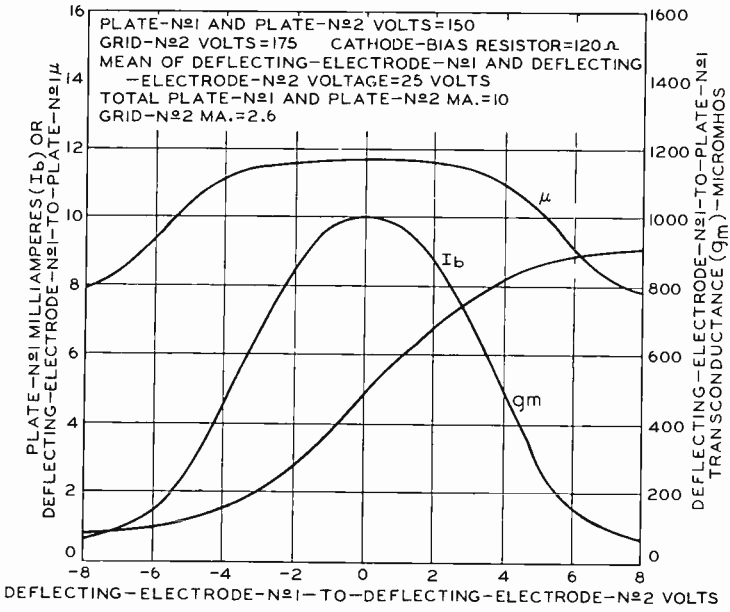

Fig. 5—Curves of 7360 showing plate current, transconductance, and μ as a function of differential deflecting-electrode voltage.

Differential plate voltage must also tend to deflect the beam, although the effectiveness is reduced by the deflecting-electrode-to-plate μ. It is less evident that the same effect occurs in the conventional structure shown in Figure 1; in fact, the μ of the design shown in that figure is almost the same as that indicated in Figure 5. The μ and plate resistance could be increased in either type of structure by the use of additional screen grids, but the grids would add considerable complexity.

The screen-grid voltage has a significant influence on deflection

characteristics. An optimum screen-grid voltage may be found for each value of beam current, although a range of plus or minus 25 volts from the optimum is not serious. This effect is illustrated by the two sets of curves shown in Figure 6. Both curves have the same

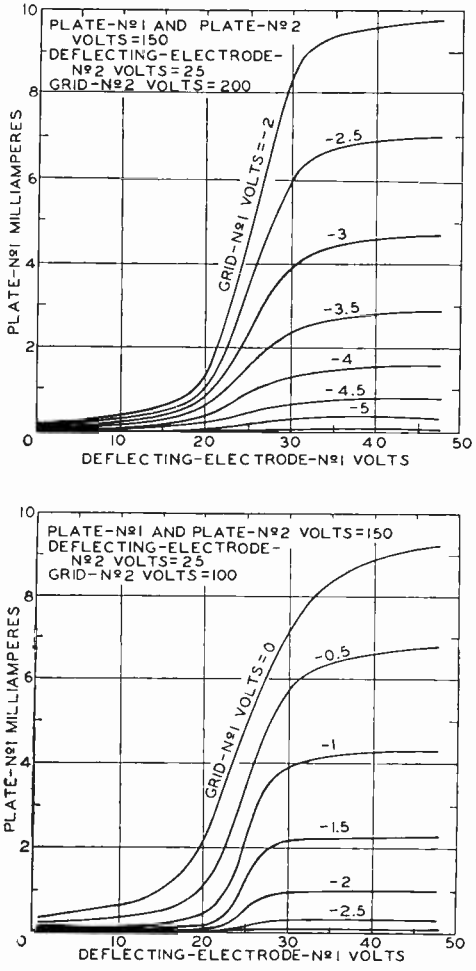

Fig. 6—Curves of 7360 showing influence of control-grid and screen-grid voltages on the linearity of deflection characteristics.

plate-current and differential deflecting-electrode voltage scales but represent different screen-grid voltages. Mean deflecting-electrode voltage was set at the optimum value for each screen-grid voltage. Deflection transconductance (slope of the plate-current curves) at low

currents is best at the lower screen-grid voltage, while the higher screen-grid voltage is best at higher currents. The implication of these characteristics in obtaining linear deflection characteristics when the grid is operated under class-C conditions in some circuits will be discussed later.

The internal capacitances and average characteristics of the 7360 are given in Table I. One bit of additional information regarding capacitances may be useful in some circuits; although the internal cage shield is shown connected to the cathode, the mica and stem shields are connected to the screen grid for convenience and for heat radiation. It is usually preferable, therefore, to have both cathode and screen grid at r-f ground potential.

General Product-Modulator Considerations

The beam-deflection tube is intended to be used as a product modulator. To the extent that the output of the tube is the mathematical product of the two input signals, two sine-wave inputs will give an output proportional to the product of the amplitudes of the input signals. The frequencies of the output will be the sum and difference frequencies of the input signals. If the input signals are of the same frequency, the output will comprise a second-harmonic component and a direct-current component. The direct-current component will be proportional to the cosine of the phase difference between the two input signals. If the input signals have a direct-current component, the output will include components at the input frequencies. This type of output is usual because most product devices must be biased in a manner such that the input signals have, in effect, a direct-current component. In applications of this type, one of the input frequencies may be eliminated from the output by balanced operation of the beam-deflection tube. In addition to the output components mentioned above, other components will be produced by distortion in the product device.

The basic product modulator may be used to perform many circuit functions, including modulation in transmitters; frequency conversion in superheterodyne receivers; and product detection for single-sideband reception, synchronous detection, and frequency-modulation detection.

Efficiency and Gain Considerations

In most circuits utilizing a product modulator, one of the input signals, the CW signal, has constant amplitude, while the other signal contains the communicated information. The CW signal input is often

Table I — General Data

Electrical:

Heater, for Unipotential Cathode:		
Voltage (AC or DC)	6.3 ± 10%	volts
Current	0.35	amp
Direct Interelectrode Capacitances (With no external shield):		
Grid No.1 to all other electrodes except plates	7.5	μμf
Grid No.1 to deflecting-electrode No.1	0.015	μμf
Grid No.1 to deflecting-electrode No.2	0.015	μμf
Grid No.1 to plate No.1	0.003	μμf
Grid No.1 to plate No.2	0.003	μμf
Plate No.1 to all other electrodes except deflecting-electrode No.1	0.8	μμf
Plate No.2 to all other electrodes except deflecting-electrode No.2	0.8	μμf
Plate No.1 to plate No.2	0.3	μμf
Deflecting-electrode No.1 to all other electrodes except plate No.1	4.6	μμf
Deflecting-electrode No.2 to all other electrodes except plate No.2	4.6	μμf
Deflecting-electrode No.1 to plate No.1	4.0	μμf
Deflecting-electrode No.2 to plate No.2	4.0	μμf
Deflecting-electrode No.1 to deflecting-electrode No.2	1.4	μμf

Characteristics, Class A1 Amplifier:

Plate-No.1 Voltage	150	volts
Plate-No.2 Voltage	150	volts
Deflecting-Electrode-No.1 Voltage	25	volts
Deflecting-Electrode-No.2 Voltage	25	volts
Grid-No.2 Voltage	175	volts
Cathode Bias Resistor	150	ohms
Total Beam Current (Plate-No.1 Current plus Plate-No.2 Current)	8.5	ma
Grid-No.2 Current	2.1	ma
Transconductance, between grid No.1 and plates connected together	5400	μmhos
Deflecting-Electrode No.1 Transconductance to Plate No.1	800	μmhos
Deflecting-Electrode No.2 Transconductance to Plate No.2	800	μmhos

Maximum Ratings, Absolute-Maximum Values:

Plate-No.1 Voltage	300 max.	volts
Plate-No.2 Voltage	300 max.	volts
Deflecting-Electrode-No.1 Voltage	±100 max.	volts
Deflecting-Electrode-No.2 Voltage	±100 max.	volts
Grid-No.2 (Screen-Grid) Voltage	250 max.	volts
Plate-No.1 Dissipation	1.5 max.	watts
Plate-No.2 Dissipation	1.5 max.	watts
Grid-No.2 Input	0.5 max.	watt

overdriven to minimize the effects of variations in its amplitude so that the output will be proportional only to the information-bearing signal. The efficiency and gain are improved when sufficient amplitude to saturate one input is used. The ultimate theoretical efficiency is 25 per cent with linear operation, but rises to 31.8 per cent when one input is overdriven. In circuits in which outputs insensitive to either input amplitude and responsive only to phase difference are desired (as in phase detectors and FM detectors), both inputs may be overdriven. Maximum efficiency with both inputs overdriven is 50 per cent. Furthermore, the output is more nearly a linear function of phase difference with this type of operation than it is when linear, or class A, operation is used. Use of only one output current, as required with conventional grid-No.3 control, reduces the efficiencies to one half the above values.

CW Signal Input

The CW signal may be applied to either the control grid or the deflecting electrodes depending upon the operating characteristics desired. In general, it is preferable to apply the CW signal to the deflecting electrodes in small-signal circuits, such as frequency converters in receivers, where maximum gain is desired. In detectors, modulators, and transmitter frequency converters, lack of distortion may be more important than gain, and operation with the CW signal on the grid is preferable.

Either type of input may be used to convert on a harmonic of the CW signal. Although gain and noise performance are sacrificed by harmonic operation, the result may be more economical in some applications than the use of frequency multipliers preceding the converters.

CW Signal Applied to Grid

When the CW signal is applied to the grid and the information-bearing signal is applied to the deflecting electrodes, the information-bearing signal and the modulation products are in push-pull at the two plates, while the CW signal components are in the same phase. Because they are in the same phase, the CW signal components may be cancelled out in a balanced load circuit. The information-bearing signal may be applied to the deflecting electrodes in either a single-ended or a push-pull arrangement; it is the voltage difference between deflecting electrodes that produces deflection. At very high frequencies, however, push-pull operation has the advantage of lower effective input capacitance.

Small-signal performance may be conveniently analyzed by the use

of frequency-converter theory.[3] For determination of conversion transconductance, deflecting-electrode-to-plate transconductance is plotted as a function of control-grid voltage, as shown in Figure 7. Then, with assumed conditions of control-grid bias and CW-signal amplitude, the deflecting-electrode-to-plate transconductance (g_m) curve as a function of time is analyzed by Fourier methods for the fundamental frequency component. This component gives the conversion transconductance (g_c). After a few calculations from trial grid-voltage conditions, inspection of the curves reveals that the average grid voltage

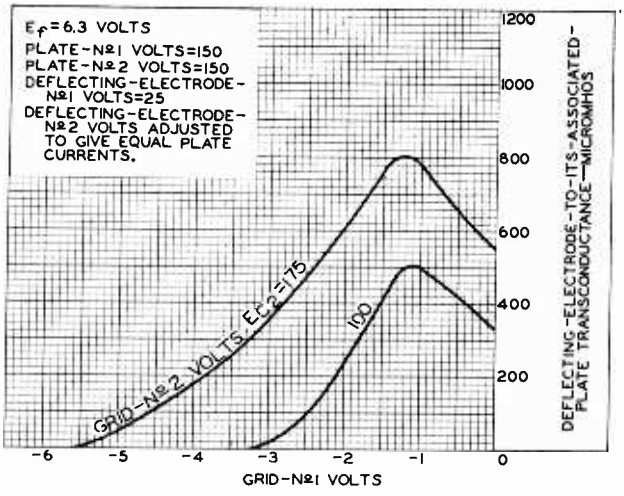

Fig. 7—Curves of deflecting-electrode-to-plate transconductance.

should be placed near cutoff on the g_m curve, and that the CW signal should swing slightly past the peak of the g_m curve for maximum conversion transconductance. Operation under these conditions of grid voltage and signal input results in a conversion transconductance of 25 to 30 per cent of the peak g_m; 300 to 350 micromhos is the maximum obtainable within tube ratings.

The effective plate resistance, r_p, at the output frequency may be determined from the same data used to find conversion transconductance. The average g_m is calculated; average r_p is the quotient of the deflecting-electrode-to-plate μ (about 13) and the average g_m. The average of the g_m curve is slightly higher than the fundamental com-

[3] E. W. Herold, "The Operation of Frequency Converters and Mixers for Superheterodyne Reception," *Proc. I.R.E.*, Vol. 30, No. 2, February, 1942.

ponent (g_c). Therefore, the product of g_c and r_p, the maximum possible conversion voltage gain, is slightly less than the deflecting-electrode-to-plate μ, or about 10. This maximum gain is not critically dependent upon control-grid operating conditions; small changes in grid conditions, in the direction that will reduce g_c, usually raise r_p. This characteristic is sometimes useful in that it is possible to increase grid drive to raise r_p, and thereby to accommodate a convenient circuit impedance more easily.

The conditions for maximum conversion gain require that the peak positive excursion of the grid voltage be about −2 volts. The conditions for minimum distortion are similar, as may be seen qualitatively by examination of the curves of Figure 6. Although the transfer curve for each grid voltage has a long straight portion, the grid swings through a range of voltages, and the conversion transfer curve is a composite of the curves shown. It is clear that the upper set of curves provides a more linear composite. When the CW signal is supplied from an external source, the bias and signal amplitude can be set so that the instantaneous grid voltage will be at least two volts negative at all times. Self-bias obtained from grid current may be desired, however, because it is relatively noncritical to CW signal amplitude and is the most convenient way to limit the amplitude of oscillation in a self-excited circuit. The advantage of grid-resistor bias may be obtained by use of a diode suitably biased so that it conducts while the grid is still negative. It is best to obtain the bias voltage from a cathode resistor, as shown in the circuits of Figures 9, 10, 11. Additional circuit stability may be obtained in this manner.

The "electron-gun" section of the beam-deflection tube can serve as a good oscillator for self-excited circuits. Feedback can be obtained from cathode current, screen-grid current, or total plate current. The use of cathode current in the Hartley circuit commonly used with frequency converters is usually preferable. In this circuit, the r-f cathode voltage is in the proper phase to place the cathode above ground potential during the cathode current pulse. The resulting reduction in effective deflecting-electrode bias should be considered in choosing the average deflecting-electrode-to-ground voltage.

CW Signal Applied to Deflecting Electrodes

When the CW signal is applied to the deflecting electrodes, the conversion transconductance may be determined by the same type of analysis used when the CW signal was applied to the grid. A plot of grid-to-plate g_m as a function of differential deflecting-electrode voltage is used as the starting point. This curve will follow the pattern

of the plate-current versus differential-deflecting-electrode-voltage curves shown in Figures 5 and 6. The g_c to each plate may be as high as about 30 per cent of the peak g_m to each plate. A g_c of 1500 micromhos is readily obtained under the operating conditions given in Table I, which shows a g_m of 5500 micromhos at 10 milliamperes of beam current. The differential r_p is approximately 14,000 ohms at the instant that the beam current is equally divided between the plates, but is very high when the current is fully switched to one plate. The average differential r_p is, therefore, a function of the amplitude of the deflecting-electrode signal; the amplitude of the signal determines the fraction of the cycle during which the r_p is low. The average differential r_p may be as high as several hundred thousand ohms under practical operating conditions. The conversion gain, therefore, may be higher than that of the best pentagrid tubes, and about equal to that of a good pentode mixer in which both signals are applied to the control grid. It is difficult to apply automatic gain control to the beam-deflection tube. In this respect, it is no better than the pentode. The oscillator-to-signal coupling and the oscillator radiation are, however, lower in the beam-deflection tube than they are in the pentode.

Noise in beam-deflection-tube converters that have the CW signal on the deflecting electrodes is comparable to that in good pentode mixers. The main contribution to noise is made by partition noise from the screen-grid current. In the 7360, the screen grid collects about the same fraction of the space current as it does in pentodes, and much less than it does in pentagrid converters. At high frequencies, the noise factor of the 7360 is degraded by fairly high input loading. This loading results from the cathode-lead inductance which is higher than normally found in pentodes. Tubes made with a special basing arrangement to reduce cathode-lead length provided noise figures of about 11 decibels at 100 megacycles and conversion power gain of about 16 decibels. This basing arrangement has not been adopted, however, because it is inferior for other applications.

The converter may be made self-exciting by use of the deflecting electrodes and plates for the oscillator. Although the deflection transconductance is rather low compared to the transconductance of triodes, oscillation up to about 200 megacycles has been obtained with a balanced oscillator having a tuned circuit between plates, and capacitance coupling from each plate to the opposite deflecting electrode. Inductive coupling may also be used with a single tuned circuit or with tuned circuits between plates and between deflecting electrodes. The oscillator circuit for a converter is complicated by the presence of the inter-

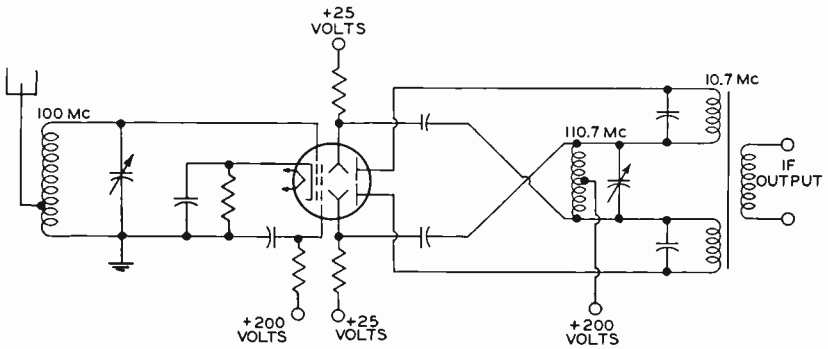

Fig. 8—Diagram illustrating use of 7360 as a self-excited frequency converter for FM receivers.

mediate-frequency transformer, but a circuit like that shown in Figure 8 has been made to work in the FM band.

Balanced-Modulator Application

The balanced modulator used to generate single-sideband signals makes especially good use of the beam-deflection-tube characteristics. The main technical requirements in this application are stability of carrier balance and low distortion. Low distortion implies carrier

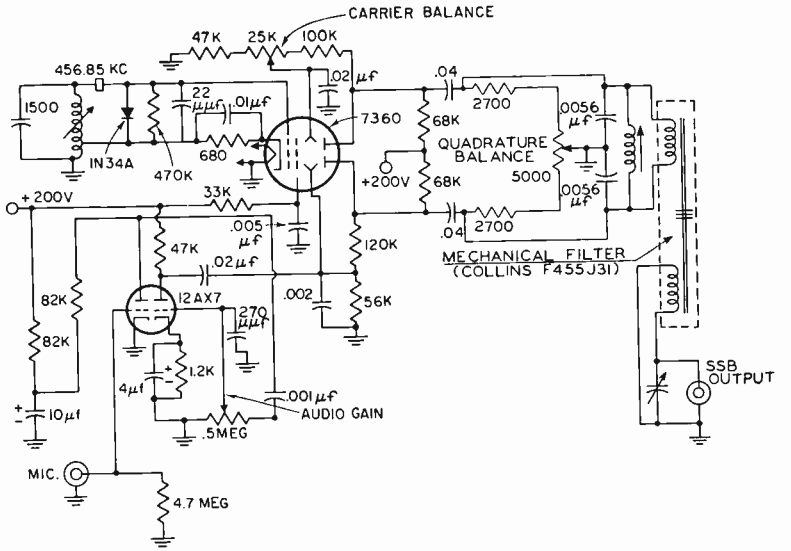

Fig. 9—Schematic of experimental single-sideband modulator using 7360.

suppression at various signal levels, and minimum spurious outputs. For economic reasons, it is desirable to have input signals at convenient voltage and impedance levels and to have some gain to reduce requirements for subsequent amplification.

The structure of the 7360 is particularly well suited to achieving stable balance of plate currents, because both plate currents originate from the same cathode face, grid, and screen grid. It also lends itself to simple and effective feedback stabilizing circuits. The deflection characteristics have very good linearity, and substantial power gain can be obtained.

The features of the tube in this application may be conveniently described by examination of a laboratory single-sideband generator that was built to investigate circuit design and tube performance. The schematic diagram of Figure 9 shows the carrier oscillator, audio amplifier, balanced modulator, and mechanical filter. The mechanical-filter system, which eliminates one sideband, was chosen as the most straightforward way to study balanced-modulator performance. The tube, however, should work well in phasing systems also.

The beam-deflection tube, used in a crystal-oscillator circuit with cathode-current feedback, provides the carrier at approximately 455 kilocycles. The proper grid-to-cathode signal amplitude of 5 to 10 volts peak-to-peak is easily provided by this type of crystal-oscillator circuit, as well as by several other types. The diode is used in conjunction with cathode bias to clamp the grid signal so that the grid swings no more positive than —2 volts.

The audio signal from a crystal microphone is amplified by a two-stage amplifier. The 270-micromicrofarad capacitor at the grid of the second stage was needed to reduce coupling of the carrier into the audio channel even though there is a carrier-frequency bypass capacitor (0.002 microfarad) from deflecting electrode to ground.

The d-c resistance in the deflecting-electrode circuit is preferably limited to about 50,000 ohms because of the flow of current to the deflecting electrodes. Furthermore, the nonlinearity of the current as a function of deflecting-electrode voltage has been considered even though the current is small. Equal d-c resistance is used in each deflecting-electrode circuit to minimize shift in carrier balance with audio-signal level. The coupling capacitor to the driven deflecting electrode is made large for minimum source impedance to minimize distortion of the audio signal from the nonlinear load. The undriven deflecting electrode is bypassed for audio frequencies to ensure that the current flow in that deflecting electrode does not set up a distorted audio voltage.

The 12AX7 provides an audio signal of 5 to 10 volts peak-to-peak. The plate load resistance is rather low for a high-μ tube, and it would be somewhat easier to drive the deflecting-electrode from a medium-μ triode. If a medium-μ tube were used, however, it might be best to use a pentode in the preamplifier stage to make up for the lower gain.

The transducer coil of the mechanical filter could be used as the push-pull load circuit except for the fact that the output of the beam-deflection tube is so large that there is severe distortion in the mechanical filter. (Double-sideband output of 40 volts peak-to-peak is readily obtained in high-impedance loads.) It is desirable to use the full output capabilities of the tube to realize the best relative carrier suppression. Consequently, the load impedance was reduced to about 2500 ohms by means of a tuned circuit in parallel with the filter input. The net Q of the output circuit was also increased in this way; the filter input coil has a Q of about 10. The tube output could have been reduced by decreasing screen-grid voltage, but the oscillator performance would have been impaired.

Each plate of the 7360 is shunt-fed through a 68,000-ohm resistor to achieve stable balance. Any unbalance in plate currents produces a voltage difference between plates which opposes the unbalance. The d-c feedback obtained in this manner amounts to 9 decibels in the circuit shown. For reduced distortion, the negative feedback can be extended through the audio range by coupling the output to the load with about 0.002-microfarad capacitors in place of the 0.04-microfarad capacitors shown. This audio feedback was not used in the experimental circuit because the audio amplifier had excessive distortion at the high output level required. However, the 0.04-microfarad capacitors used provide some hum reduction by feedback at 60 cycles.

Additional d-c feedback is provided by obtaining deflecting-electrode voltage with bleeders from the plates. In this way, part of the plate voltage change, caused by shifts in plate-current balance, is applied to the deflecting electrodes to oppose the change. The total d-c feedback is 17 decibels. This feedback is a substantial aid to stability of carrier balance. It should be noted, however, that feedback to the deflecting electrodes shifts some of the burden of stability from the tube to the resistors in the two bleeders. If this type of feedback is not used, a common bleeder should be used for deflecting-electrode voltage so that resistor changes primarily affect mean deflecting-electrode voltage rather than the differential deflecting-electrode voltage.

Adjustment of plate-current balance is provided by making one deflecting-electrode voltage variable. The adjustment is the main carrier balance control, but, for excellent carrier balance, the phases of

the currents being balanced must be equal within very small tolerance. An adjustment of quadrature balance, therefore, is usually required. In the circuit of Figure 9, the tuned load circuit has a high C/L ratio; unbalance of resistances across each half of the balanced circuit provides adjustment of quadrature balance almost independent of in-phase balance. The resistance in the quadrature-balance circuit must be fairly high compared to the resonant impedance of the tuned circuit to preserve the independence of the balance adjustments.

Another method of obtaining quadrature balance has been tested successfully. In this method, some carrier signal is applied to the appropriate side of the balanced load circuit through a small adjustable capacitor to provide 90 degrees phase shift. The use of a differential capacitor connected to both plates provides a practical means to adjust the amplitude of the inserted carrier at either plus or minus 90 degrees. Alternatively, a variable capacitor can be connected from the grid to one plate, and a fixed capacitor with a value at about the center of the range of the variable capacitor can be connected from the grid to the other plate. The necessary phase corrections are so small that capacitance values less than one micromicrofarad are needed when the carrier signal is obtained from the grid. More commonplace values of capacitance can be used if the carrier is fed from a lower voltage point, such as the cathode in the circuit of Figure 9.

The mechanical filter attenuates the carrier frequency about 20 decibels, and carrier balance of 90 decibels below peak signal output is readily obtained. The significant feature of performance, however, is that carrier suppression remains better than 60 decibels with 10 per cent variations of heater voltage, B voltage, or both.

Balanced-Mixer Application

Tube operation in the balanced-mixer circuit is much like that in the balanced modulator. The balanced mixer is frequently used in single-sideband transmitters. When modulation is performed at a low frequency, the signal is translated to the carrier frequency by mixing, or heterodyning, with appropriate frequencies. The modulation must not be distorted as it would be in a frequency multiplier. There is a restriction on the frequency of the CW signal relative to the frequency of the information-bearing signal, because the CW signal and the unwanted "beat" signal must be far enough from the desired "beat" signal to be conveniently eliminated by the selectivity of the tuned circuits. This restriction is eased by the use of a balanced mixer which substantially attenuates the CW signal. The balance requirements are

not as severe as they are for the balanced modulator, however, because simple selective circuits capable of adequately attenuating the undesired beat also considerably attenuate the CW signal frequency. Balance is consistent enough among 7360 tubes that a balance adjustment is unnecessary if oscillator signal level up to about 20 decibels below the desired signal (excluding circuit selectivity) is tolerable.

Figure 10 shows an experimental balanced-mixer circuit. This unit was used in conjunction with the single-sideband generator of Figure 9. An intermediate amplifier was also required for experimental work

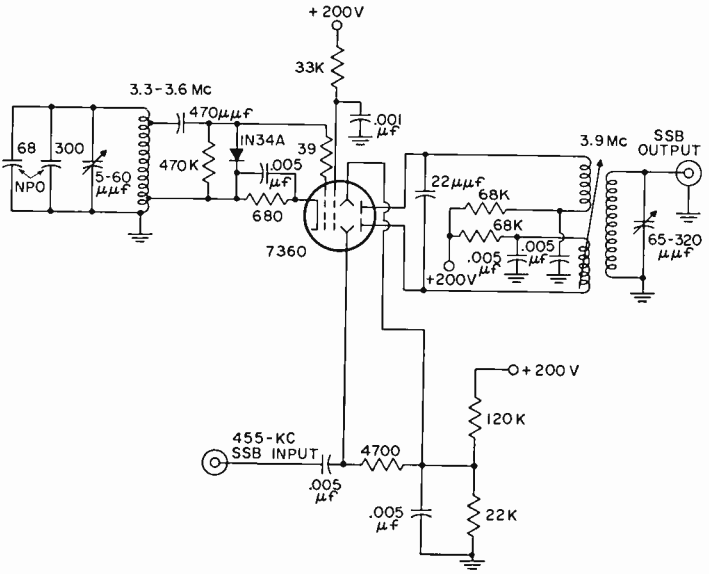

Fig. 10—Schematic of experimental balanced mixer using 7360.

because the mechanical filter was incapable of enough output to drive the mixer adequately.

The beam-deflection tube is also used as a variable-frequency oscillator made stable by the well-known technique of tapping the tube down on a stable, high-Q, tuned circuit having fairly high C/L ratio. Single-sideband input of up to 5 volts peak-to-peak is fed, single-ended, to one deflecting electrode. The push-pull plate circuit is arranged so that the currents from the two plates flow through separate 68,000-ohm resistors to stabilize balance. The plate coils of the output transformer are bifilar-wound to assure tight coupling and accurate center tap for good balance. This output circuit was double-tuned for ade-

quate selectivity; a low-impedance output was used to minimize detuning when various experimental uses were made of the output.

Observations made with limited equipment indicated that the distortion was low even at signal levels considerably higher than those normally possible with other types of mixers. The simplicity of using a single tube as oscillator and balanced mixer is evident. In some transmitter systems it may be possible to eliminate frequency multipliers for the CW signal because the relatively large signal levels handled by the beam-deflection tube may make conversion on harmonics of the CW signal practical despite the lower gain.

Product Detector Application

Another very promising modulator application of the beam-deflection tube is as the product detector used in single-sideband receivers. The "beat-frequency oscillator" (BFO) signal is applied to the control grid. The 7360 may serve as its own oscillator as in the above applications. The intermediate-frequency signal is applied to the deflecting electrodes, preferably in push-pull, and the demodulated output is taken from the plates either single-ended or push-pull.

Although considerable input signal can be handled with low distortion, a sharp overload point is reached at slightly higher levels so that good limiting of impulse noise is provided in the detector. Even at overload, however, the deflection characteristics are symmetrical, and there is little undesired signal rectification or "envelope detection." The detector has substantial gain and enough output to drive a power amplifier directly. The BFO signals are in phase at the plates and may be balanced out with the use of a suitable output transformer. The transformer requirements are especially practical with low intermediate frequencies, which are difficult to filter adequately when unbalanced detectors are used.

Figure 11 shows the schematic diagram of an experimental product detector. This unit was built as an adapter for a war-surplus communication receiver having a 910-kilocycle intermediate frequency.

The oscillator uses the principles discussed above for frequency stability and for grid-voltage conditions to secure optimum detection linearity. Balanced signal input is used to minimize coupling of signal to the oscillator grid and to minimize coupling of the oscillator into the i-f amplifier. Coupling of the signal to the oscillator grid tends to lock the oscillator on the signal frequency. In the test circuit, the oscillator did not lock until a CW signal of normal amplitude was brought to within about 5 to 10 cycles of the oscillator frequency. If

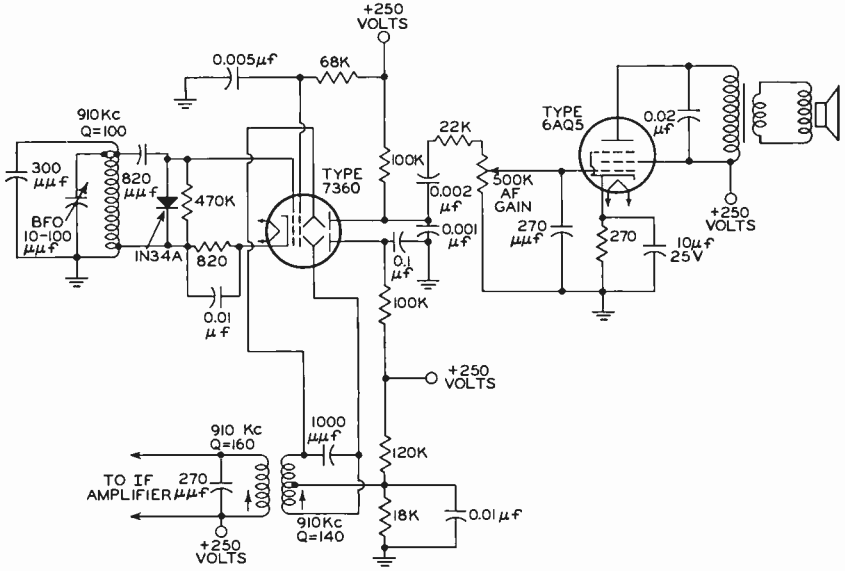

Fig. 11—Schematic of experimental product detector using 7360 for single-sideband or CW reception.

desired, the locking tendency could be reduced by provision for adjustable neutralizing of the signal-to-oscillator coupling or by use of a separate oscillator. Oscillator locking was used for synchronous

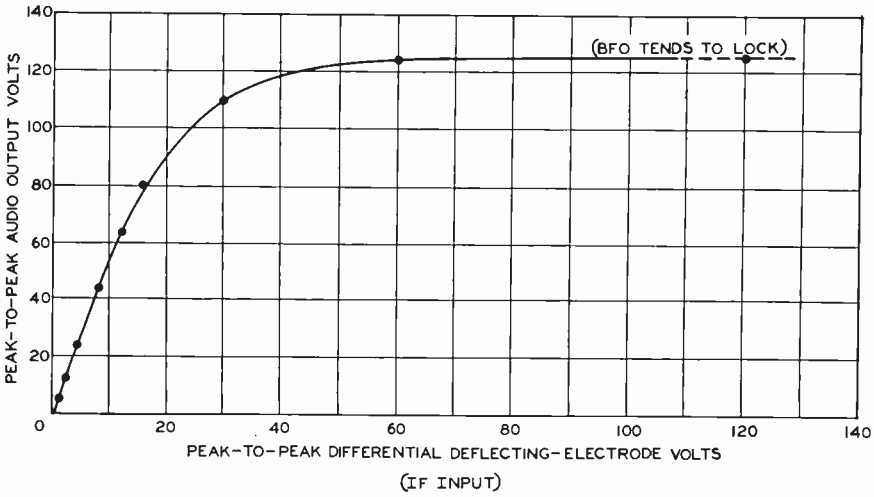

Fig. 12—Curve showing linearity and overload characteristics of product detector circuit (Figure 11).

detection of AM signals by including a switch (not shown) to lower the oscillator-circuit Q and to add resistive signal-to-oscillator coupling so that the oscillator would lock in the proper phase on a carrier within about 200 cycles of the natural oscillator frequency.

RC filtering was sufficient to attenuate the BFO frequency in this instance, and single-ended output to a power amplifier tube formed a simple circuit arrangement. Note that equal plate-load resistors are used to obtain the proper d-c voltages, but that one plate is bypassed for audio frequencies. This bypassing permits full differential r_p to be obtained and, thus, increases the gain at the plate used for output.

Conversion voltage gain, linearity, and limiting characteristics are shown in Figure 12.

Other Circuit Applications

There are many possible circuit applications outside of the communications field. The tube may be useful in pulse-combining circuits. The deflecting-electrode characteristics are such that a signal may be clipped at both positive and negative peaks at the same time. Two signals may be added in well-isolated inputs by feeding one signal to each deflecting electrode. Output signals of both polarities are obtained, and the effective polarity of an input signal can be changed by switching it from one deflecting electrode to the other.

Acknowledgment

The author wishes to acknowledge the valuable assistance of Robert S. Nelson and Joseph Pastor, Jr. during the advanced development phases of tube design and circuit development. Product development of the 7360 was carried out by several other people, principally G. H. Foster and B. Levine on tube design, and J. T. Maguire on circuit evaluation.

RCA TECHNICAL PAPERS†

First Quarter, 1960

Any request for copies of papers listed herein should be addressed to the publication to which credited.

"Electrostatic Imaging and Recording," E. C. Hutter, J. A. Inslee, and T. H. Moore, *Jour. S.M.P.T.E.* (January) 1960

"Hi-Fi Applications of New Triode-Pentode," W. Austin, *Electronics World* (January) 1960

"Image Sensors and Space Environment," M. Ritter and M. H. Mesner, *Jour. S.M.P.T.E.* (January) 1960

"Lamp and Receptacle Provide Standby Power and Appliance Checker," J. B. Powell, *Electronic Design* (January) 1960

"Miniature High-Frequency Magnetic Amplifiers for Magnetic Memory Sensing," G. R. Briggs and K. C. Hu, *Communication and Electronics* (January) 1960

"Nomographs Simplify Electron Tube Design (Part I)," R. D. Reichert, *Electronic Industries* (January) 1960

"The Optimum Noise Performance of Tunnel-Diode Amplifiers," K. K. N. Chang, *Proc. I.R.E.* (January) (Letter to the Editor) 1960

"Particle Interaction in Magnetic Recording Tapes," J. G. Woodward and E. Della Torre, *Jour. Appl. Phys.* (January) 1960

"Pictorial Data Transmission from a Space Vehicle," J. F. Baumunk and S. H. Roth, *Jour. S.M.P.T.E.* (January) 1960

"Rectangular Hysteresis Loop Ferrites with Large Barkhausen Steps," A. P. Greifer and W. J. Croft, *Jour. Appl. Phys.* (January) 1960

"Root Locus Properties and Sensitivity Relations in Control Systems," H. Ur, *Trans. I.R.E. PGAC* (January) 1960

"Space Technology and Image Sensing: Summary and Conclusions," S. Sternberg, *Jour. S.M.P.T.E.* (January) 1960

"SSB and ISB Systems for Long Distance Radio Telegraph," W. Lyons, *Communication and Electronics* (January) 1960

"Television and Lunar Exploration," S. W. Spaulding, *Jour. S.M.P.T.E.* (January) 1960

"A Two-Transistor Regenerative Receiver for 80 and 40 Meters," E. M. Washburn, *RCA Ham Tips* (January-February) 1960

"Influence of Degeneracy on Recombination Radiation in Germanium," J. I. Pankove, *Phys. Rev. Letters* (January 1) 1960

"Missile Interference: Cause and Cure," G. W. Soderquist, *Electronics* (January 8) 1960

"Measuring Critical Current in Cryogenic Circuits," J. I. Pankove and R. Drake, *Electronics* (January 22) 1960

"Compandor Loading and Noise Improvement in Frequency Division Multiplex Radio-Relay Systems," E. M. Rizzoni, *Proc. I.R.E.* (February) 1960

"Nomographs Simplify Electron Tube Design," R. D. Reichert, *Electronic Industries* (February) 1960

"Photoelectronic Analysis of High Resistivity Crystals: (a) GaAs, (b) Sb_2S_3," R. H. Bube, *Jour. Appl. Phys.* (February) 1960

"Pictorial Data Transmission from a Space Vehicle," J. F. Baumunk and S. H. Roth, *Elec. Eng.* (February) 1960

"SSB/ISB Systems for Long-Distance Radiotelegraphy," W. Lyons, *Elec. Eng.* (February) 1960

† Report all corrections or additions to RCA Review, RCA Laboratories, Princeton, N. J.

"TM Waves in Submillimetric Region," C. A. Martin, *Proc. I.R.E.* (February) (Correspondence) 1960
"A Transport Mechanism Design for the Television-Tape Recorder," J. G. Lee, *Jour. S.M.P.T.E.* (February) 1960
"Vapor-Zone Refining," L. R. Weisberg and F. D. Rosi, *Rev. Sci. Instr.* (February) (Notes) 1960
"Variation in Ear Protector Attenuation as Measured by Different Methods," L. Weinreb and M. L. Touger, *Jour. Acous. Soc. Amer.* (February) 1960
"Origin of the Photomagnetism Anomaly in Germanium," A. R. Moore and J. O. Kessler, *Phys. Rev. Letters* (February 1) ... 1960
"Ferroelectricity in Tetramethylammonium-Trichloro-Mercurate," E. Fatuzzo and R. Nitsche, *Phys. Rev.* (February 15) 1960
"All New Monochrome Studio Camera, Type TK-12," J. H. Roe, *Broadcast News* (March) 1960
"Application of the Sampling Function to Circuit Analysis of Modulators and Demodulators using Diodes," A. Feller, *RCA Review* (March) 1960
"Automatic Sensitivity Control for Monochrome Film Cameras," S. L. Bendell and K. Sadashige, *Broadcast News* (March) .. 1960
"Consider Interference in Systems Design," R. F. Ficcki," *Electronic Industries* (March) 1960
"Constant-Ratio Code and Automatic-RQ on Transoceanic HF Radio Services," J. B. Moore, *Trans. I.R.E. PGCS* (March) 1960
"Design Considerations for Integrated Electronic Devices," J. T. Wallmark, *Proc. I.R.E.* (March) 1960
"Double-System Recording and Editing With Video Tape," O. F. Wick, *Jour. S.M.P.T.E.* (March) 1960
"Effect of Temperature on Photovoltaic Solar Energy Conversion," J. J. Wysocki and P. Rappaport, *Jour. Appl. Phys.* (March) .. 1960
"Electromagnetic Properties of High-Temperature Air," M. P. Bachynski, T. W. Johnston, and I. P. Shkarofsky, *Proc. I.R.E.* (March) 1960
"Electronic Music Synthesis," H. F. Olson, H. Belar, and J. Timmens, *Jour. Acous. Soc. Amer.* (March) 1960
"A Frequency-Locked Grid-Controlled Magnetron," C. L. Cuccia, *RCA Review* (March) 1960
"How Design of Tape Transport Mechanism Improves Performance of TV Tape Recorder," J. G. Lee, *Broadcast News* (March) .. 1960
"Improved Antennas of the Rhombic Class," E. A. Laport and A. C. Veldhuis, *RCA Review* (March) 1960
"The Influence of Magnetic Tape on the Field of a Recording Head," E. Della Torre, *RCA Review* (March) 1960
"Intermodulation Distortion and Efficiency Analysis of Multicarrier Repeaters," *Trans. I.R.E. PGCS* (March) 1960
"Maximum Stable Collector Voltage for Junction Transistors," R. A. Schmeltzer, *Proc. I.R.E.* (March) 1960
"Measurement of Semiconductor Properties through Microwave Absorption," R. D. Larrabee, *RCA Review* (March) 1960
"Measuring Techniques for FM Main and Subcarrier Deviation," I. H. Lubash, *Broadcast News* (March) 1960
"More on 7-Transistor Pocket Radio," H. Wittlinger, *Radio-Electronics* (March) (Correspondence) 1960
"New 1000 Watt FM Transmitter," J. A. Aurand, *Broadcast News* (March) 1960
"New Equipment for Measuring Envelope Delay," E. N. Luddy, *Trans. I.R.E. PGB* (March) 1960
"New High-Efficiency 5-KW AM Transmitter," I. R. Skarbek, *Broadcast News* (March) 1960
"New 10-KW FM Transmitter," A. H. Bott, *Broadcast News* (March) 1960
"New Velocity Microphone Type BK-11A," *Broadcast News* (March) 1960

"On the Nonconservation of Noise Parameters in Multivelocity Beams," J. Berghammer and S. Bloom, *Jour. Appl. Phys.* (March) 1960

"Nonlinear Theory of a Velocity-Modulated Electron Beam with Finite Diameter," F. Paschke, *RCA Review* (March) 1960

"Nonreciprocal Attenuation of Ferrite in Single-Ridge Waveguide," T. S. Chen, *Trans. I.R.E. PGMTT* (March) (Correspondence) 1960

"Operation of a Chromium Doped Titania Maser," H. J. Gerritsen and H. R. Lewis, *Jour. Appl. Phys.* (March) (Letters to the Editor) 1960

"Optimum Estimation of Impulse Response in the Presence of Noise," M. J. Levin, *Trans. I.R.E. PGCT* (March) 1960

"Pattern Recognition and Display Characteristics," W. R. Bush, R. B. Kelly, and V. M. Donahue, *Trans. I.R.E. PGHFE* (March) 1960

"A Resonant Coaxial-Stub as an Automatic Equalizer," G. V. Rao, *Trans. I.R.E. PGB* (March) 1960

"Ringing in Horizontal-Deflection and High-Voltage Television Circuits," T. Murakami, *RCA Review* (March) 1960

"Simultaneous Signal Separation in the Tricolor Vidicon," H. Borkan, *RCA Review* (March) 1960

"A Special-Effects Amplifier for Noncomposite or Composite, Monochrome or Color Television Signals," R. C. Kennedy, *Jour. S.M.P.T.E.* (March) 1960

"S.S.B. Exciter Circuits Using a New Beam-Deflection Tube," H. C. Vance, *QST* (March) 1960

"A Statistical Analysis of Cross-Track Errors in a Navigation System Utilizing Intermittent Fixes," H. Staras and R. W. Klopfenstein, *Trans. I.R.E. PGANE* (March) 1960

"10 Watt Transistor Monitor Amplifier," *Broadcast News* (March) 1960

"Test Set for Displaying the Volt-Ampere Characteristics of Tunnel Diodes," A. M. Goodman, *Rev. Sci. Instr.* (March) 1960

"Theoretical and Experimental Study of Wide-Band Paraboloid Antenna with Central-Reflector Feed," P. Foldes and S. G. Komlos, *RCA Review* (March) 1960

"Transistor AC Amplifier with High Input Impedance," J. J. Davidson, *Semiconductor Products* (March) 1960

"Electric Field Induced Light Absorption in CdS," R. Williams, *Phys. Rev.* (March 15) 1960

AUTHORS

T. N. CHIN received the B.S. degree from the National Tsing Hua University, Kunming, China, in 1942, and the M.S. and Ph.D. degrees from the University of Illinois, Urbana, in 1949 and 1952, respectively. From 1942 to 1945 he worked at the Central Radio Manufacturing Works in Kunming, and from 1945 to 1947 he served as an instructor in the National Tsing Hua University, Peiping, China. After being associated with the Electron Tube Research Laboratory at the University of Illinois, Dr. Chin joined the RCA Electron Tube Division, Lancaster, Pa., in 1955. In 1957, he was transferred to the RCA Laboratories Division at Princeton, N.J. where he is engaged in research on display devices.

C. LOUIS CUCCIA (See *RCA Review*, Vol. XXI, No. 1, March 1960, p. 146.)

RALPH W. ENGSTROM received the B.S. degree from St. Olaf College in Northfield, Minnesota in 1935. He subsequently attended Northwestern University in Evanston, Illinois, and received the M.S. degree in 1937 and the Ph.D. in 1939. He joined the RCA Tube Division in Harrison, N. J. in 1941, and was engaged for several years in the development of multiplier phototubes and related devices. He is now manager of the Photo and Image Tube Development Group in Lancaster, Pennsylvania. Dr. Engstrom is a member of the honorary physical society Sigma Psi, and is a Fellow of the American Physical Society.

L. E. FLORY received the B.S. degree in Electrical Engineering, University of Kansas in 1930. He was with the research division of RCA Manufacturing Co., Camden, N. J. from 1930 to 1942 during which time he was engaged in research on television tubes and related electronic problems, particularly in the development of the iconoscope. In 1942 he was transferred to the RCA Laboratories Division, Princeton, N. J. From 1949 to 1954 he was in charge of work on storage tubes, and since 1949 he has been in charge of work on industrial television. More recently he has been concerned with applications of transistors to television circuits and with medical electronics problems. Mr. Flory is a member of Sigma Xi and a Fellow of the Institute of Radio Engineers.

ROBERT D. GOLD received the B.E.E. degree from City College of New York in 1953. He spent three months with the RCA Victor Division as a Specialized Trainee before entering the U.S. Army. He worked on feasibility studies of radar counter-measure systems while in service. From 1955-1957 he attended Cornell University, where he received the M.S. degree in Electrical Engineering. He joined RCA Laboratories in 1957, where he has worked on television circuits and kinescopes, and on semiconductor devices. He has also given lectures in Electrical Engineering at City College of New York. Mr. Gold is a member of the Institute of Radio Engineers, Tau Beta Pi, and Eta Kappa Nu.

GEORGE W. GRAY attended Princeton University as a civilian and in the Navy V-12 Program until 1943 when he was assigned to active duty in the Navy. After release to inactive duty in 1946, he returned to Princeton University and received the B.A. degree in Physics. In March of 1947 he joined the technical staff of RCA Laboratories Division at Princeton, N. J. He is at present a member of the Electronic Research Laboratory engaged in television research. Mr. Gray is a member of Sigma Xi.

KARL G. HERNQVIST graduated in Electrical Engineering at the Royal Institute of Technology, Stockholm, Sweden, in 1945. He received the Licentiate of Technology degree in 1951 and the Doctor of Technology degree in 1959. From 1946 to 1952 he was employed by the Research Institute of National Defense in Stockholm working in the field of microwave electronics. From 1948 to 1949, Mr. Hernqvist was a trainee of the American-Scandinavian Foundation at RCA Laboratories, to which he returned in 1952; he is presently working on thermionic power conversion. Dr. Hernqvist is a Member of the Institute of Radio Engineers and Sigma Xi.

JACK HILIBRAND received the B.S.E.E. degree from the City College of New York in 1951. He was a National Science Foundation Fellow at the Massachusetts Institute of Technology for two years and a Research Assistant at the Research Laboratory of Electronics for two years. In 1956 he received the Sc.D. degree from M.I.T. for work in the analysis of excess physical noises. Since graduation he has been a Member of the Technical Staff of RCA Laboratories in Princeton, N. J., where he is engaged in semiconductor device design and analysis. He also holds the rank of Lecturer at the Graduate Division of the School of Technology, City College of New York. Dr. Hilibrand is a member of Eta Kappa Nu, Tau Beta Pi, and Sigma Xi.

RALPH C. KENNEDY received the B.A. degree from the San Jose State College in 1943, the M.A. degree from Stanford University in 1945 and the E.E. degree from the same institution in 1946. He joined the Development Group of the National Broadcasting Company in 1946. Since that time, he has worked on various phases of monochrome and color television. He is Adjunct Professor in the Graduate School of Engineering of New York University and Lecturer in the Graduate School of Electrical Engineering at the City College of New York. Mr. Kennedy is a member of Sigma Pi Sigma.

HARRY KIHN received the B.S. degree in Electrical Engineering from the Cooper Union Institute of Technology in 1934 and the M.S. degree from the University of Pennsylvania in 1952. Prior to joining RCA he was employed by the Hygrade-Sylvania Co., Polytherm (his own company), and the Ferris Instrument Company. He joined the RCA Manufacturing Company in Camden in 1939 and engaged in television field testing, receiver circuit development, and research in frequency modulation, fluctuating noise, ferromagnetic materials, and the APN-1 radio altimeter. In 1942, he was transferred to RCA Laboratories in Princeton, where he engaged in research on X-band receivers, silicon crystals, frequency modulation radar, automatic bombing devices, and the APN-22 altimeter. With the advent of color television, he participated in the research and development of the field test receivers. In 1953, he transferred to the System Research Laboratory, where he did research on millimeter-wave high-resolution radar. He directed research in pulse code and microminiature digital communication systems resulting in the "Megacoder" and data link developments. He was head of the Space Systems Research Group with responsibility in IR and radar systems and the research application of devices developed in the Laboratories. Mr. Kihn is a Senior Member of the IRE, of Sigma Xi, and a member of the Operations Research Society of America.

RICHARD J. KLENSCH received the B.S. degree in Electrical Engineering from the University of Illinois in 1951. From 1952 to the present time he has taken graduate courses, as an incidental student, at Princeton University. After a brief stay with Motorola, Inc., as an engineer in their test laboratory, he joined RCA Laboratories in 1952 where he engaged in millimeter wave high resolution radar research dealing with r-f, i-f, a-f-c, and computer circuitry. From 1954 to 1956 he was a radar instructor while serving in the U. S. Army. In 1956 he returned to RCA Laboratories and did research on microwave scanning antennae, low-noise infra-red detection systems, and micro-miniature multiplexing systems. Currently, he is doing research in the general field of communications. Mr. Klensch is an associate member of the Institute of Radio Engineers and is a member of the Professional Group on Antennas, Professional Group on Instrumentation, and Professional Group on Telemetry and Space Electronics.

M. BERWYN KNIGHT received the B.S. degree in Electrical Engineering from the University of Wisconsin in 1948. He joined RCA in the specialized training program that year, and was subsequently assigned to the Electron Tube Division in Harrison, N.J. He worked on circuit applications of electron tubes, particularly for television receivers, in the Receiving Tube Application Laboratory until 1954. He then transferred to Receiving Tube Advanced Development to develop special tubes and circuits for color television receivers. He is currently responsible for tube application engineering, primarily with "Nuvistor" tubes, in Receiving Tube Advanced Development. Mr. Knight is a Senior Member of the Institute of Radio Engineers.

JEREMIAH M. MORGAN studied at Drexel Institute. In 1929 he was employed by the Victor Talking Machine Company in Camden, N. J. in the test department. With the absorption into the RCA Manufacturing Co. in 1930, he was transferred to the television laboratory engaged in circuit design. He has continued in this line doing circuit development work on electron miscroscopes, television and special test equipment, transferring to the RCA Laboratories in Princeton, N. J. in 1942. Since 1948 he has been engaged in the development of industrial television equipment. Mr. Morgan is a Member of the Institute of Radio Engineers and an Associate Member of the Franklin Institute.

WINTHROP SEELEY PIKE received the B.A. degree in Physics in 1941 from Williams College. He served with U. S. Army Signal Corps during World War II as radar officer and later as project officer in charge of the Signal Corps Moon Radar project. In 1946 he joined the research staff of RCA Laboratories Division at Princeton, N. J., where he has worked on sensory aids for the blind, storage tube applications, color television and industrial television. Mr. Pike is a Member of Sigma Xi and the American Guild of Organists.

ALLEN H. SIMON received the B.E.E. degree from the Cooper Union in 1957 and, in the same year joined RCA Laboratories as a student trainee. His training assignments included research on a microminiature pulse-position modulation system and some theoretical investigations related to magnetic tape recording. He is now a member of the Mathematical Services group, and is working toward a Ph.D. degree in Electrical Engineering at Princeton University.